Ph.D. THESIS

Fatigue Reliability Assessment Considering Multiple Crack Coalescence

다중균열의 병합을 고려한 피로신뢰도 평가

2019년 2월

서울대학교 대학원

건설환경공학부

박 준 용

ABSTRACT

Fatigue Reliability Assessment Considering Multiple Crack Coalescence

Jun Yong Park
Department of Civil and Environmental Engineering
Seoul National University

Assessment method including analysis methods for multiple crack growth and coalescence and a probability model of initial crack size and distance between initial cracks is suggested to evaluate fatigue reliability reflecting actual fatigue mechanism. Probabilistic assessment to predict the fatigue performance of general welded connections is possible with suggested model instead of existing deterministic assessment based on measured multiple crack.

Analysis methods for multiple crack growth and coalescence were determined by referring to existing analysis methods. LEFM is adopted to simulate the propagation of single crack. Since the crack growth model proposed by Paris and Erdogan is based on large crack data, simulation of crack growth can be difficult in fatigue details with small cracks. Crack growth model suitable for the size of investigated crack should be adopted. However, it is difficult to establish the crack growth model as in the large crack since crack growth rate of small crack is affected by the grain size, grain orientation, and crack shape. To overcome this problem, EIFS concept, which

utilize equivalent virtual crack size, is adopted. When EIFS is considered as initial crack size instead of actual initial crack size, crack growth simulation can be done with large crack growth model which is used to determine EIFS even if the initial crack size lies in the small crack region. Back-extrapolation method, which find the initial crack size having the same life with experimental fatigue life, is adopted to estimate EIFS.

When multiple crack coalescence is simulated, the crack shape gradually differs from idealized semi-elliptical crack during crack coalescence. Therefore, FEA is adopted to simulate the crack coalescence since it is difficult to simulate the change of SIF occurring in the crack coalescence with existing solutions. For this reason, a re-characterization rule is adopted to replace the complex simulation of crack coalescence. Among the many proposed rules, re-characterization rule proposed by Kamaya is adopted. In this rule, coalesced crack can be simulated by introducing a single crack having the same area with sum of two adjacent cracks.

For probabilistic simulation of multiple crack condition, probability model of initial crack size and distance that constitute the initial conditions of multiple cracks was developed by analyzing the fatigue fracture surface obtained from the actual fatigue tests performed in NCHRP Project 10-70. Crack initiation point is estimated based on beach mark and ratchet mark on the fracture surface. From 6 to 23 of crack distance data were identified from each specimen and total 209 distance data were utilized to develop probability model of distance between initial cracks. As a result of goodness-of-fit test,

the Lognormal distribution with a mean of 8.3 mm and a standard deviation of 4.4 mm is the most suitable distribution.

Since the initial crack size is not a variable that can be obtained directly from the fracture surface, it should be estimated based on the experimental results. Initial crack size model suitable for the target structure was determined using the EIFS concept. In order to obtain EIFS, material parameters *C*, *m* and SIF equations appropriate for the target fatigue detail are necessary. Material parameters *C* and *m* are considered to be distribution model based on the experimental data of Barsom. Since the material parameter *C* has a distribution, samples of *C* are generated based on experimental data of Barsom and then EIFS distribution corresponding to the samples of *C* is obtained. All EIFS distribution data obtained from each crack initiation point of the specimen is assembled and the probability model of the EIFS is suggested using these data. Most suitable distribution is Lognormal distribution with a mean of 0.58mm and a standard deviation of 0.91mm.

Multiple crack condition is not determined depending on the type of structure, but is common conditions in welded connection. In addition, general structural steel is utilized in test specimen and there is no significant difference with other type of structures in terms of welding materials and methods. Therefore, the distribution characteristics of the initial cracks extracted in Chapter 2 can be sufficiently applied to welded connection of other kinds of structures such as bridge. Welded details in bridge were selected for example to verify the validity of the developed assessment model.

The validity of the developed assessment model was identified by comparing distribution of the fatigue life presented in the NCHRP Reports and that of the fatigue life obtained by the developed assessment model. In addition, distribution of fatigue life obtained by applying single crack model is also considered to compare with multiple crack model. As a result, it can be seen that the fit with the experimental fatigue life is high when the multiple crack conditions are considered. In case of transverse stiffener, model for multiple crack gives conservative results. On the other hand, the result of simulation assuming the conventional single crack condition always gives overestimated fatigue life. Through the assessment of the three welded details, the basis for application of welded details of various steel structures are identified.

Keywords: Fatigue reliability; LEFM; Multiple crack coalescence; Equivalent initial flaw size (EIFS); Re-characterization rule

Student Number: 2011-20977

TABLE OF CONTENTS

LIST OF FIGURES

LIST OF TABLES

ABBREVIATIONS

LEFM	Linear Elastic Fracture Mechanics
SIF	Stress Intensity Factor
SCF	Stress Concentration Factor
EIFS	Equivalent Initial Flaw Size
NDI	Non-Destructive Inspection
TTCI	Time To Crack Initiation
DOB	Degree Of Bending
KS test	Kolmogorov-Smirnov test
MCS	Monte-Carlo Simulation

GLOSSARY

a	Depth of surface crack or half-length of through-thickness crack
a_0	Depth of initial crack
b	Half-width of plate
C	Material parameter in Paris' law
c	Half-length of surface crack
a/c	Crack aspect ratio
d	Distance between crack initiation points
da/dN	Crack growth rate
F_s	Front surface correction factor
F_w	Back surface correction factor
F_e	Shape correction factor
F_g	Stress gradient correction factor
ΔK	Stress intensity factor range
ΔK_{th}	Fatigue crack propagation threshold
L/T	Weld footprint width
M_{km}	Stress gradient correction factor subjected to membrane stress
M_{kb}	Stress gradient correction factor subjected to bending stress
m	Material parameter in Paris' law
N	Number of cycles
R	Stress ratio(ratio of minimum stress to maximum stress)
r	Radius of tube

S_r	Applied nominal stress range
$S_{r,th}$	Stress range threshold
$S_{r,hs}$	Range of hot spot stress
T	Thickness of plate
T_{cp}	Thickness of cover plate
Y	Correction factor for stress intensity factor
Y_m	Flat plate SIF equations subjected to membrane stress
Y_b	Flat plate SIF equations subjected to bending stress
Z	Height of weldment
θ	Weld angle

CHAPTER 1

INTRODUCTION

1.1 Research background

In general, single crack is assumed for the fatigue reliability assessment (Chen et al., 2011; Leander and Al-Emrani, 2016; Lukic and Cremona, 2001; Maljaars et al., 2012). However, the fatigue crack forms in actual weldment by growth of multiple initial cracks coalescence (Ali et al., 2008; Fisher et al., 1974; Frise and Bell, 1992; Harrington, 1995; Lin and Smith, 1997). Ali et al. (2008) found that the fatigue mechanism of the aluminum alloy specimen was due to the coalescence of multiple cracks. They found that the number of coalesced cracks is greatly affected by the distance between cracks, and they have developed a modelling of crack coalescence. In many NCHRP reports considering fatigue detail in bridges, growth and coalescence of multiple crack are identified from fatigue tests (Fisher et al., 1974; Fisher et al., 1980; Fisher et al., 1970) Frise and Bell (1992) modelled crack growth and coalescence through experimental and analytical approaches. In addition, they emphasized the importance of crack growth model considering coalescence since large percentage of fatigue life is spent in the process of crack growth and coalescence. They also mentioned that typically there are crack initiation points per meter of weldment from 100 to 200. Therefore, in order to perform a realistic fatigue assessment, assessment should be

performed through a model reflecting actual fatigue mechanism.

Actually in general welded detail, fracture surfaces show various range of approximate size and distance between cracks, as shown in Figure 1. In order to predict the fatigue performance of general welded connections, probabilistic approach for size and distance between cracks is required along with a crack growth model considering multiple crack coalescence.

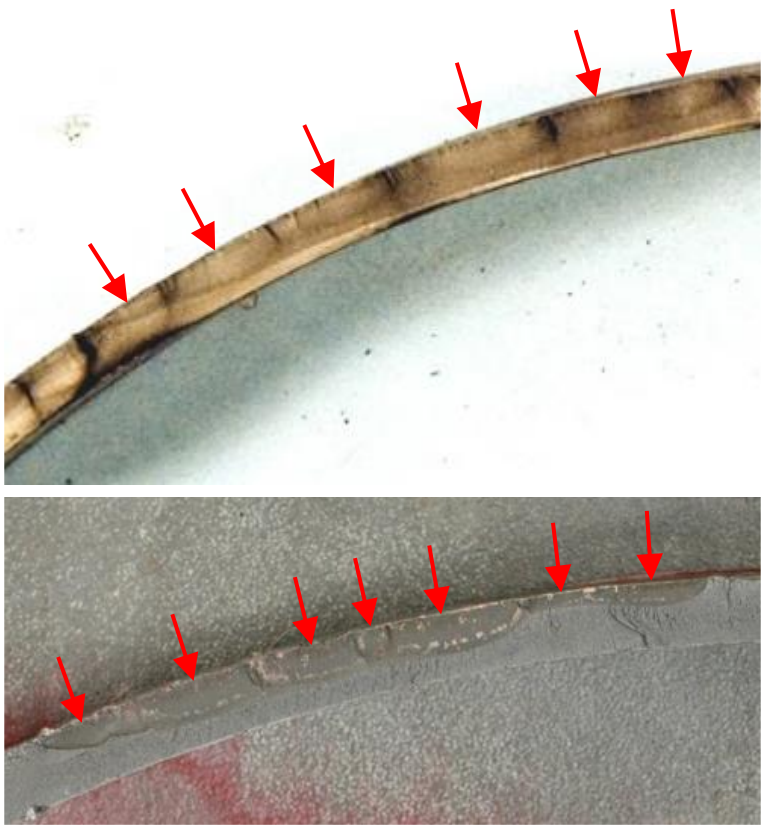

Figure 1. Multiple crack propagation and coalescence in actual fracture surfaces

In previous studies, deterministic assessment was carried out according to the measured position and size of the cracks. Chew and Pang (2016) developed a crack growth modeling algorithm considering crack closure

concept and multiple crack coalescence and estimated fatigue S-N curves. Non-propagating crack size suggested by El Haddad et al. (1979b) is utilized as initial crack size. Crack coalescence is simulated by re-characterizing adjacent cracks into a single crack, which is called re-characterization rule. Result of fatigue life prediction was compared with experimental S–N curve to verify developed algorithm. However, distance between cracks are not applicable to general welded detail since they considered periodic clad-toe surface cracks. In addition, crack growth modeling algorithm considering crack closure concept cannot apply to general welded detail since crack closure generally occurs at stress-relieved condition. Bowness and Lee (2002) emphasizes importance of number of initial crack in order to predict fatigue life. They identified effect of the number of crack on fatigue life since multiple crack growth are typical in most welded joints. Simplified multiple crack condition was adopted in which a number of equally spaced initial crack.

1.2 Literature survey

1.2.1 Crack growth model for single crack simulation

Linear elastic fracture mechanics (LEFM) is the most widely adopted methodology to simulate fatigue crack propagation. Paris and Erdogan (1963) conducted fatigue testing for metal specimens under constant amplitude loading and isolated three distinct phases in crack propagation, as shown in

Figure 2. Phase I is a non-propagation stage wherein fatigue cracking does not propagate when the applied stress intensity factor (SIF) range (ΔK) at the crack tip is lower than the fatigue crack propagation threshold (ΔK_{th}). If the applied ΔK at the crack tip is greater than ΔK_{th}, cracks begin to propagate, and that is Phase II. The rate of the crack propagation is measured via the increment of crack length per fluctuation of applied stress, and it is proportional to ΔK. Phase III is a fracture stage. Once a fatigue crack reaches a critical crack size, catastrophic fracture occurs.

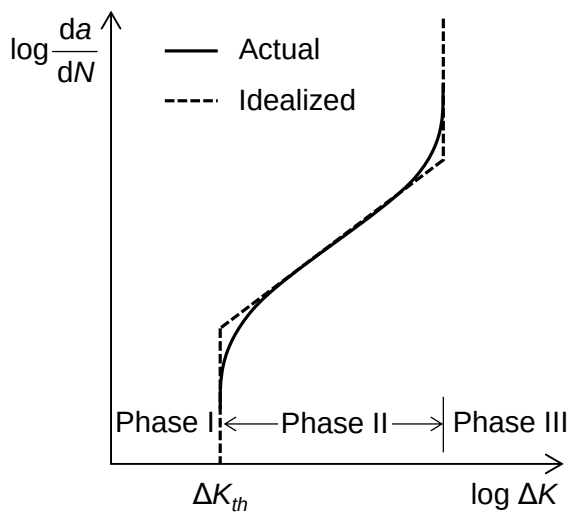

Figure 2. Fatigue crack growth in steel

Crack growth model proposed by Paris and Erdogan (1963) was adopted to simulate fatigue crack growth using Eq. (1).

$$\frac{da}{dN} = \begin{cases} 0 & for\ \Delta K_a < \Delta K_{th} \\ C(\Delta K_a)^m & for\ \Delta K_{th} \le \Delta K_a \end{cases}$$
$$\frac{dc}{dN} = \begin{cases} 0 & for\ \Delta K_c < \Delta K_{th} \\ C(\Delta K_c)^m & for\ \Delta K_{th} \le \Delta K_c \end{cases} \quad (1)$$

In that equation, a is the crack depth, c is half length of the crack, N is the number of loading cycles, da/dN is the crack growth rate and C and m are the material parameters. Range of SIF including ΔK_a and ΔK_c is considered for the crack in Mode I which is opening mode, since propagation of fatigue cracks investigated in this study are mostly affected by opening mode. This equation is only valid in Phase II which has proportional relationship between rate of the crack propagation and ΔK. The range of SIF which is important variable to determining rate of the crack propagation was determined using Eq. (2).

$$\begin{aligned} \Delta K &= Y(a) S_r \sqrt{\pi a} \\ &= F_s F_w F_e F_g S_r \sqrt{\pi a} \end{aligned} \quad (2)$$

In that calculation, $Y(a)$ is a SIF correction factor that deals with the crack shape, the crack size and geometry of the connection detail, F_s is front surface correction factor, F_w is back surface correction factor which should be applied at finite width, F_e is shape correction factor that considers shape of the crack front, F_g is a stress gradient correction factor that considers the stress distribution through the thickness direction, and S_r is the applied nominal stress range.

Crack shape can be classified into two types, as shown in Figure 3. In first type, semi-elliptical surface crack propagates until depth of crack attain

thickness of plate. After crack penetrated plate, type of crack changed to through-thickness crack. Immediate transitions can be assumed since transition occurred during considerably short period of time (Fisher et al., 1974). In this study, direction of crack propagation is not changed since direction of principal stress is assumed to be perpendicular to crack front during crack propagation.

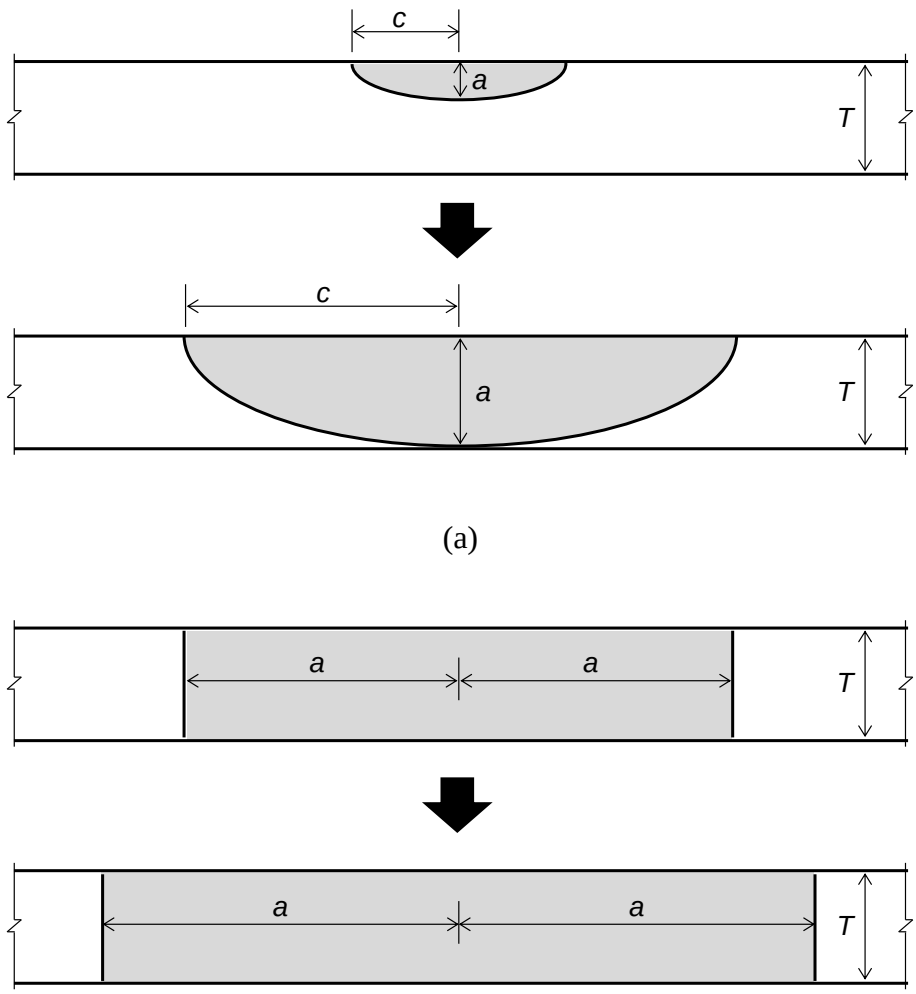

Figure 3. Two types of crack shape during crack propagation: (a) semi-elliptical surface crack; and (b) through-thickness crack

1.2.2 Probability model for variables in crack growth model

The variables used in the crack growth model show the distribution characteristics. Therefore, each variable is applied as a probability model for reliability assessment. Probabilistic variables consist of initial crack size (a_0), material parameter (C, m) in Paris' law and fatigue crack propagation threshold (ΔK_{th}).

Many papers dealing with LEFM-based fatigue assessment refer to existing probability model of initial crack size. As shown in Table 1, mean of initial crack sizes range from 0.1mm to 6.3mm, and Exponential and Lognormal are usually utilized as the probability model (Becher and Hansen, 1974; Bokalrud and Karlsen, 1982; Engesvik and Moan, 1983; Hudak Jr et al., 1990; JCSS, 2011; Marshall, 1982; Recho, 1984).

Table 1. Existing probability models of initial crack size

Reference	Distribution	Mean (mm)	Standard deviation (mm)
JCSS (2011)	Lognormal	0.150	0.100
Engesvik and Moan (1983)	Lognormal	0.125	0.045
Marshall (1982)	Exponential	6.250	6.250
Bokalrud and Karlsen (1982)	Exponential	0.110	0.110
Becher and Hansen (1974)	Lognormal	1.810	1.780
Recho (1984)	Lognormal	0.089	0.089
Hudak Jr et al. (1990)	Lognormal	0.539	0.516

Bokalrud and Karlsen (1982) identified 325 undercuts at 827 measurement sites and suggests the Exponential model of initial crack size based on measured size of undercut. Recho (1984) also suggests a Lognormal model of initial crack size based on the measured data identical with data used by Bokalrud and Karlsen (1982). Engesvik and Moan (1983) proposed a distribution model by combining the data used in various studies including the measured data utilized by Bokalrud and Karlsen (1982). Thus, it is identified that the initial crack size varies due to measurement methods and material property.

Table 2. Material parameter C and m (in SI unit)

		ln$C$			
Reference	m	Type	Mean	Standard deviation	Mean+2sd.
Barsom and Rolfe (1999)	3.0	Deterministic	-	-	-29.15
BSI (2015)	3.0	Deterministic	-	-	-28.28
Hirt and Fisher (1973)	3.0	Deterministic	-29.72	-	-
King (1998)	3.0	Normal	-29.02	0.37	-28.28
DNV (1984)	3.1	Normal	-29.84	0.55	-28.74
Snijder et al. (1987)	2.8	Normal	-27.76	0.23	-27.30

The material parameters C and m of the crack growth model vary depending on the material and stress ratio (R) (BSI, 2015; King, 1998). As shown in Table 2, probability model of material parameters or material constants are proposed for various materials, however, it is important to apply

C and *m* suitable for the material and stress ratio of the target structure (Barsom, 1971; BSI, 2015; DNV, 1984; Hirt and Fisher, 1973; King, 1998; Snijder et al., 1987).

Fatigue crack propagation threshold (ΔK_{th}) also vary depending on the material and stress ratio (R). In BSI (2015), fatigue crack propagation threshold which is strongly dependent on R is recommended to apply the lower bound value obtained at high R for assessment of welded detail. This is because the R is generally high at the weldment due to the residual stress, and the recommended threshold value for welded detail is 63 N/mm$^{3/2}$. Barsom and Rolfe (1999) proposed the equation of fatigue crack propagation threshold according to R as follows:

$$\Delta K_{th} = 221(1-0.85R) \text{ N/mm}^{3/2} \tag{3}$$

JCSS (2011) proposed a fatigue crack propagation threshold in the form of a probability model which is Lognormal distribution with a mean of 140 N/mm$^{3/2}$ and a standard deviation of 56 N/mm$^{3/2}$.

1.2.3 Correction factors for stress intensity factor (SIF) equation

For reasonable simulation of the crack growth, proper Y should be applied according to the conditions such as the type of details indicating the steel plate, the round steel pipe, the shape of the crack indicating the surface crack and edge crack, and the welding condition. Except for the specific details, generally factor which is appropriately adopted from the existing solutions is

used for fatigue evaluation (Leander and Al-Emrani, 2016; Lukic and Cremona, 2001; Pang et al., 2017; Pipinato et al., 2011; Zhang et al., 2002; Zhou et al., 2016).

Cracks in weldment occur mainly at the boundary between weldment and base metal, and are categorized as semi-elliptical surface cracks because they usually have semi-elliptical shapes. Various SIF equations for semi-elliptical surface cracks are presented in papers (Barsom and Rolfe, 1999; Fisher, 1984; Irwin, 1962; Newman and Raju, 1981; Paris and Sih, 1965). SIF equations developed by experiment and analysis have differences in results depending on the geometry of crack, detail and loading conditions. SIF equations proposed by Newman and Raju (1981), Barsom and Rolfe (1999) and Fisher (1984) are compared.

The SIF equation of Newman and Raju (1981) consists of Eq. (4) to(10). As a result of evaluating the equations for surface cracks based on fracture data, Newman and Raju's equation has the advantage that the standard deviation of the SIF values is the smallest and the stability of the equation is high (Newman, 1979). Newman and Raju (1981) proposed SIF correction factors for surface cracks on the base metal, therefore, stress gradient correction factor (F_g) is not suggested in paper. In other words, correction factors corresponding to a front surface correction factor (F_s), a back surface correction factor (F_w), and a shape correction factor (F_e), which are commonly applied to a semi-elliptical surface crack, is proposed. However, in the SIF equation, three kinds of correction factors including F_s, F_w and F_e

are complexly integrated.

$$\begin{aligned}\Delta K &= Y(a)S_r\sqrt{\pi a} \\ &= \left[M_1 + M_2\left(\frac{a}{T}\right)^2 + M_3\left(\frac{a}{T}\right)^4 \right] f_\phi g f_w S_r \sqrt{\frac{\pi a}{Q}}\end{aligned} \tag{4}$$

$$M_1 = 1.13 - 0.09\left(\frac{a}{c}\right) \tag{5}$$

$$M_2 = -0.54 + \frac{0.89}{0.2 + (a/c)} \tag{6}$$

$$M_3 = 0.5 - \frac{1.0}{0.65 + (a/c)} + 14\left(1.0 - \frac{a}{c}\right)^{24} \tag{7}$$

$$g = 1 + \left[0.1 + 0.35\left(\frac{a}{T}\right)^2 \right](1 - \sin\phi)^2 \tag{8}$$

$$f_\phi = \left[\left(\frac{a}{c}\right)^2 \cos^2\phi + \sin^2\phi \right]^{1/4} \tag{9}$$

$$f_w = \sqrt{\sec\left(\frac{\pi c}{2b}\sqrt{\frac{a}{T}}\right)} \tag{10}$$

The SIF equation of Barsom and Rolfe (1999) consists of Eq. (11) to (14). Correction factors including F_s, F_w and F_e which are commonly applied to semi-elliptical surface cracks, are suggested respectively.

$$\Delta K = Y(a)S_r\sqrt{\pi a} = F_s F_w F_e F_g S_r \sqrt{\pi a} \tag{11}$$

$$F_s = 1.12 \tag{12}$$

$$F_w = \begin{cases} 1.0 & for\ a/T < 0.5 \\ 1.0 + 1.2\left(\dfrac{a}{T} - 0.5\right) & for\ a/T \geq 0.5 \end{cases} \tag{13}$$

$$F_e = \frac{1}{\int_0^{\pi/2}\left[1 - \dfrac{c^2 - a^2}{c^2}\sin^2\theta\right]^{1/2} d\theta} \tag{14}$$

The SIF equation of Fisher (1984) consists of Eq. (15) to (18). Correction factors including F_s, F_w and F_e are suggested respectively as Barsom and Rolfe (1999). Equation of Fisher (1984) was used in crack growth analysis to investigate fatigue tests performed in several NCHRP projects.

$$\Delta K = Y(a)S_r\sqrt{\pi a} = F_s F_w F_e F_g S_r \sqrt{\pi a} \tag{15}$$

$$F_s = 1.211 - 0.186\sqrt{\frac{a}{c}} \tag{16}$$

$$F_w = \sqrt{\sec\frac{\pi a}{2T}} \tag{17}$$

$$F_e = \frac{1}{\int_0^{\pi/2}\left[1 - \dfrac{c^2 - a^2}{c^2}\sin^2\theta\right]^{1/2} d\theta} \tag{18}$$

The validity limits of SIF equations are also important point to determine

proper SIF equation. In case of equation of Fisher (1984), value of SIF diverges when the depth of crack grows to thickness of plate because F_w used by Fisher is only valid in a range where a/T is less than 0.7. When crack growth from surface crack to through-thickness crack is simulated, validity limit of a/T is important. In such perspective, equations of Newman and Raju (1981) and Barsom and Rolfe (1999) give valid values even if the depth of crack grow to the thickness of plate.

Since F_g is a factor that varies depending on the degree of stress concentration, it is determined according to investigated fatigue detail. In case of transverse stiffener in bridge, SIF equations developed by Zettlemoyer and Fisher (1977) and Bowness and Lee (2002) can be adopted to calculate F_g. F_g of Zettlemoyer and Fisher (1977) could be calculated by:

$$F_{g,a} = \frac{\mathrm{SCF}}{1 + \frac{1}{0.3602}\left(\frac{a}{T}\right)^{0.2487}} \tag{19}$$

$$\mathrm{SCF} = 1.621 \log\left(\frac{Z}{T}\right) + 3.963 \tag{20}$$

In that equation, SCF is the stress concentration factor, T is the flange thickness, and Z is the weld height. SCF is affected by geometry of fatigue detail and weldment.

As mentioned above, there are many kinds of SIF equations and it plays an important role in assessment because different values can be obtained for each proposed SIF equation. To identify the significance of the proper SIF equation, a fatigue life estimation was performed on the transverse stiffener

detail. All variables in the crack growth model are the same and only the SIF equation is applied differently. Four possible combinations of SIF equation are considered. The results of the fatigue life estimation are shown in Figure 4, which shows that up to 44% fatigue life difference occurs.

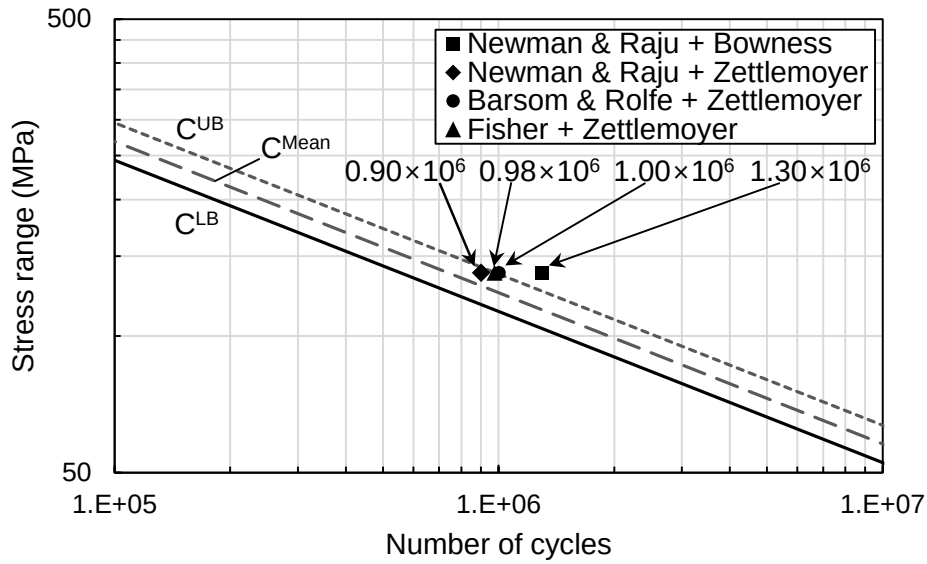

Figure 4. Difference of fatigue life according to SIF equation

1.2.4 Large crack and small crack

Since the crack growth model proposed by Paris and Erdogan (1963) is based on large crack data, simulation of crack growth can be difficult in fatigue details with small cracks (El Haddad et al., 1979a; Miller, 1987; Newman et al., 1999; Ritchie and Lankford, 1986; Venkateswaran et al., 2005). However, as shown in Table 1, mean size of initial defect in weldment has various sizes ranging from 0.1mm to 6.3mm according to research group (Becher and

Hansen, 1974; Bokalrud and Karlsen, 1982; Engesvik and Moan, 1983; Hudak Jr et al., 1990; JCSS, 2011; Marshall, 1982; Recho, 1984). Therefore, crack growth model proposed by Paris and Erdogan (1963) cannot be adopted to every cases since most initial defects are located in small crack region.

As shown in Figure 5, the significant difference between the behavior of large crack and that of small crack is that the crack can grows in the ΔK lower than the large crack threshold (ΔK_{th}) (Liu and Mahadevan, 2009; Newman et al., 1999). Furthermore, crack growth rates are also faster than large cracks. However, crack growth rate of small crack is affected by the grain size, grain orientation, and crack shape, and has considerable uncertainties. This makes it difficult to establish the crack growth model as in the large crack (Liu and Mahadevan, 2009).

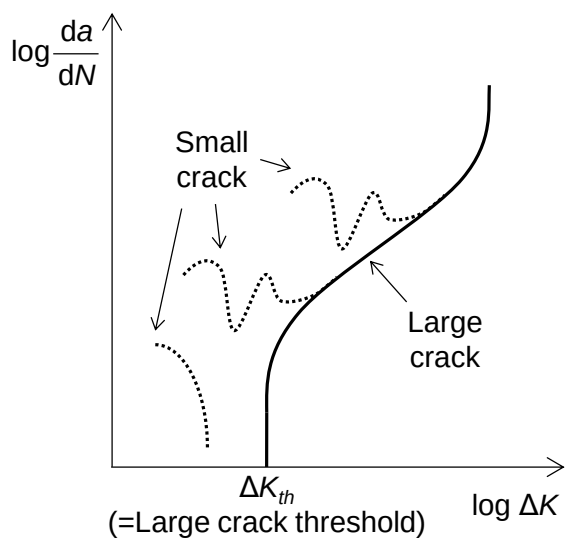

Figure 5. Fatigue crack growth behavior for small and large cracks (Liu and Mahadevan, 2009; Newman et al., 1999)

Through experimental approach, Frost (1959)and El Haddad et al. (1979b) obtained the stress amplitude threshold according to crack length. As shown in Figure 6, it was found that the tendency was different around 1mm. If the crack depth is larger than 1 mm, the stress range threshold ($S_{r,th}$) can be obtained using the Eq. (21).

$$\Delta K_{th} = Y(a) S_{r,th} \sqrt{\pi a} \tag{21}$$

Since ΔK_{th} is a fixed value, $S_{r,th}$ increase as the crack size decreases. However, when the crack depth is smaller than 1 mm, Eq. (21) is not valid and $S_{r,th}$ tends to converge gradually to the fatigue limit of material. For this reason, even if ΔK is smaller than ΔK_{th} in the small crack region, the crack can grow if the applied stress range is larger than the fatigue limit of material. Conversely, even if applied stress range is smaller than the fatigue limit of material in a large crack region, cracks can grow if ΔK occurred at the crack tip greater than ΔK_{th}.

In order to simulate realistic crack growth, a crack growth model suitable for the size of investigated crack should be adopted.

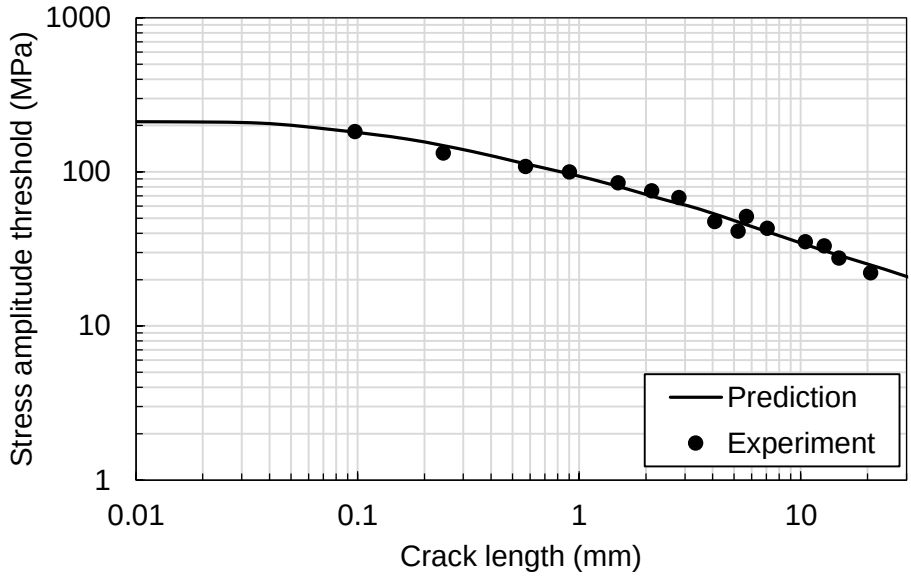

(a)

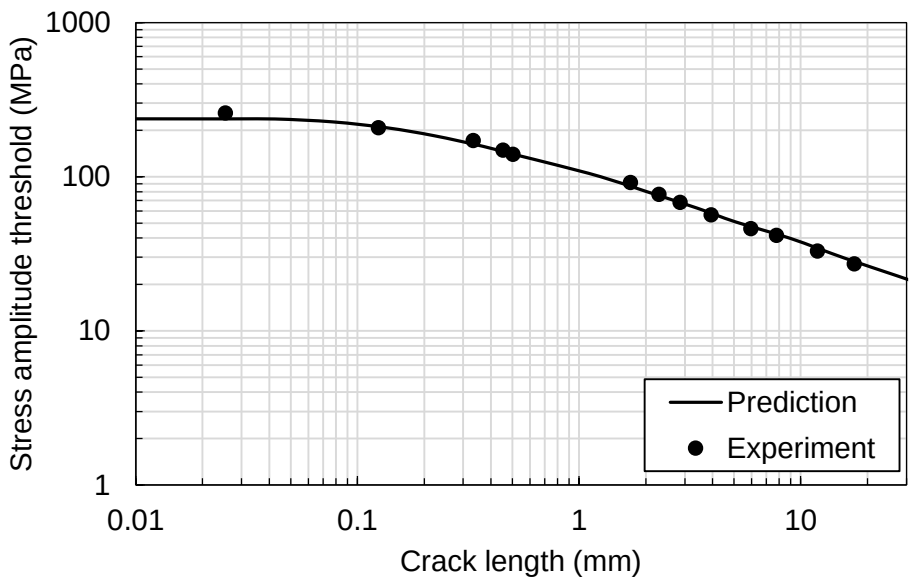

(b)

Figure 6. Change of stress amplitude threshold according to crack length: (a) experimental results of El Haddad et al. (1979b); and (b) experimental results of Frost (1959)

1.2.5 Equivalent initial flaw size (EIFS)

One of problem in fatigue assessment using fracture mechanics is that the exact initial crack size is not known and should be estimated to a specific value (Liu and Mahadevan, 2009). Fatigue life varies considerably depending on how the initial crack size is determined. The initial cracks size can be determined by using the proposed distribution model from experiments or measurements and by measuring the actual crack size of structures through non-destructive inspection (NDI) (BSI, 2014; Engesvik and Moan, 1983; JCSS, 2011). Both methods have the limitation that the accuracy of the crack size depends on the detection capability. When initial crack size is smaller than the detection capability, the detection limit can be assumed as initial crack size.

Other problem is absence of well-known crack growth model in small crack like Paris' law. When the initial crack size is small enough not to be valid with large crack growth model, fatigue assessment becomes difficult (Forth et al., 2002). To overcome this problem, EIFS, which is virtual crack size, is estimated based on experimental results. Crack growth simulation can be performed with large crack growth model when EIFS is adopted as initial crack size.

The EIFS concept was first used by Rudd and Gray (1976) for assessing the manufacturing quality of the aircraft in the McDonnell Douglas F-4C / D aircraft structural integrity program. Three commonly used methods for

estimating EIFS are the back-extrapolation method, the Kitagawa-Takahashi (KT) diagram method, and the time to crack initiation (TTCI) method (Shahani and Moayeri Kashani, 2013). The back-extrapolation method is a method to find the initial crack size having the same life with experimental fatigue life of the investigated specimen through crack growth simulation. Kitagawa-Takahashi diagram method combines the concepts that fatigue failure does not occur at the fatigue limit of the S-N approach and that the crack does not grow below the SIF threshold of LEFM as shown in Figure 7. Assuming EIFS as a material constant, the SIF threshold and the fatigue limit of the material are used to calculate EIFS as Eq. (22).

$$a = \frac{1}{\pi}\left(\frac{\Delta K_{th}}{\Delta \sigma_f}\right)^2 \tag{22}$$

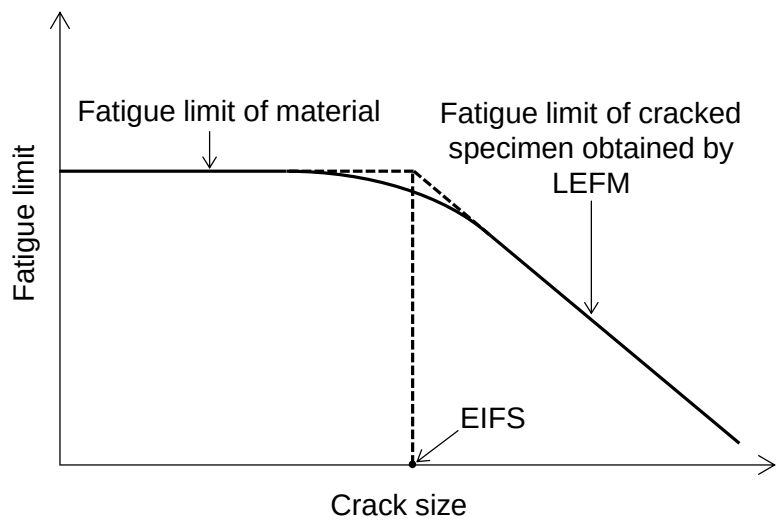

Figure 7. Kitagawa-Takahashi (KT) diagram

TTCI method estimates the initial crack size by fitting curve indicating

relationship between crack size and cycle based on the measured crack size history.

In this study, back-extrapolation method is adopted to estimate EIFS based on experimental. In the case of the Kitagawa-Takahashi diagram method, it is not applicable because there is no ΔK_{th} information of specimens. TTCI method is also not applicable to the estimation because there is no crack growth history and the accuracy is lower than other two methods (Shahani and Moayeri Kashani, 2013).

The EIFS determination using back-extrapolation method has the same procedure regardless of type of crack growth model used for simulation, as shown in Figure 8. When the fatigue life or crack growth history information is obtained through experiments, crack growth simulation is performed while changing the initial crack size to find best fitted initial crack size with experimental result. Variable in crack growth simulation is only initial crack size and the remaining variables indicating loading condition, geometry of detail and SIF are applied as constant value according to the experimental conditions. If material properties are unknown, material properties are also applied as variable. In this case, EIFS distribution can be obtained instead of only one EIFS value. As a result, EIFS is defined as the initial crack size that best fit the experimental result among the prediction results. This kind of approach to estimate initial crack size is called as back-extrapolation method (Liu and Mahadevan, 2009).

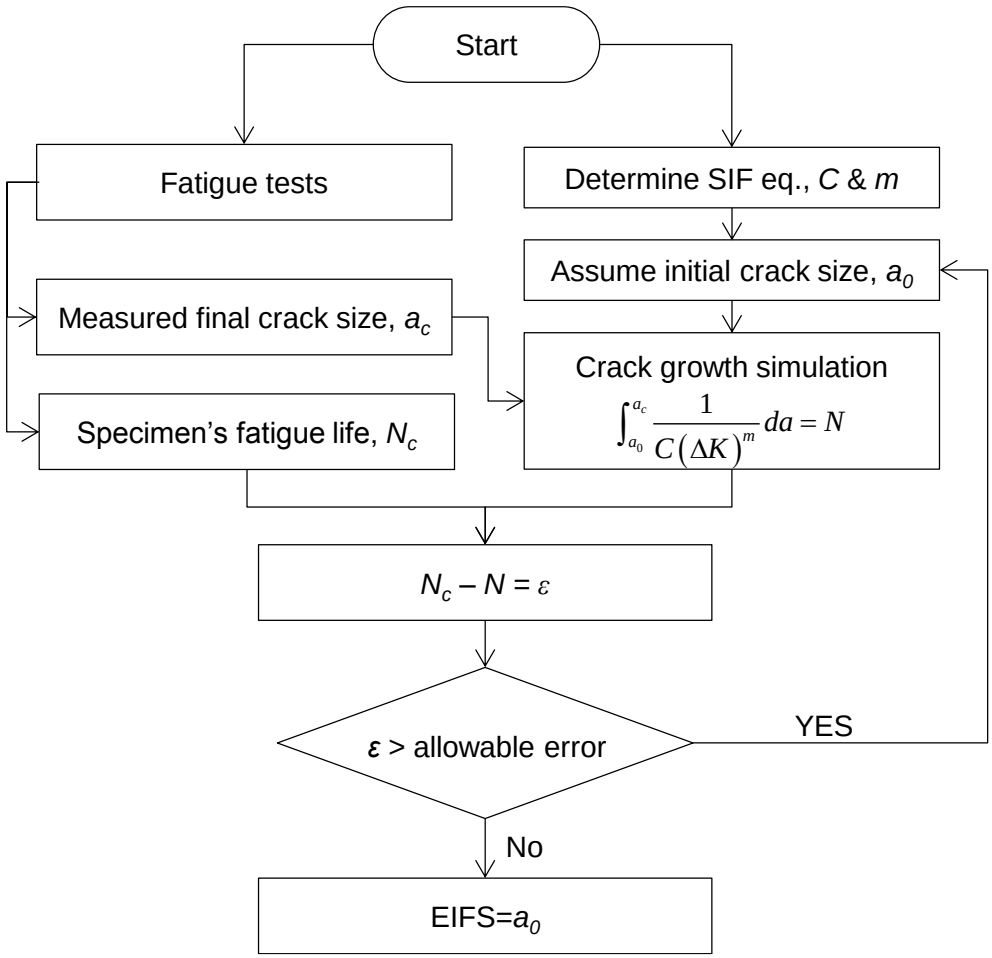

Figure 8. Algorithm of EIFS determination using back-extrapolation method

As shown in Figure 9, back-extrapolation is performed from measured crack size to initial crack size. In case of extrapolation of initial crack size from final crack size instead of measured crack sizes during fatigue test, it is more prone to error since there is only one reference point (Fawaz, 2003). Since EIFS is a virtual crack size estimated based on the experimental results rather than the actual initial crack size, crack growth simulation can be done with large crack growth model which is used to determine EIFS even if the initial crack size lies in the small crack region (Liu and Mahadevan, 2009).

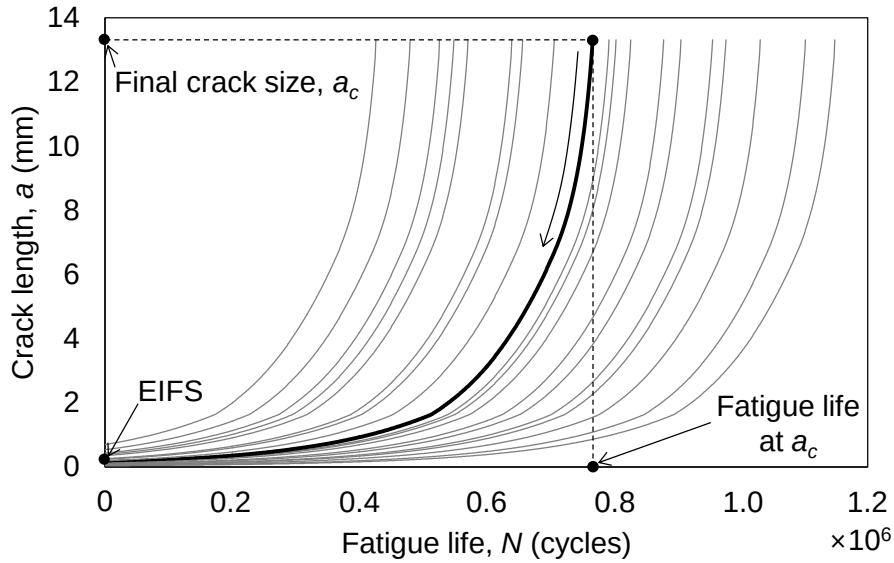

Figure 9. Schematic of approach to determine the EIFS

Despite this strong point, the reason why EIFS is not widely used is that experimental data should be sufficient to obtain a reliable EIFS value (Fawaz, 2000). By applying this procedure to several cracks, EIFS distribution can be obtained and can be used as a probabilistic model for fatigue reliability assessment of other similar structures (Johnson, 2010).

1.2.6 Crack coalescence

Typically in weldment, there are 100~200 crack initiation points per meter (Frise and Bell, 1992). Crack coalescence is a process which cracks are joining with adjacent crack during crack growth. Considering multiple fatigue cracks, fatigue life can be significantly reduced compared to the estimated fatigue life assuming a single crack (Ali et al., 2008; Bowness and Lee, 2002;

Tanaka et al., 1985).

In order to investigate the effect of crack coalescence, the change of SIF before and after coalescence was simulated. The fatigue detail used in this simulation is the tube-to-transverse plate welded connection that is mostly used in the highway sign, signal, and luminaire support structures. Applied parameters are specified in Table 3. In the process of crack coalescence, the cracks become gradually lengthen and also a/c becomes lower. As shown in Figure 10, the SIF in the depth direction increases as the crack become wide and shallow shape. Therefore, as multiple cracks existing in the weldment gradually coalesce, the SIF in the depth direction also gradually increases, thereby reducing the fatigue life.

Table 3. Simulation condition used for identifying effect of crack coalescence

Parameters	Values
Range of hot spot stress, $S_{r,hs}$	100 MPa
Degree of bending(*DOB*)	0.5
Thickness of tube, T	4.5 mm
Radius of tube, r	127 mm
Weld angle, θ	45 degrees
Weld footprint width, L/T	2.75
Crack aspect ratio, a/c	0.25

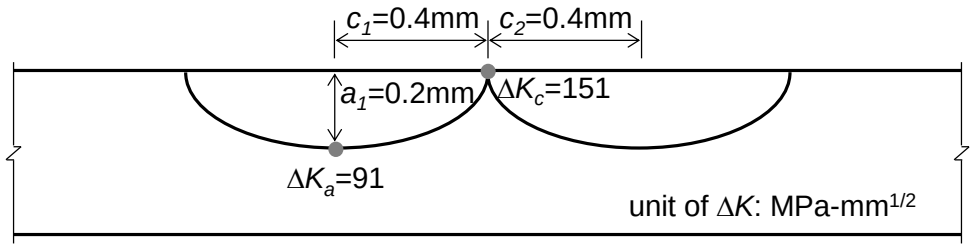

(a)

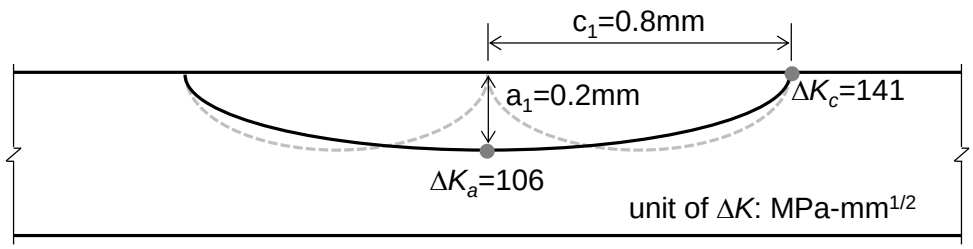

(b)

Figure 10. Change in SIF during crack coalescence: (a) before crack coalescence; and (b) after crack coalescence

In this simulation, the process of determining the depth and length of coalesced crack to simulate crack coalescence is called re-characterization. And the crack growth rate is accelerated in the inner crack tip of the adjacent crack, which is called the interaction. Many papers that have studied the crack coalescence have focused on re-characterization and interaction. Iida and Kawahara (1980) experimentally simulated the crack coalescence and found that the interaction between adjacent cracks is not apparent. Vialaton et al. (1976) found that interaction is negligible when the distance between two cracks is greater than the crack length. They also conclude that if distance between two cracks is smaller, the interaction occurs, but there is no general

interaction rule for simulation and exact calculation though structural analysis is required to consider the interaction. Twaddle and Hancock (1988) identified that little interaction occurs before coalescence, but a significant increase in SIF occurs in the region of inner crack tip of the adjacent crack after coalescence. This phenomenon causes the two cracks to turn into a single crack with a semi-elliptical shape rapidly.

1.2.7 Simulation of crack coalescence

Generally, when crack growth simulation is performed, the shape of fatigue crack is idealized as semi-elliptical surface crack and SIF equations are also adopted using existing equations proposed for a semi-elliptical surface crack. However, the crack shape gradually differs from semi-elliptical crack during crack coalescence. At this time, SIF may increase or decrease in region of inner crack tip of the adjacent crack due to interaction between two cracks (Kamaya, 2008b). Magnitude of interaction is influenced by factors such as relative crack size, distance, and crack shape, so it is difficult to simulate the change of SIF occurring in the crack coalescence with existing solutions (Kamaya, 2008a). For this reason, a re-characterization rule has been developed to determine the depth and length of a coalesced crack which has equivalent fatigue life in order to replace the complex simulation of crack coalescence (API, 2007; ASME, 1995).

In API (2007) and ASME (1995), the re-characterization rule was applied

when the distance between two cracks became closer than a specified value. The depth of the coalesced crack is defined as depth of deeper cracks between the two cracks, and depth of the coalesced crack is defined as sum of lengths of the two cracks. However, there are many researches that this method is relatively overestimation compared to the actual crack coalescence and growth (Frise and Bell, 1992; Iida and Kawahara, 1980; Leek and Howard, 1996; Soboyejo et al., 1990). Therefore, re-characterization rule solving this problem has been proposed through many studies (Frise and Bell, 1992; Grandt et al., 1986; Iida and Kawahara, 1980; Kamaya, 2008a; Leek and Howard, 1996; Soboyejo et al., 1990). Among the many proposed rules, re-characterization rule proposed by Kamaya (2008a) is adopted for this study since it is verified to be highly compatible with the experimental results by Pang et al. (2017).

Kamaya (2008a) found that if the area of the crack is the same, the average of SIF along the crack front is also same by considering various shapes of crack through FEA. Murakami and Nemat-Nasser (1983) also found that the area of the cracks correlated with maximum SIF at arbitrary-shaped surface cracks. This means that the area of crack can be a representative parameter for crack growth. In other words, the coalesced crack can be simulated by introducing a single crack having the same area with sum of two adjacent cracks, as shown in Figure 11 (Kamaya, 2008a).

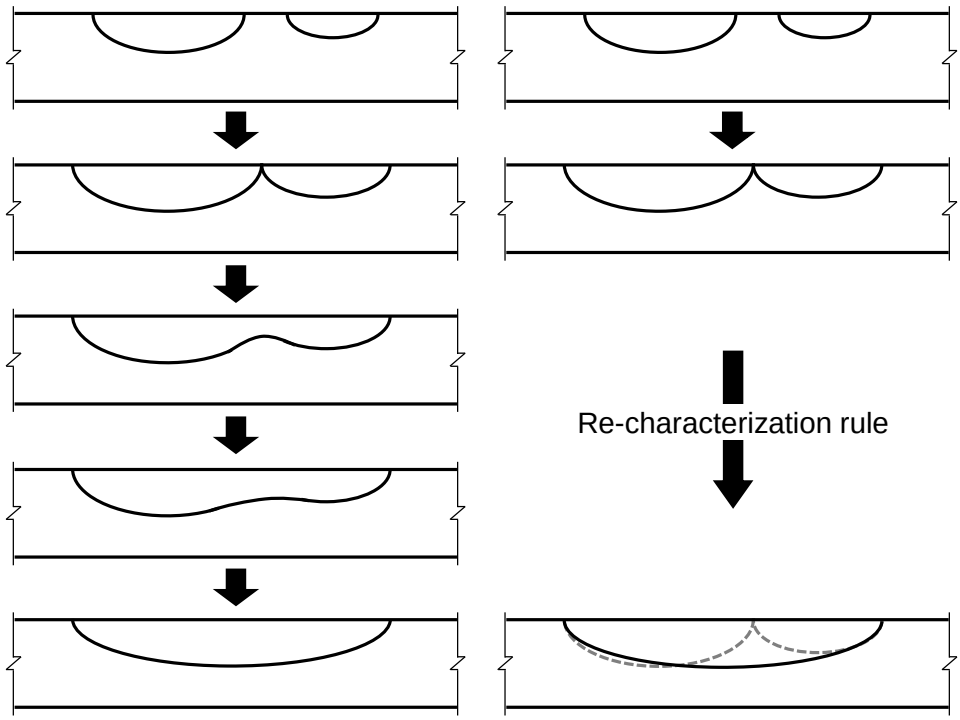

(a) (b)

Figure 11. Procedure for crack coalescence: (a) actual crack coalescence; and (b) simulation of crack coalescence using re-characterization rule

In order to apply crack coalescence to the fatigue assessment, position of multiple cracks and size of multiple cracks as well as the re-characterization rule are needed as initial conditions. The location and size of the cracks will be determined based on the experimental results and are utilized to develop probability model for fatigue reliability assessment. This will be provided in Chapter 2.

1.3 Objective and scope

In order to evaluate fatigue reliability considering multiple crack coalescence, both analysis methods for multiple crack growth and coalescence and a probability model of initial crack size and distance are needed. In Chapter 1, analysis methods for multiple crack growth and coalescence were determined by referring to existing analysis methods. In Chapter 2, the probability model of initial crack size and distance that constitute the initial conditions of multiple cracks was developed by analyzing the fracture surface of the specimens obtained from the actual fatigue test. From Chapter 3 to Chapter 5, the fatigue reliability assessment method considering multiple crack coalescence is applied to the welded details of bridge to verify applicability to other types of structures with welded connection.

CHAPTER 2

DISTRIBUTION CHARACTERISTICS OF INITIAL CRACKS

The size of the initial cracks and distance between initial cracks for estimating realistic fatigue reliability were determined from the actual fatigue tests performed in NCHRP Project 10-70 (Roy et al., 2011). The size and distance of the initial cracks were inversely estimated from the fatigue fracture surface and fatigue life, and a probability model was established based on estimated information of initial cracks. Since the general structural steel is utilized in test specimen and there is no significant difference on the welding materials and methods, the distribution characteristics of the initial cracks extracted in Chapter 2 can be sufficiently applied to welded connection of other kinds of structures such as bridge.

2.1 Sampling of fatigue fracture surface

Fatigue tests were performed on 78 specimens in the ATLSS Center for the purpose of developing the cost-effective fatigue resistant connections of signs, luminaire and traffic signal support structures as shown in Figure 12 (Roy et al., 2011). The test specimens are divided into six types of round steel tubes and six types of multi-sided steel tubes. In multi-sided tubes, high stress concentration occurs at the folded region. Therefore, arrangement of crack

initiation points are relatively regular and fracture is likely to be originated from a single crack initiation point at folded region. On the other hand, it is likely that several crack initiation points occur at round tube since there is no large difference of stress in the circumferential direction as shown in Figure 13. Round tubes were selected to identify the effect of multiple crack initiation point. Fatigue details are fillet-welded connection of mast arm-to-base plate, and pole-to-base plate as shown in Figure 12(a).

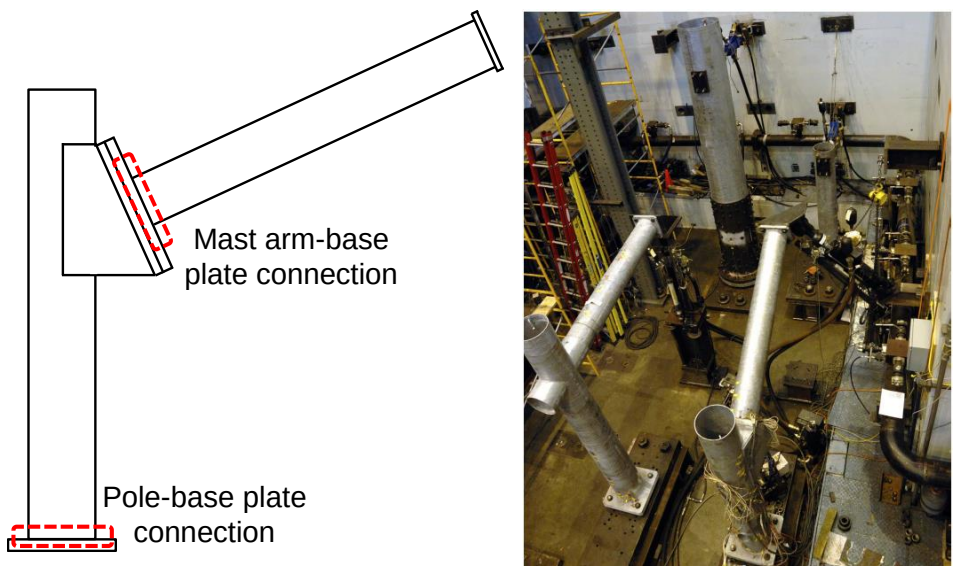

(a) (b)

Figure 12. Specimen of fatigue tests: (a) investigated fatigue details; and (b) test setups (Roy et al., 2011)

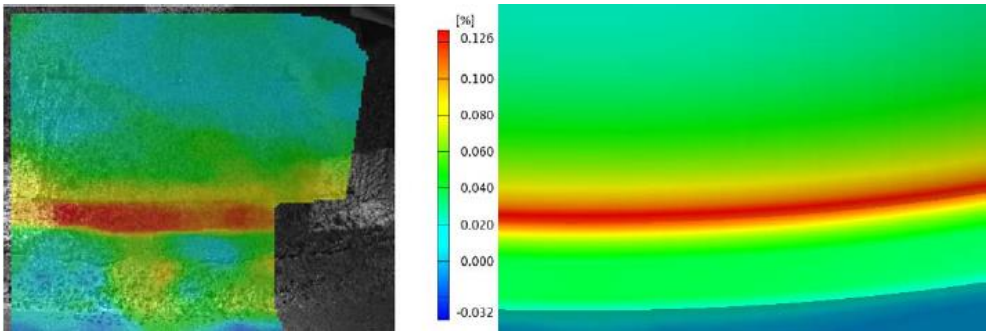

(a) (b)

Figure 13. Stress contour obtained on pole-base plate connection of specimen Type I: (a) obtained from measurement; and (b) obtained from FEA (Roy et al., 2011)

Experimental fatigue life and fracture surfaces obtained by the actual fatigue test were utilized to estimate the initial crack size and distance between cracks. As shown in Figure 14, specimens were selected except for the cases which the condition of fracture surface were poor or the specimens were fractured at other fatigue detail. As shown in Table 4, 12 specimens were selected from mast-arm connections and four specimens were selected from pole connections.

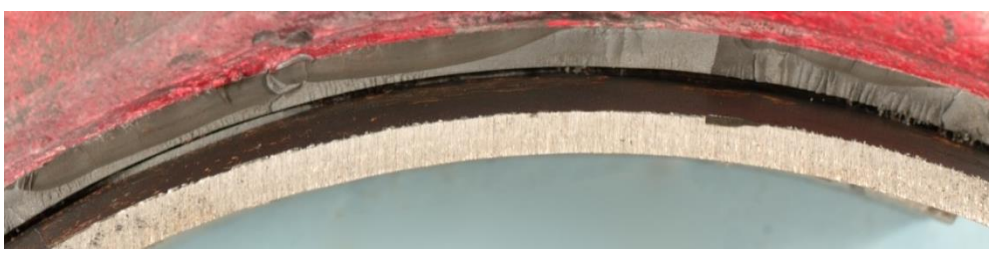

(a)

(b)

Figure 14. Fracture surfaces: (a) surface included for the investigation; and (b) surface excluded for the investigation

Table 4. Selected specimens

		Number of specimens	
Specimen ID	Types of connection	Mast-arm	Pole
I	Socket connection	7	2
II	Groove-weld connection	-	1
III	Groove-weld connection	5	-
V	Groove-weld connection	-	1

2.2 Characteristics of fatigue fracture surface

In order to estimate the crack information, beach mark and ratchet mark on the fracture surface is utilized as shown in Figure 15. Beach mark is generated by showing a curved line in the circumferential direction as an indication of the growth of individual cracks in the fracture surface. The Ratchet mark occurs in the vertical direction as an indication that cracks are coalesced during crack growth.

(a)

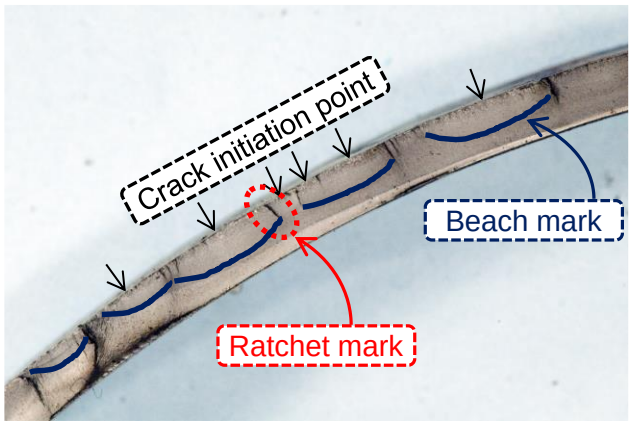

(b)

Figure 15. Fatigue fracture surface: (a) original picture; and (b) identified crack initiation point based on beach mark and ratchet mark

2.3 Probability model for distance between initial cracks

Fatigue fracture surfaces of 16 specimens were analyzed on the basis of ratchet mark and beach mark. As shown in Figure 16, 13 crack initiation points were identified in the Type-II-1-Pole test specimen, and 12 distance data were obtained as shown in Table 5. Crack distance data identified from

each specimen ranges from 6 to 23 and total 209 distance data were identified. Detailed results are described in Appendix A.

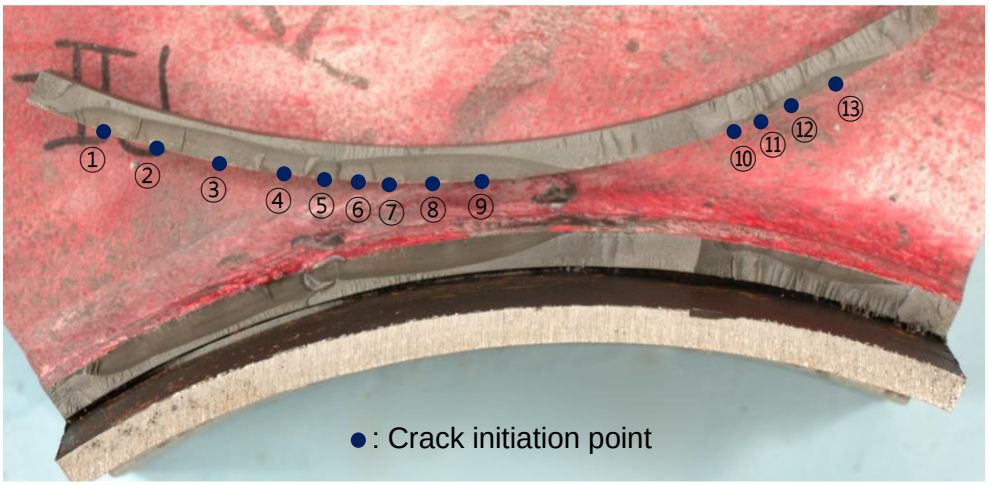

Figure 16. Crack initiation points in specimen Type II-1-Pole

Table 5. Distance between cracks in specimen Type II-1-Pole

Adjacent cracks	Distance between cracks (mm)
1, 2	9.8
2, 3	11.2
3, 4	11.7
4, 5	7.0
5, 6	5.5
6, 7	6.1
7, 8	6.6
8, 9	7.7
9, 10	47.1
10, 11	4.5
11, 12	6.4
12, 13	8.5

Distance data were analyzed by dividing into three groups: arm group, pole group, and total groups. Arm group contains distance data obtained from specimen of arm connection. Pole group contains distance data obtained from specimen of pole connection. Total group consists of data of two group. Histograms of three groups are shown in Figure 17, and the mean and standard deviation of the distance data for each group are shown in Table 6. Based on the average distance of the three groups, it can be seen that the average number of cracks per 1 m of weld length is 108 to 125, which is similar range of 100 to 200 specified by Frise and Bell (1992).

Probability model of crack distance is developed by using the data obtained from the total group as shown in Figure 18, since there is no significant difference between three groups. As shown in Table 7, the lognormal distribution showed the most suitability as a result of the Kolmogorov-Smirnov test which is one of goodness-of-fit test.

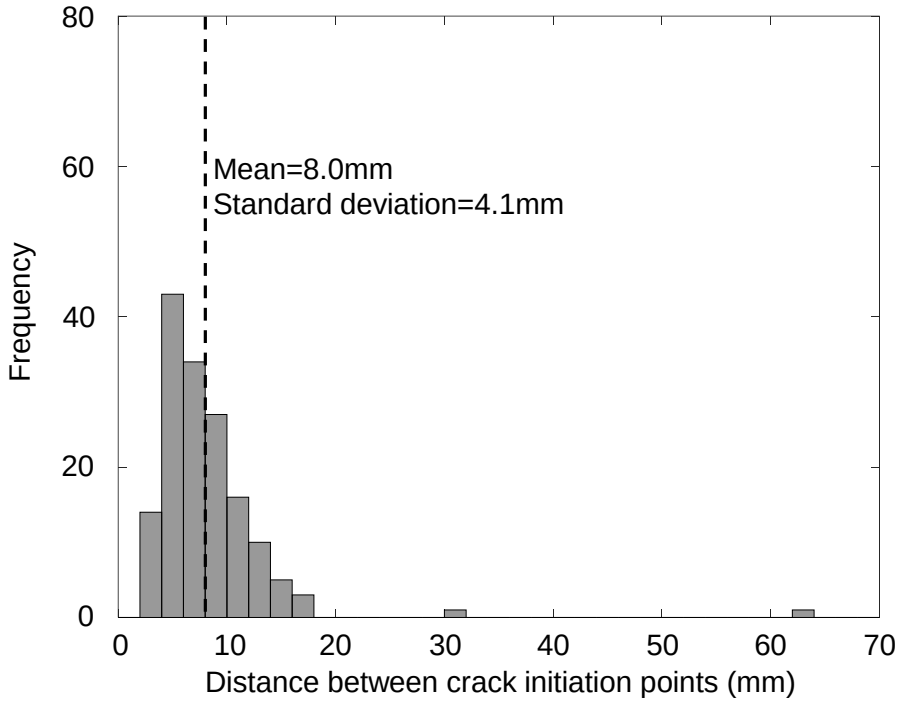
Mean=8.0mm
Standard deviation=4.1mm
Frequency
Distance between crack initiation points (mm)
0
20
40
60
80
0
10
20
30
40
50
60
70

(a)

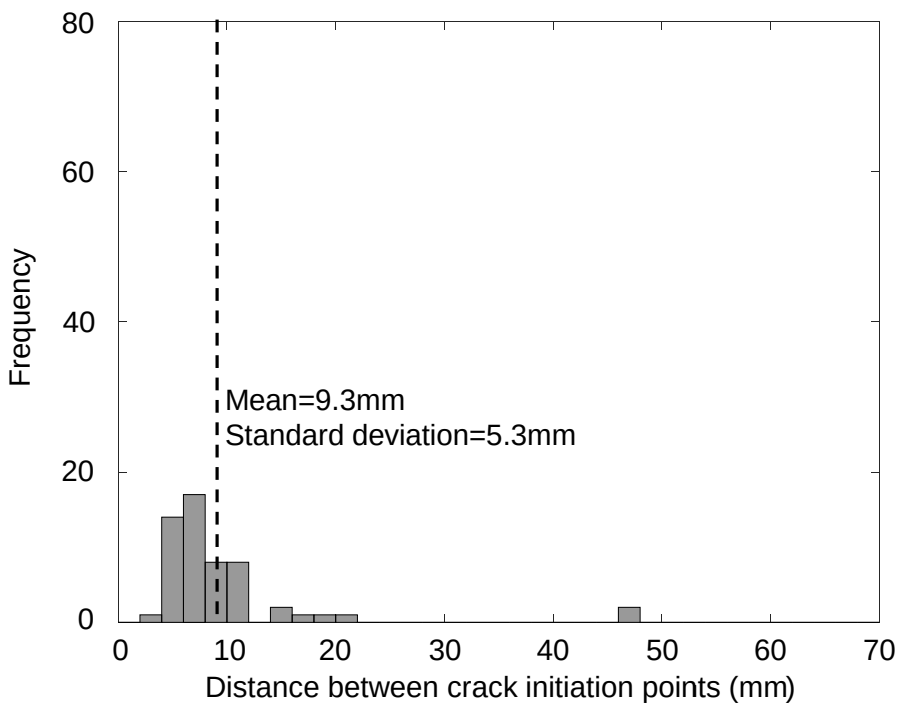
Mean=9.3mm
Standard deviation=5.3mm
Frequency
Distance between crack initiation points (mm)
0
20
40
60
80
0
10
20
30
40
50
60
70

(b)

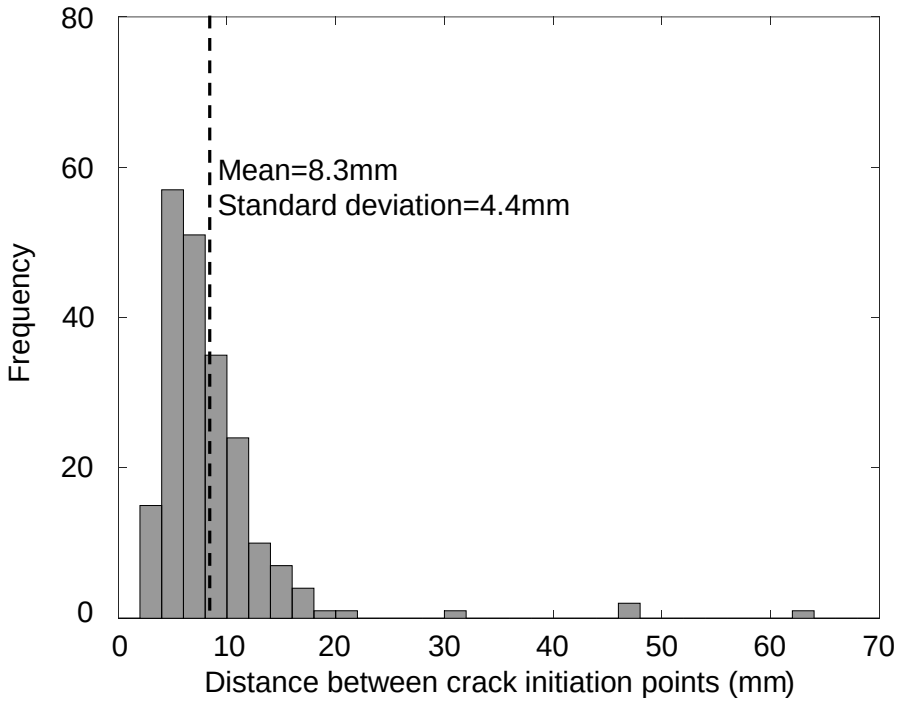

(c)

Figure 17. Histogram of distance between cracks: (a) arm group; (b) pole group; and (c) total group

Table 6. Statistical characteristics of distance data

Group	Mean(mm)	Standard deviation(mm)
Arm	8.0	4.1
Pole	9.3	5.3
Total	8.3	4.4

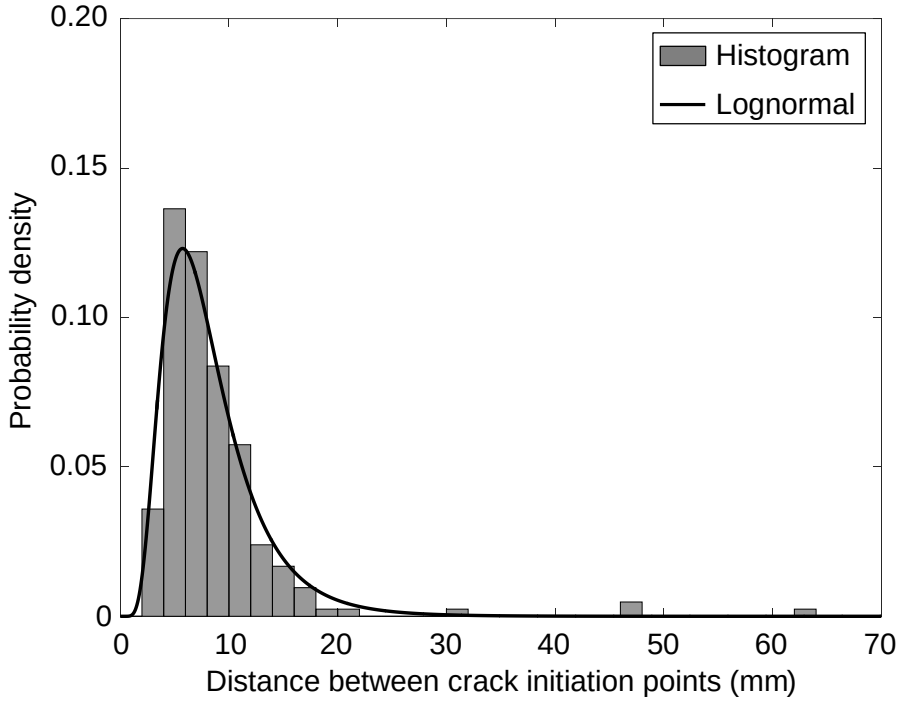

Figure 18. Developed probability model of crack distance

Table 7. Results of KS goodness-of-fit test

Types of distribution	KS statistics	Rank
Normal	0.18	4
Lognormal	0.07	1
Exponential	0.31	6
Weibull	0.16	3
Rayleigh	0.21	5
Gamma	0.11	2

2.4 Probability model for initial crack size

Initial crack size model suitable for the target structure was determined using the EIFS estimated by applying the back-extrapolation method to the actual

fatigue test results. In order to obtain EIFS, material parameters *C*, *m* and SIF equations appropriate for the target fatigue detail are necessary. Material parameters *C* and *m* are considered to be distribution model instead of specific values, since material parameter varies depending on the material and manufacturing process even the same material. SIF equation suitable for fatigue detail is determined in Section 2.4.1, and distribution model of material parameters *C* and *m* for fatigue reliability assessment is determined in Section 0. EIFS distribution was obtained for each crack initiation point of the specimen in Section 2.4.3. In Section 2.4.4, every EIFS distribution data is collected and the probability model of the EIFS to be used in the fatigue reliability assessment is suggested.

2.4.1 SIF equation for round tube to transverse plate fillet-welded connection

Since the results of the fatigue test on the round steel tube specimen performed in NCHRP Project 10-70 are utilized, the fatigue test results should be analyzed by applying appropriate SIF equation to the fatigue detail of specimen(Roy et al., 2011). The fatigue detail of the investigated structure is determined to be a round tube to transverse plate fillet-welded connection and a semi-elliptical surface crack is assumed as initial condition.

In case of plate to plate fillet-welded connections, various SIF equations have been proposed including the F_g taking into account the effects of welds

(Chew and Pang, 2016; Hobbacher, 1993; Lie et al., 2017; Newman and Raju, 1981; Norris and Fisher, 1981; Pang et al., 2016). However, since it is difficult to find a study on SIF equation for round tube to plate fillet-welded connection including the F_g, the proposed SIF equations for round tube is considered as an alternative. Raju and Newman (1986) proposed a SIF equation for circumferential semi-elliptical surface cracks in pipes and rods. They also examined the internal radius to wall thickness (R/T) from 1 to 10 and found that the SIF getting closer to the SIF of flat plate as the R/T increases, and the SIF increases as the R/T decreases due to the effect of curvature. However, SIF equation is proposed without considering stress concentration due to welding indicating F_g. Bergman (1995) also proposed SIF for circumferential surface cracks in pipes without considering F_g. Hoh et al. (2016) propose a SIF equation for circumferential surface crack of pipe in welding, but crack depth to thickness of plate (a/T) is limited from 0.05 to 0.5. Using this SIF equation, it is difficult to simulate a crack growth up to thickness in the depth direction. There is a considerable difference in connection type since it is a horizontal connection between pipes indicating girth-welded pipe rather than a perpendicular connection which is the same connection type with investigated fatigue detail. *British Standard 7910* (2015), which is one of the most referenced standard in LEFM-based fatigue assessment papers, suggests that SIF equations for surface cracks at weld toes can be referred to the paper by Bowness and Lee (2002). Bowness and Lee (2002) proposed equation of weld toe cracks in tubular joint using SIF

equation of T-butt joint. In the case of a tubular joint, equation is proposed only for the basic joint configuration. In order to obtain equation for all the other conditions, it requires a significant amount of analysis. To overcome this problem, they verified applicability to the tubular joint using equation of surface weld toe cracks in T-butt joint. Zhang et al. (2002) applied the equations of Bowness and Lee (2002) to the girth-welded pipe and identified that it shows higher applicability than other equations.

Based on Raju and Newman (1986), SIF is expected to be similar to those of the flat plate because R/T of target structure is approximately 55. Therefore, SIF equations of Bowness and Lee (2002), which is proved to be applicable to tubular joint and girth-welded pipe, is applied in this study.

The range of SIF (ΔK) can be determined using Eq. (23).

$$\Delta K = [Y_m M_{km}(1-DOB) + Y_b M_{kb} DOB] S_{r,hs} \sqrt{\pi a} \tag{23}$$

In that equation, Y_m and Y_b are flat plate SIF equations subjected to membrane stress and bending stress proposed by Newman and Raju (1981), respectively. M_{km} and M_{kb} are indicating stress gradient correction factor subjected to membrane stress and bending stress proposed by Bowness and Lee (2002), respectively. Degree of bending (*DOB*) is the ratio of bending stress to total applied stress. *DOB* was calculated by taking into account the hot spot stress due to membrane stress and bending stress at the point where the maximum stress was identified for each specimen. $S_{r,hs}$ is range of hot spot stress considering concentrated stress at the weld toe. Table 8 shows the condition of the fatigue test specimens. Details are introduced in Appendix A.

Table 8. Summary of fatigue test condition

Specimen type	$S_{r,hs}$ due to membrane (MPa)*	$S_{r,hs}$ due to bending (MPa)*	*DOB*	*L*/*T*	θ (degree)
Type I Arm	77.9	182.0	0.70	12.6	42(I-1)
					26(I-2)
					20(I-3)
					29.7(Others)
Type I Pole	31.0	98.6	0.76	9.4	33.6(I-5)
					35.0(I-7)
					29.7(Others)
Type II Pole	27.6	64.8	0.70	9.4	29.7
Type III Arm	77.9	107.6	0.58	12.6	29.7
Type V Pole	27.6	40.7	0.60	9.4	29.7

* Applied nominal stress is 82.7MPa in case of arm and 46.9MPa in case of pole

The validity limits of SIF equations are shown in Table 9. For crack depth ratios, it is impossible to estimate the initial cracks smaller than 0.5% of the thickness due to the validity limit of equation proposed by Bowness and Lee (2002). In case of weld angle, the measured angles were applied to the evaluation of five specimens as shown in Table 8, and 30 degrees which is lower validity limit was applied to the remaining specimens without weld angle measurement. Weld footprint width of 12.6 in arm and 9.4 in pole exceeds the validity limit. However, when *L*/*T* exceeds 1.17, the effect of weld footprint width is converged to specific value and the same fatigue life is obtained according to Bowness and Lee (2002). Therefore, the validity limit of 2.75 was applied. $S_{r,hs}$ and *DOB* are obtained based on the maximum stress

point of the test specimen. However, as the crack grows and becomes wide crack, stress can be overestimated since both ends of the crack are moved away from the maximum stress point. Plate details are not a big problem, but in the case of tube detail, it can be influential problem since the magnitude of the stress varies in the circumferential direction. However, since it is not practical to evaluate $S_{r,hs}$ and *DOB* at all points in the circumferential direction during crack growth, the evaluation is based on maximum stress point.

Table 9. Validity limit of adopted SIF equations

Parameters	Newman and Raju (1981)	Bowness and Lee (2002)
Crack aspect ratio, a/c	$0<a/c\leq1.0$	$0.1\leq a/c\leq1.0$
Crack depth ratio, a/T	$0\leq a/T<1.0$	$0.005\leq a/T<1.0$
Crack length ratio, c/b	$c/b<0.5$	-
Weld angle, θ	-	$30°\leq\theta\leq60°$
Weld footprint width, L/T	-	$0.5\leq L/T\leq2.75$

* *b*: half width of plate

When type of crack changes from surface crack to through-thickness crack, SIF equations for through-thickness flaws in plate proposed by BSI (2015) is utilized using Eq. (24).

$$\begin{aligned}\Delta K &= Y(a)S_r\sqrt{\pi a} \\ &= \sqrt{\sec\left(\frac{\pi a}{2b}\right)}S_r\sqrt{\pi a}\end{aligned} \tag{24}$$

2.4.2 Distribution of material parameter in Paris' law

The material parameters *C* and *m* of the crack growth model significantly vary depending on the material and stress ratio (*R*) (BSI, 2015; King, 1998). Probability model of material parameters or material constants are proposed for various materials, however, it is important to apply *C* and *m* suitable for the material and stress ratio of the target structure (Barsom, 1971; BSI, 2015; DNV, 1984; Hirt and Fisher, 1973; King, 1998; Snijder et al., 1987).

Barsom (1971) conducted fatigue tests on four type of ferrite-pearlite steel, which are mainly used as structural steels. Crack growth rate according to SIF were derived as shown in Figure 19. The stress ratio was considered from 0 to 0.7, however the tendency to the stress ratio was not observed. Conservatively, the lower bound of *C* is proposed.

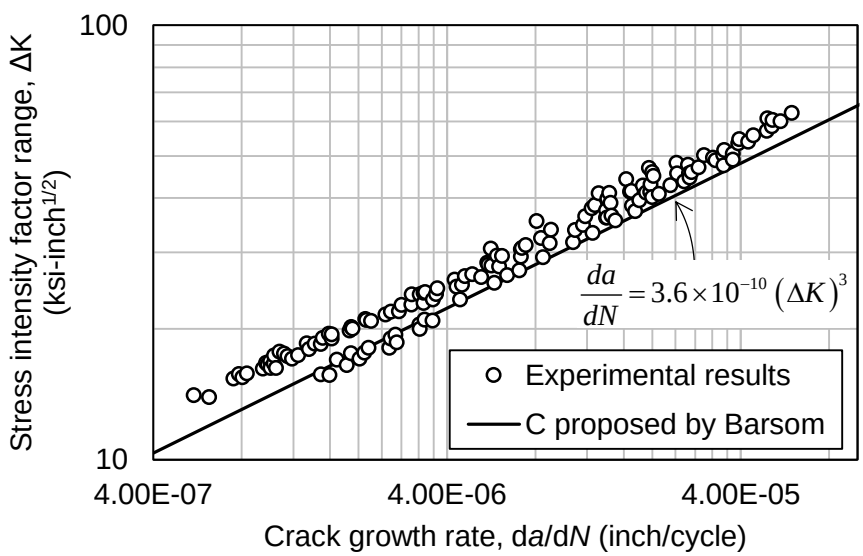

Figure 19. Fatigue crack growth data for ferrite-pearlite steels

For reliability assessment, statistical characteristics were extracted based on the experimental data of Barsom as shown in Figure 20. As shown in Table 10, mean value of *C* was -29.48, the standard deviation was 0.20, and m was 2.98, however *m* is determined to be 3.0, which is widely used as *m* value of steel.

Table 10. Statistical characteristics of material parameters

Material parameter	Lower 95% (Mean – 2σ)	Mean	Upper 95% (Mean + 2σ)
lnC	-29.88	-29.48	-29.08
C	1.06×10^{-13}	1.58×10^{-13}	2.35×10^{-13}
m	3.0	3.0	3.0

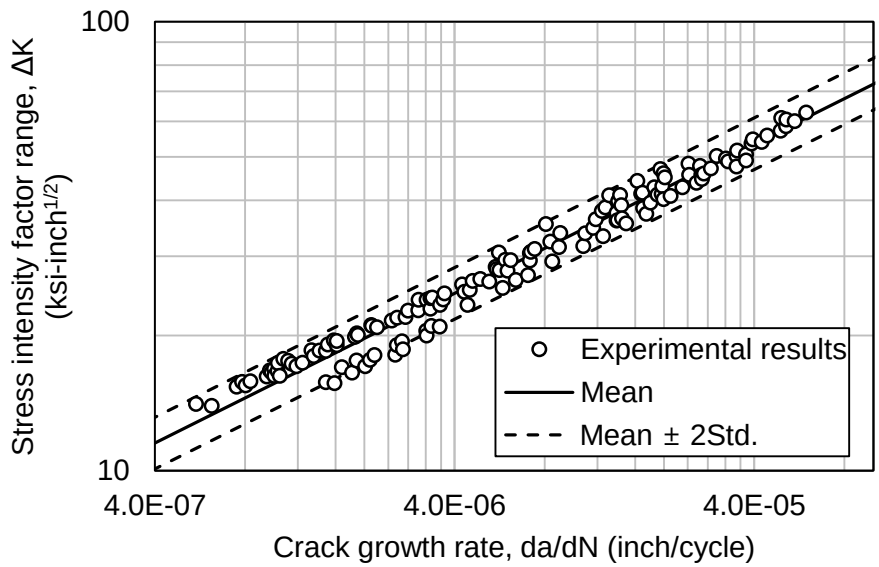

Figure 20. Statistical characteristics based on experimental data of Barsom

2.4.3 Distribution of EIFS

Since the initial crack size is not a variable that can be obtained directly from

the fracture surface, it should be estimated based on the experimental results. Therefore, the back-extrapolation method is applied to the experimental results to estimate the EIFS, which is regarded as the initial crack size. There are various sizes of cracks that bring same experimental results since the size of the crack consists of two variables, the depth and the length of the crack. Therefore, *a*/*c* of the initial crack was fixed to a specific value in order to determine it as one crack size. Initial *a*/*c* refer to the existing models for the initial aspect ratio as shown in Table 11. Existing models were proposed as mean values of 0.2 ~ 0.67. Mean value of proposed model from Yamada and Nagatsu (1989), which is close to the median of proposed initial *a*/*c* values, was applied.

Table 11. Existing model of initial crack shape (*a*/*c*)

Reference	Types of distribution	Mean (mm)	Standard deviation (mm)
JCSS (2011)	Lognormal distribution	0.62	0.25
Yamada and Nagatsu (1989)	Lognormal distribution	0.39	0.16
Engesvik and Moan (1983)	Formula	0.3 ~ 0.4	-
El Haddad et al. (1980)	Deterministic	0.2	-
Beier et al. (2015)	Deterministic	0.3	-
Yazdani and Albrecht (1990)	Deterministic	0.25 (Cover plate) 0.50 (Stiffener) 0.67 (Rolled beam)	-

Using Algorithm for EIFS determination described in Section 1.2.5, EIFS was estimated for every crack initiation points in 16 specimens. In this calculation, allowable error for determining EIFS is one percent. EIFS was estimated by different approach depending on the type of crack at the time of fracture. As shown in Figure 21 (a), when specimen is fractured at state of coalesced through-thickness crack and size of coalesced crack is only identified, same EIFS is assumed at every crack initiation point, since it is impossible to distinguish each size of crack. As shown in Figure 21 (b), when specimen is fractured at state of coalesced surface crack and each depth of crack can be identified, different EIFS are estimated at every crack initiation point based on depth of crack at the time of fracture.

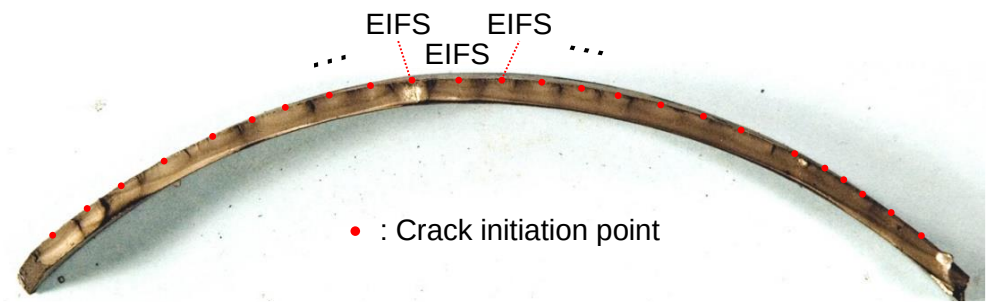

(a)

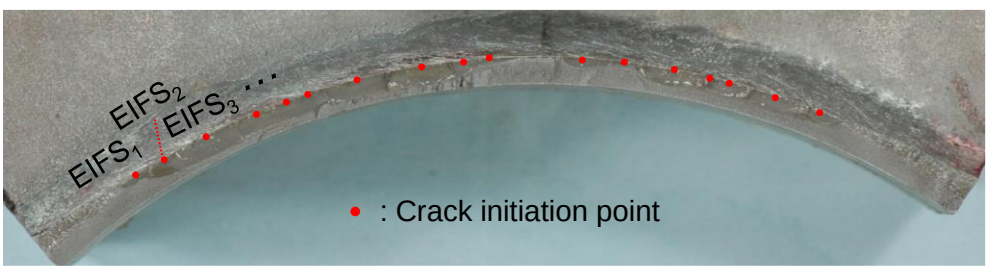

(b)

Figure 21. Type of fracture surface (a) fractured specimen at state of coalesced through-thickness crack; and (b) fractured specimen at state of coalesced surface crack

Since the material parameter C has a distribution, samples of C are generated based on experimental data of Barsom (1971) and then EIFS distribution corresponding to the samples of C is obtained. In order to identify the convergence of the results obtained from the generated samples, the mean and standard deviation of the EIFS obtained from the Type I-1 arm specimen were obtained as shown in Figure 22. The mean and standard deviation of the EIFS are found to be less than 1% of the difference from considering 3000 samples. Therefore, the other samples were analyzed using 3000 samples.

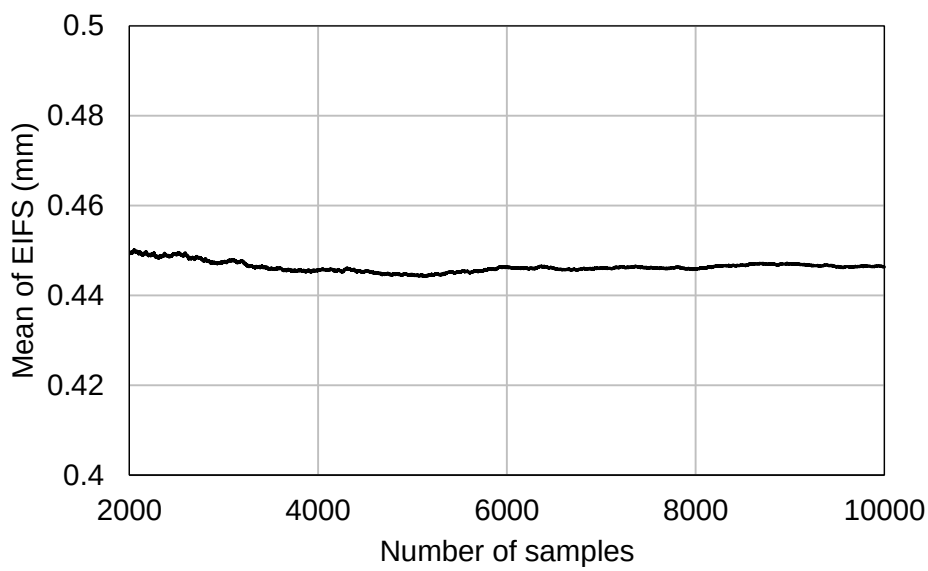

(a)

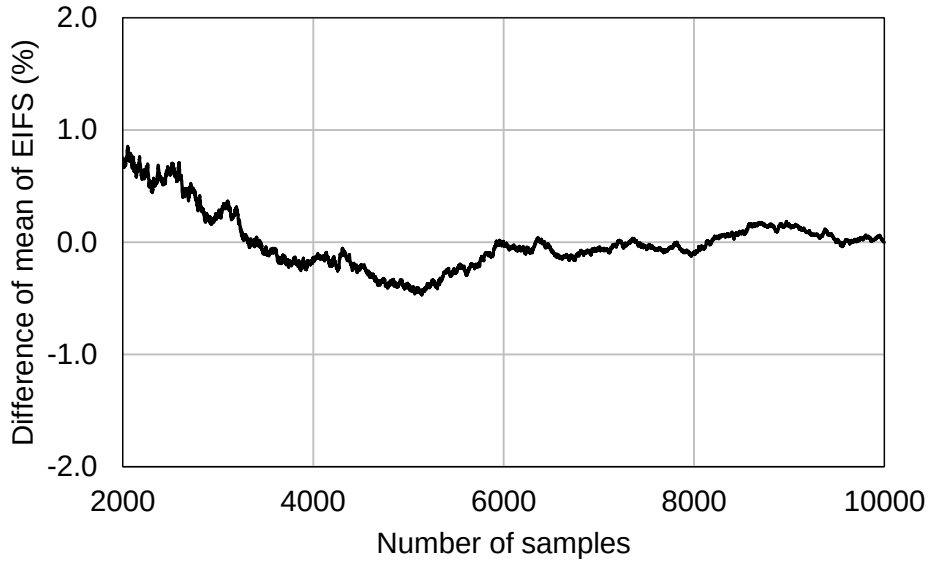
2.0
1.0
0.0
-1.0
-2.0
Difference of mean of EIFS (%)
2000
4000
6000
8000
10000
Number of samples

(b)

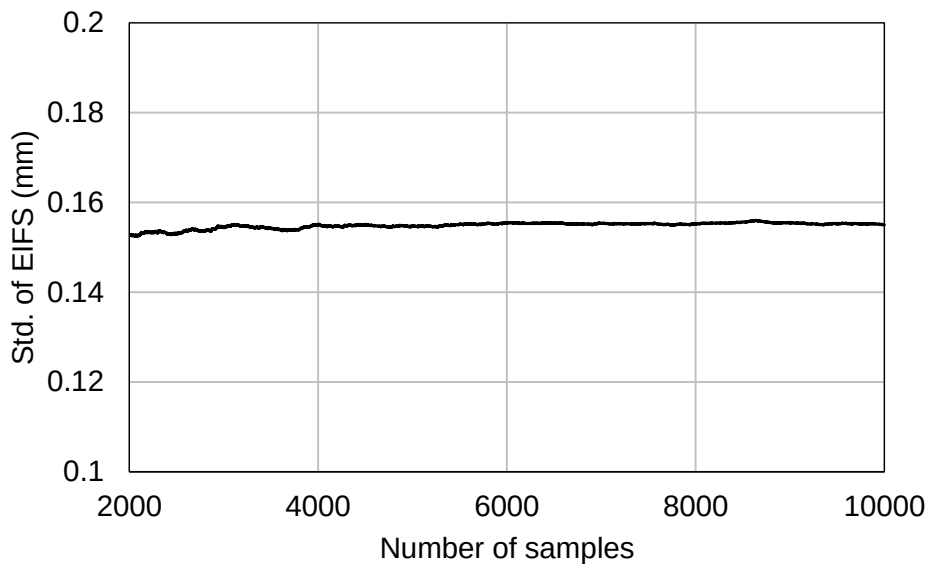
0.2
0.18
0.16
0.14
0.12
0.1
Std. of EIFS (mm)
2000
4000
6000
8000
10000
Number of samples

(c)

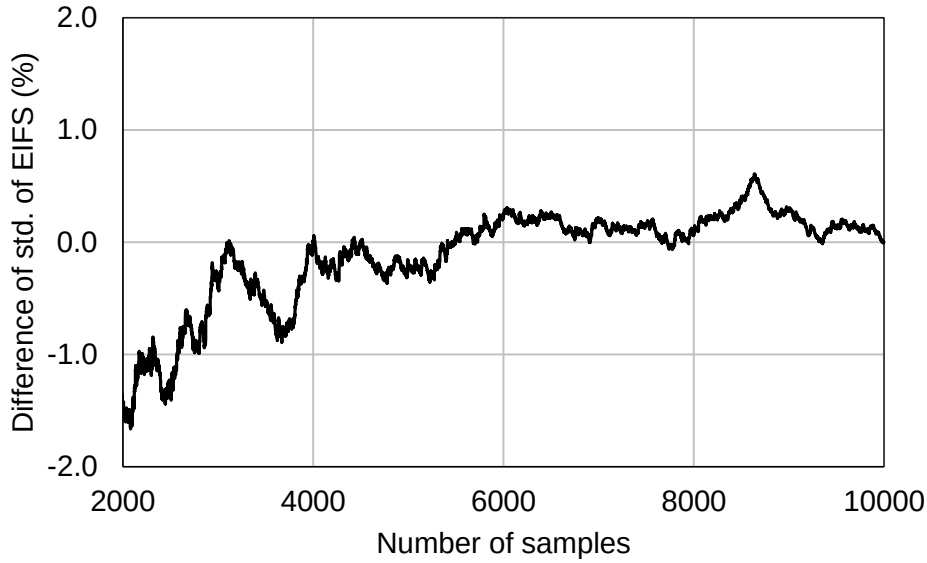

(d)

Figure 22. Convergence tests in specimen of Type I-1 Arm: (a) Mean of EIFS according to number of samples; (b) difference of mean of EIFS according to number of samples; (c) std. of EIFS according to number of samples; and (d) difference of std. of EIFS according to number of samples

Total 46 EIFS distributions were estimated from 16 specimens. As shown in Figure 23, the EIFS distribution has various distribution characteristics depending on specimen and location of crack initiation point. Figure 23(a) shows the whole histogram indicating relatively large size of EIFS. On the other hand, as shown in Figure 23(b) and (c), it failed to obtain whole histogram due to considerable amount of invalid EIFS. This is due to the validity limit of crack depth in the SIF equation of Bowness and Lee (2002) used for EIFS estimation. The lower bound of validity limit is 0.5% of plate thickness, and this value is 0.023mm for arm and 0.031mm for pole. EIFS estimated to be less than the validity limit has a ratio of 0 to 100% depending

on the location of the crack initiation point. Detail results about 46 EIFS distributions are described in Appendix B. The probability model of initial crack size was developed using valid EIFS.

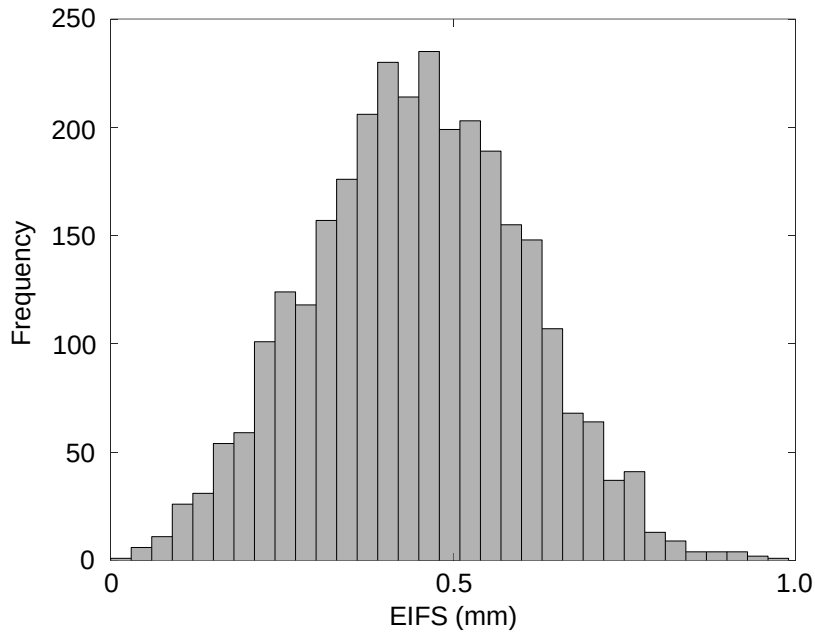

(a)

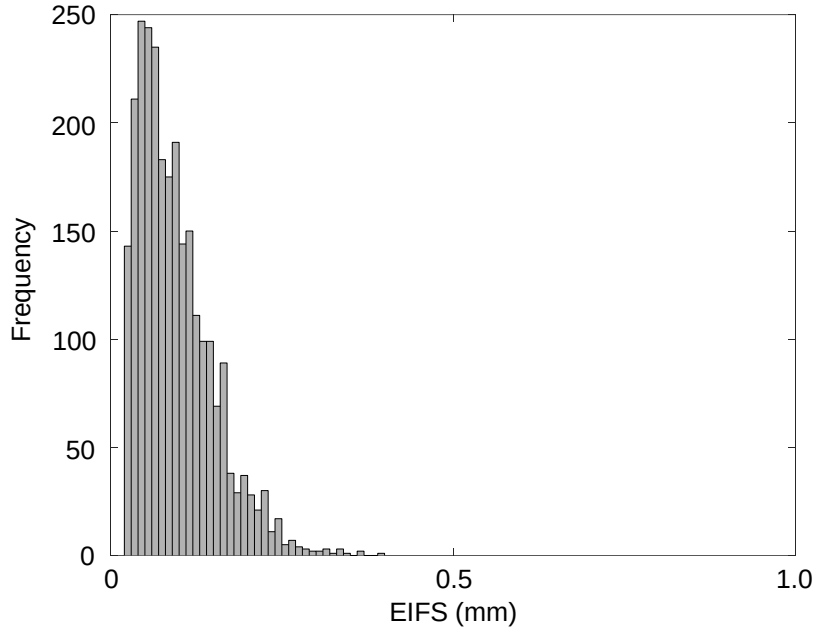

(b)

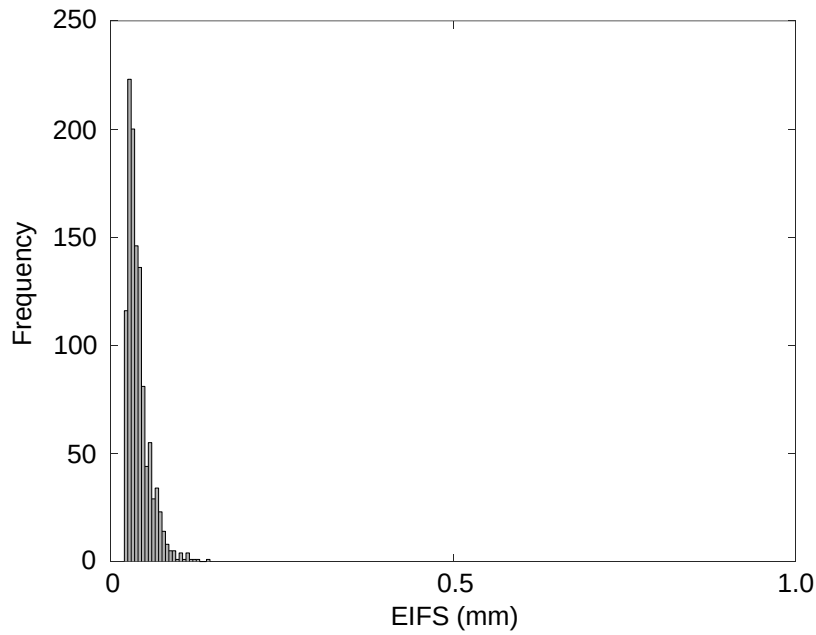

(c)

Figure 23. Histogram of EIFS (a) Type I-1 arm specimen; (b) 1st crack of Type I-2 arm specimen; and (c) 10th crack of Type I-2 arm specimen

2.4.4 Determination of probability model of EIFS

EIFS distributions including 138,000 EIFS are obtained from 46 crack initiation points in 16 specimens. Distance data were analyzed by dividing into three groups as development of probability models of crack distance: arm group, pole group, and total groups. Arm group represents the 36 EIFS distributions from 12 arm specimens, and pole group represents the 10 EIFS distributions from 4 pole specimens. Histograms of EIFS of each group are shown in Figure 24. It can be seen that most of the EIFS is gathered at less than 1mm in histogram of arm group as shown in Figure 24(a). On the other hand, it can be seen that EIFS is relatively scattered and many peaks are found in histogram of pole group as shown in Figure 24(b). It means that pole group can be difficult to represent the distribution property due to insufficient specimens. Therefore, probability model of initial crack size is developed by using the data obtained from the total group as shown in Figure 24(c).

As shown in Table 12, the lognormal distribution showed the most suitability as a result of the Kolmogorov-Smirnov test which is one of goodness-of-fit test. Figure 25 shows lognormal distribution with a mean of 0.58mm and a standard deviation of 0.91mm indicating probability model of initial crack size.

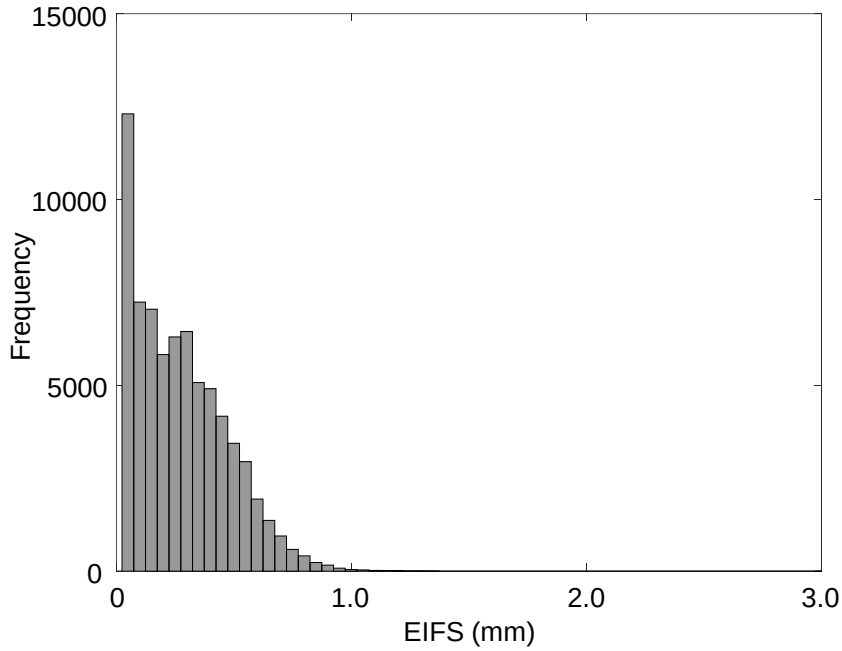
15000
10000
5000
0
Frequency
0
1.0
2.0
3.0
EIFS (mm)

(a)

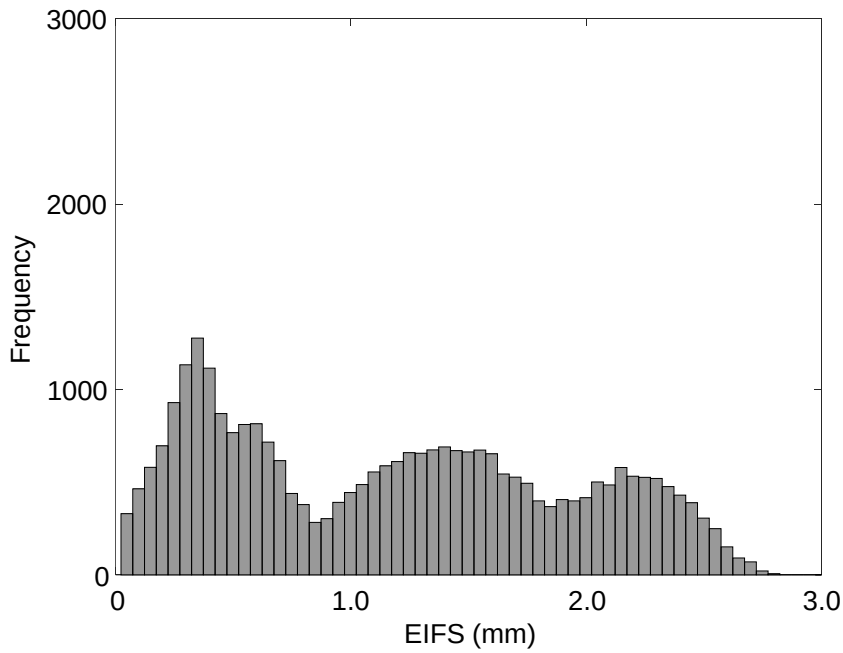
3000
2000
1000
0
Frequency
0
1.0
2.0
3.0
EIFS (mm)

(b)

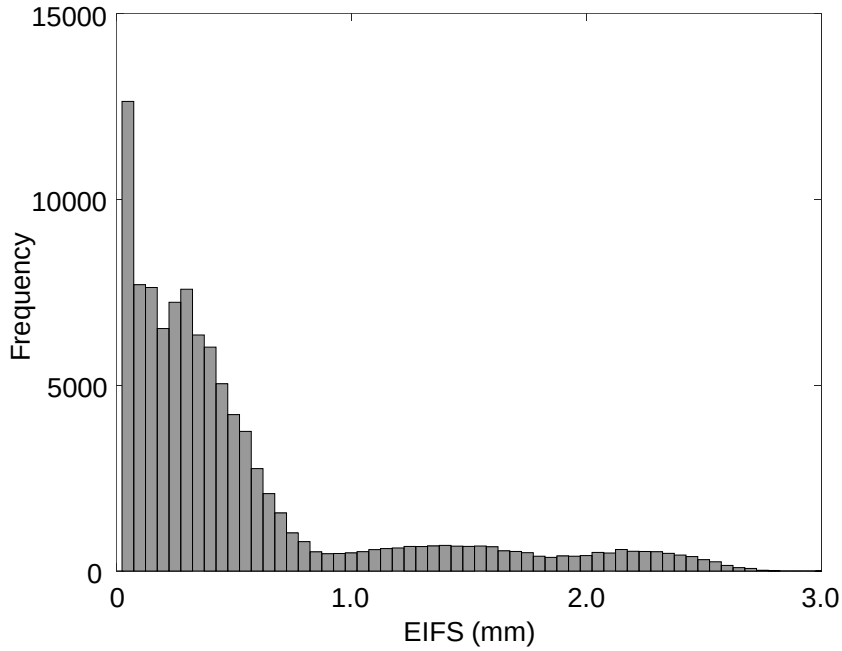

(c)

Figure 24. Histogram of EIFS: (a) arm group; (b) pole group; and (c) total group

Table 12. Results of KS goodness-of-fit test

Types of distribution	KS statistics	Rank
Normal	0.22	5
Lognormal	0.05	1
Exponential	0.08	3
Weibull	0.08	2
Rayleigh	0.37	6
Gamma	0.09	4

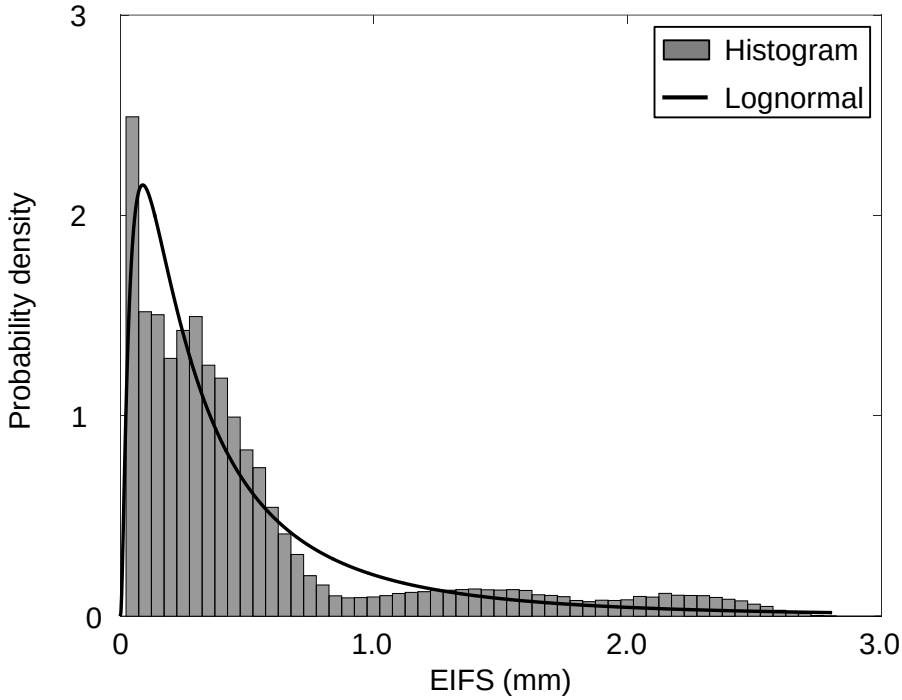

Figure 25. Developed probability model of initial crack size

2.5 Correlation between initial crack size and distance between initial cracks

Correlation should be identified to utilize the initial crack size and distance between initial cracks, which are random variables obtained from fracture surface of the same specimens, for probabilistic assessment. Mean value of the distance located on the left and right of the crack was used as a representative value, nevertheless, distance between initial cracks is originally derived from the two cracks. Since both the size and distance of initial crack are distributed as Lognormal, the size and distance of initial crack for each crack initiation points are drawn in the log scale as shown in Figure

26. The correlation coefficient between the two variables is 0.17, which means that the correlation is considerably small. Therefore, statistically independence is assumed in the probabilistic assessment.

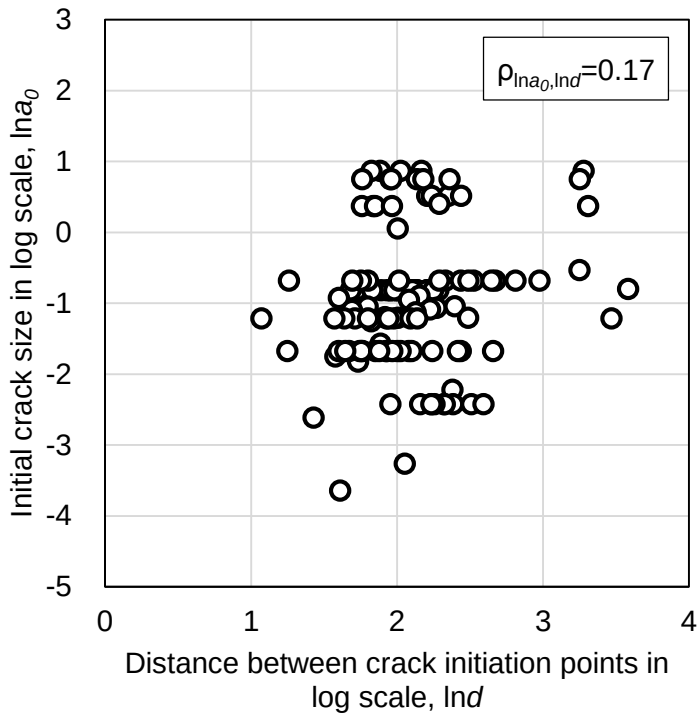

Figure 26. Correlation between initial crack size and distance between initial cracks in log scale

CHAPTER 3

VERIFICATION FOR APPLICABILITY OF DEVELOPED PROBABILITY MODEL OF INITIAL CRACK TO COVER PLATE DETAIL

Probability model of crack distance and initial crack size developed for the assessment of fatigue reliability considering multiple cracks are based on the experimental results of welded connection in support structures. Since multiple crack condition is not determined depending on the type of structure, but is common conditions in welded connection, developed models are applied to welded connection in other structure, which is determined to bridge in this study. NCHRP Reports are referred to utilize specimens of welded connection in bridge and results of actual fatigue test (Fisher et al., 1974; Fisher et al., 1980; Fisher et al., 1970; Keating and Fisher, 1986). Results of the fatigue tests presented in the NCHRP Reports were statistically analyzed to suggest the fatigue strength in the form of the SN curve of the log scale. Results of the fatigue tests on the log scale show characteristics of normal distribution. The lower 2.5 percentile of the normal distribution is suggested as the design fatigue strength in AASHTO(2012). The validity of the developed assessment model was identified by comparing distribution of the fatigue life obtained from the fatigue test and that of the fatigue life obtained by the developed assessment model. In addition, distribution of fatigue life obtained by applying single crack model is also considered to identify the validity of multiple crack model for simulating actual fatigue test results.

Through the assessment of the three welded details, the basis for application of welded details of various steel structures are identified. Welded details were selected from long to short weldment to reflect the characteristics of the crack distance model for simulating multiple crack condition.

3.1 Assessment method

3.1.1 Basic parameters for crack growth simulation

In order to simulate crack growth, it is required that initial crack size including length and depth of crack, material parameters in Paris' law, fracture crack size. The size of the initial crack can be determined by the depth and the aspect ratio of crack which is ratio of depth to half-length of crack. Depth of initial crack was determined using the lognormal distribution with mean of 0.58 mm and a standard deviation of 0.91mm described in Section 2.4.4.

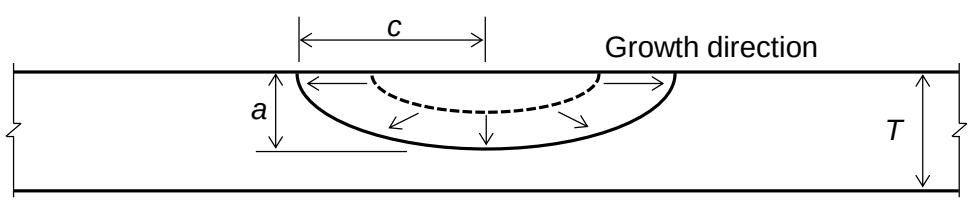

Figure 27. Growth direction of semi-elliptical surface crack

Semi-elliptical surface crack grows radially as shown in Figure 27. Crack growth occurs only in critical section and direction of crack growth remains constant since direction of principal stress is assumed to be perpendicular to

crack front during crack propagation. The shape of the crack can be defined by calculating the propagation in the length and depth of the crack. Shape of the crack can be determined in two methods. The first method is a method of analyzing the depth direction of crack and the length direction of crack, respectively, and the growth of depth and length is determined based on geometry of crack and detail and loading conditions. The second method is to determine the shape of the cracks according to the relation between *a* and *c* based on the information of experimental aspect ratio obtained by the experiment, and then only crack growth analysis in the depth direction is performed. as Fisher (1984) did. Since the information of crack shape obtained from fatigue tests is utilized, multiple crack coalescence is considered in the formulation of relation between *a* and *c*. Tendency of shape development of crack is mainly affected by types of detail. Therefore, if there is insufficient information about the tendency of shape development, it cannot be practical approach (Fisher, 1984; Fisher et al., 1980; Yazdani and Albrecht, 1990). Fisher (1984) performed crack shape measurements on cover plate and stiffener detail and proposed an empirical relationship between *a* and *c*. Aspect ratio in cover plate details ranges from 0.1 to 0.3 as shown in Eq. (25). Different formula is suggested according to depth of crack in web attachment details of Category E, as shown in Eq. (26) (Fisher et al., 1980).

$$c = 5.457a^{1.133} \text{ (in.)} \tag{25}$$

$$\begin{aligned} c &= 3.55 + 1.29a \quad \text{if } a \le 4\text{mm} \\ c &= 1.506a^{1.241} \quad \text{if } a > 4\text{mm} \end{aligned} \tag{26}$$

Yazdani and Albrecht (1990) suggest 0.25 of a/c in the cover plate, 0.5 of a/c in the stiffener, and 0.67 of a/c as a representative value, despite scattering in result of crack shape measurement. It is presumed that crack shape is close to the circular shape because it is difficult to coalesce the cracks when the weldment is absent or the length of weldment is short and the stress concentration is small. On the contrary, when the length of weldment is long and the stress concentration is large, it is presumed that a/c has a low value. In order to avoid the disadvantage of requiring shape development information of various details, first method which consider depth and length direction is adopted to simulate the crack growth. Mean value of probability model of a/c suggested by Yamada and Nagatsu (1989) is applied as initial value of a/c.

Probability model of Barsom (1971), which was considered in the development of the probability model of initial crack size in Section 0, was applied for the material parameters C and m of Paris' law. The variables used in the evaluation for applicability of developed model are summarized in Table 13.

Table 13. Variables for fatigue reliability assessment

Variables	Descriptions	Types of distribution	Mean	C.O.V.
a_0	Initial crack depth (mm)	Lognormal	0.578	1.58
$(a/c)_0$	Initial ratio of depth to half-length of crack	Deterministic	0.39	-
ln$C$	Material parameter	Normal	-29.48	0.01
m	Material parameter	Deterministic	3.0	-
d	Distance between crack initiation points (mm)	Lognormal	8.33	0.53

The criterion for determining the failure of the specimen was referred to the criterion defined in the NCHRP Report (Fisher et al., 1974; Fisher et al., 1980; Fisher et al., 1970). Deflection criterion is used to define failure of specimen and fatigue tests were stopped at increase in mid-span deflection of 0.5mm. When this criterion is met, most of the plate section is lost due to the crack, which causes the yield of section. In case of cover plate, cracked area is from 50 percent to 75 percent of flange area. The transverse stiffener and web attachment also satisfied the failure criteria at a similar point in time. As a result of the fatigue test, the deflection criterion was satisfied at the through-thickness crack. In order to predict fatigue life considering stage of through-thickness crack, crack growth analysis based on fracture mechanics should be consider other factors loading and strength condition will be change since when crack area propagates to most of plate section. Therefore, in this study, interpretation of stage of surface crack is only done using LEFM to ensure the validity of crack growth analysis. Since 96 percent of fatigue life is

consumed at stage of surface crack in transverse stiffener detail and about 60 to 85 percent of fatigue life is consumed at stage of surface crack in web attachment detail, prediction of fatigue life can be underestimated in comparison to experimental fatigue life.

Increment of crack growth in length and depth of crack, as shown in Figure 27, is calculated for each integration interval. The integration interval should be sufficiently narrow for the convergence of fatigue life which is result of crack growth analysis. As shown in Table 14, the error of fatigue life at each integration interval was calculated based on the example described in Section 3.1.6. Since the error is sufficiently converged at 100 cycles of integration interval, every simulation of crack growth were performed in this integration interval.

Table 14. Convergence of fatigue life according to integration interval

Integration interval (cycles)	Fatigue life	Error from one cycle of integration interval (%)
1	243,404	-
10	243,440	0.01
100	243,700	0.12
1000	246,000	1.07

3.1.2 SIF equation for fatigue cracks in weldment

Cracks in weldment occur mainly at the boundary between weldment and base metal, and are categorized as semi-elliptical surface cracks because they usually have semi-elliptical shapes. Various SIF equations for semi-elliptical

surface cracks in opening mode are presented in papers (Barsom and Rolfe, 1999; Fisher, 1984; Irwin, 1962; Newman and Raju, 1981; Paris and Sih, 1965). SIF equations developed by experiment and analysis have differences in results depending on the geometry of crack, detail and loading conditions. Therefore, it is important to utilize SIF equation that is appropriate for the fatigue detail being evaluated. SIF equations proposed by Newman and Raju (1981), Barsom and Rolfe (1999) and Fisher (1984) are compared.

The SIF equation of Newman and Raju (1981) consists of Eq. (27) to (33). As a result of evaluating the equations for surface cracks based on fracture data, Newman and Raju's equation has the advantage that the standard deviation of the SIF values is the smallest and the stability of the equation is high (Newman, 1979). Newman and Raju (1981) proposed SIF correction factors for surface cracks on the base metal, therefore, stress gradient correction factor (F_g) is not suggested in paper. In other words, correction factors corresponding to a front surface correction factor (F_s), a back surface correction factor (F_w), and a shape correction factor (F_e), which are commonly applied to a semi-elliptical surface crack, is proposed. However, in the SIF equation, three kinds of correction factors including F_s, F_w and F_e are complexly integrated. Since F_g is a factor that varies depending on the degree of stress concentration, it is determined according to investigated fatigue detail.

$$\Delta K = Y(a)S_r\sqrt{\pi a}$$
$$= \left[M_1 + M_2\left(\frac{a}{T}\right)^2 + M_3\left(\frac{a}{T}\right)^4 \right] f_\phi g f_w S_r \sqrt{\frac{\pi a}{Q}} \tag{27}$$

$$M_1 = 1.13 - 0.09\left(\frac{a}{c}\right) \tag{28}$$

$$M_2 = -0.54 + \frac{0.89}{0.2 + (a/c)} \tag{29}$$

$$M_3 = 0.5 - \frac{1.0}{0.65 + (a/c)} + 14\left(1.0 - \frac{a}{c}\right)^{24} \tag{30}$$

$$g = 1 + \left[0.1 + 0.35\left(\frac{a}{T}\right)^2 \right](1 - \sin\phi)^2 \tag{31}$$

$$f_\phi = \left[\left(\frac{a}{c}\right)^2 \cos^2\phi + \sin^2\phi \right]^{1/4} \tag{32}$$

$$f_w = \sqrt{\sec\left(\frac{\pi c}{2b}\sqrt{\frac{a}{T}}\right)} \tag{33}$$

The SIF equation of Barsom and Rolfe (1999) consists of Eq. (34) to (37). F_s, F_w and F_e, which are commonly applied to semi-elliptical surface cracks, are suggested respectively. Since the material parameters of Barsom (1971) are used in Section 0, there is an advantage that the condition of whole assessment has unity.

$$\Delta K = Y(a)S_r\sqrt{\pi a} = F_s F_w F_e F_g S_r \sqrt{\pi a} \tag{34}$$

$$F_s = 1.12 \tag{35}$$

$$F_w = 1.0 \quad for\ a/T < 0.5 \qquad = 1.0 + 1.2\left(\frac{a}{T} - 0.5\right) \quad for\ a/T \geq 0.5 \tag{36}$$

$$F_e = \frac{1}{\int_0^{\pi/2}\left[1 - \frac{c^2 - a^2}{c^2}\sin^2\theta\right]^{1/2} d\theta} \tag{37}$$

The SIF equation of Fisher (1984) consists of Eq. (38) to (41). F_s, F_w and F_e, are suggested respectively as Barsom and Rolfe (1999). Equation of Fisher (1984) was used in crack growth analysis to investigate fatigue tests performed in several NCHRP projects.

$$\Delta K = Y(a)S_r\sqrt{\pi a} = F_s F_w F_e F_g S_r \sqrt{\pi a} \tag{38}$$

$$F_s = 1.211 - 0.186\sqrt{\frac{a}{c}} \tag{39}$$

$$F_w = \sqrt{\sec\frac{\pi a}{2T}} \tag{40}$$

$$F_e = \frac{1}{\int_0^{\pi/2}\left[1 - \frac{c^2 - a^2}{c^2}\sin^2\theta\right]^{1/2} d\theta} \tag{41}$$

Figure 28 shows comparison with SIF values obtained from three SIF

equations by applying the 0.39 of a/c which is mean value of probability model proposed by Yamada and Nagatsu (1989). Equation of Fisher (1984) shows that value of SIF diverges when the depth of crack grows to thickness of plate because F_w used by Fisher is only valid in a range where a/T is less than 0.7. In order to assess the bridge fatigue detail, it is necessary to simulate from surface crack to through-thickness crack, therefore, value of SIF should be valid up to 1.0 of a/T. Equations of Newman and Raju (1981) and Barsom and Rolfe (1999) give valid values even if the depth of crack grow to the thickness of plate. The SIF equation of Barsom and Rolfe (1999) is simple and has clearly distinguishable correction factors, so it is easy to apply each correction factor depending on the type of detail to be evaluated. Considering these points, the SIF equation proposed by Barsom and Rolfe (1999) is applied to the three fatigue detail cases to be discussed in the next section.

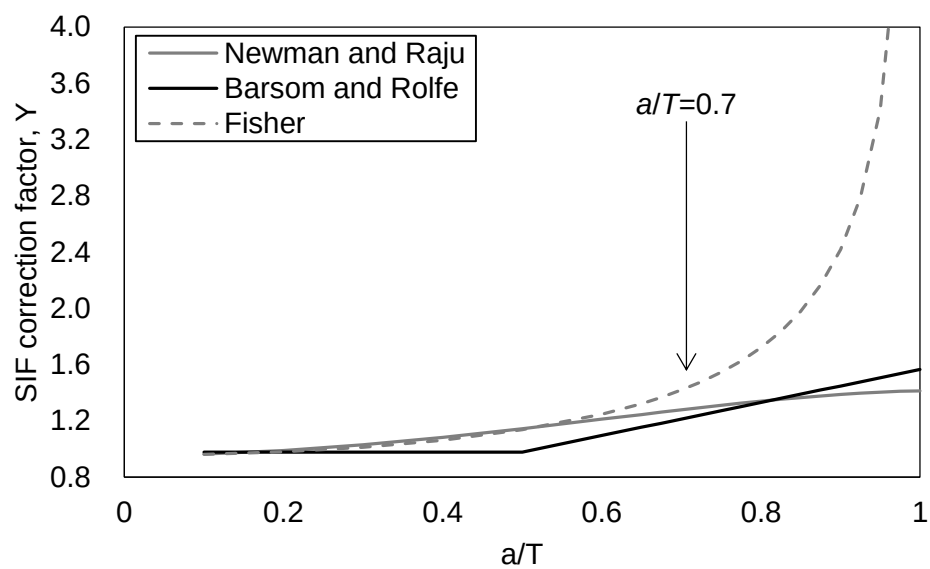

Figure 28. Change of SIF values according to type of equation

3.1.3 Simulation of multiple crack growth and coalescence

Arrangement of multiple initial crack is simulated using the probability models of initial crack size and distance between cracks developed in Section 2.3 and 2.4. Firstly, one crack initiation point is arranged in the center of weldment, and then, other initial cracks are arranged from side to side based on developed probability models about initial crack. Arrangement is performed within length of weldment.

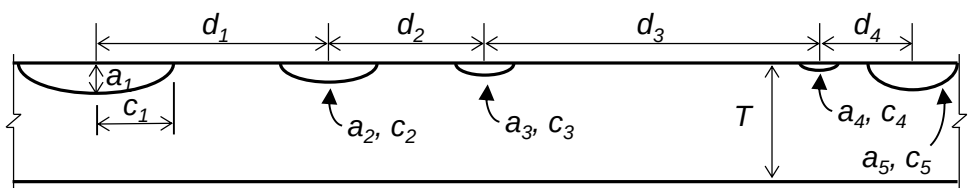

Figure 29. Arrangement of multiple initial cracks simulating actual multiple crack condition

3.1.4 Simulation of single crack growth

Conventional single crack condition was simulated for comparison with fatigue reliability assessment assuming multiple crack condition. Probability model of initial crack size is adopted to Lognormal distribution with mean value of 0.125mm proposed by Engesvik and Moan (1983), as specified in Section 1.2.2.

3.1.5 Determination of investigated fatigue detail

Among the welded details used in the bridges, fatigue details to be evaluated are determined having diversity in terms of detail category and length of weldment. The selected details are composed of the cover plate of Category E and the transverse stiffener of Category C, web attachment of Category E or E' as shown in Table 15. In case of cover plate and transverse stiffener detail, it is selected to identify the effectiveness and suitability of developed model considering multiple crack condition because the length of weldment in the expected direction of crack is long enough to satisfy the condition of multiple cracks. In the case of the web attachment detail, the length of weldment in the expected direction of the crack is relatively short, which is close to the condition of the single crack. Therefore, it is selected to identify that developed model considering multiple crack condition has sufficient applicability in details with a single crack condition.

Table 15. Selected fatigue detail according to fatigue Category and length of weldment

Types of details	Fatigue Category	Length of weldment (mm)	References
Cover plate-to-flange fillet weld	E	114	NCHRP Report 102
Transverse stiffener-to-flange fillet-weld	C	83	NCHRP Report 147
Longitudinal attachment-to-web weld	E (T<25mm)	19	NCHRP Report 227
	E′ ($T \geq 25$mm)	51	

3.1.6 Sensitivity of random variables

The sensitivity of the random variables to the distribution characteristics of fatigue life was identified by the importance vector. An importance vector for the mean and standard deviation of fatigue life is defined as Eq. (44) and (45), respectively.

$$\delta = \left[\frac{\Delta\mu_N}{\Delta\mu_{a_0}}\sigma_{a_0}, \frac{\Delta\mu_N}{\Delta\mu_d}\sigma_d, \frac{\Delta\mu_N}{\Delta\mu_{\ln C}}\sigma_{\ln C} \right] \tag{42}$$

$$\eta = \left[\frac{\Delta\sigma_N}{\Delta\sigma_{a_0}}\sigma_{a_0}, \frac{\Delta\sigma_N}{\Delta\sigma_d}\sigma_d, \frac{\Delta\sigma_N}{\Delta\sigma_{\ln C}}\sigma_{\ln C} \right] \tag{43}$$

The importance vector δ represents the sensitivity of the mean of random variable to mean of fatigue life. The importance vector η is the sensitivity of the standard deviation of random variable to standard deviation of the fatigue life. Each value in importance vector is multiplied by standard deviation for normalization. The mean and standard deviation of each variable were adjusted by 20 percent of the standard deviation since each random variables has difference standard deviation. As shown in Table 1 in Section 1.2.2, the difference between the existing probability models of initial crack size is considerably large, so the adjustment amount was set to 20 percent.

3.1.7 Assessment cases

Total four assessment cases are considered to identify the validity of suggested assessment method. Table 16 describes characteristics of each assessment case. Case I is suggested method for assessment. Case II and III utilize existing model for size of initial crack as described in Section 3.1.4. Case IV is defined to identify size of equivalent single crack giving same result as Case I in terms of fatigue life.

Table 16. Description of analysis cases

Case	Number of crack	Size of initial crack
I	Multiple cracks	Using developed model in this study
II	Single crack	Existing model of Engesvik and Moan (1983)
III	Multiple cracks	Existing model of Engesvik and Moan (1983)
IV	Single crack	Equivalent single crack giving the same result as Case I

3.2 Applicability to cover plate detail

Information of fatigue tests on cover plate detail is referred to NCHRP Report 102 (Fisher et al., 1970). The results of fatigue test were used to suggest the design fatigue strength corresponding to Category E of AASHTO LRFD through statistical analysis (AASHTO, 2012). As shown in Figure 30, a crack propagation simulation was performed for cracks occurring at the boundary between the cover plate end weld and the top flange of the test specimen.

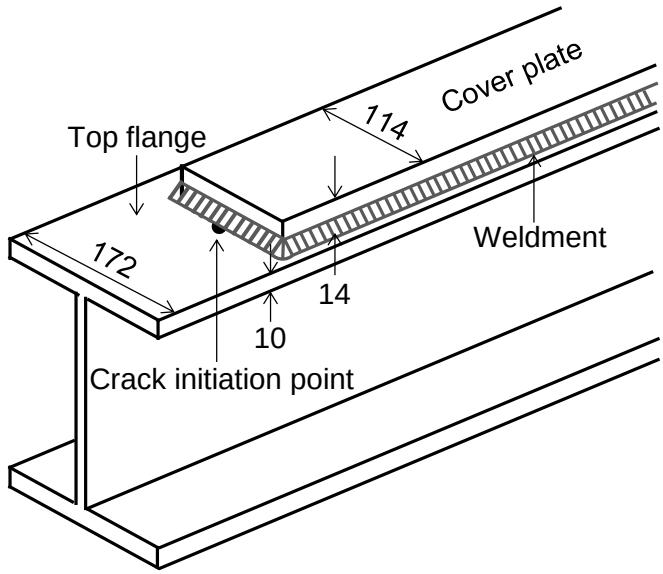

Figure 30. Cover plate detail (Fisher et al., 1970) (unit: mm)

3.2.1 SIF equation for cover plate detail

SIF Equation proposed by Barsom and Rolfe (1999) is adopted to calculate F_s, F_w, and F_e. Correction factor F_w is influenced by how much the cross section is affected by bending (Zettlemoyer and Fisher, 1978). Correction factor F_w is not applied to cover plate detail because the web in the thickness direction is resistant to the bending of the cover plate detail.

Stress gradient correction factor (F_g) considering the stress distribution in the depth direction was developed by Zettlemoyer and Fisher (1977). Stress gradient correction factor could be calculated by:

$$F_{g,a} = \frac{SCF}{1 + \frac{1}{0.1473}\left(\frac{a}{T}\right)^{0.4348}} \tag{44}$$

$$SCF = -3.539\log\left(\frac{Z}{T}\right) + 1.981\log\left(\frac{T_{cp}}{T}\right) + 5.798 \tag{45}$$

In that equation, SCF is the stress concentration factor, T is the flange thickness, T_{cp} is the thickness of the cover plate, and Z is the weld height. Equation of Zettlemoyer gives only the stress gradient correction factor in the depth direction, so F_g equation which is proposed for transverse stiffener by Bowness and Lee (2002) is referred for analysis in length direction. It is assumed that the ratio of the F_g in depth direction to the F_g in length direction is the same as that of the transverse stiffener as shown in Figure 31. Estimated $F_{g,c}$ indicating F_g in length direction is utilized for fatigue assessment.

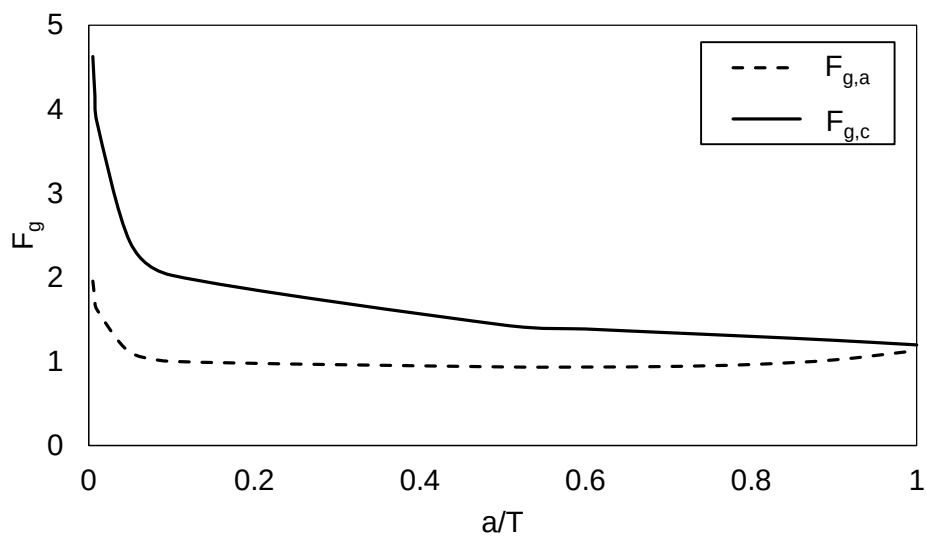

Figure 31. Value of F_g in depth and length direction proposed by Bowness and Lee (2002)

3.2.2 Characteristics of multiple crack propagation and coalescence

Before obtaining the fatigue life distribution through simulations based on the developed model, crack growth characteristics of multiple crack conditions is identified by performing multiple crack growth analysis using the mean value of each parameter. The mean values given in Table 13 are applied to multiple crack growth analysis. Based on the mean value of the distance between cracks, 13 cracks were placed with same distance at boundary between weldment and top flange. Since all the cracks are placed by same distance and initial size, they have same crack growth rate and grow together by coalescing into one crack at a time. The characteristics of multiple crack condition are investigated through crack growth analysis.

Crack shape development is identified in terms of a/c as shown in Figure 32, while the semi-elliptical surface crack grows including the coalescing process of the initial cracks. Until coalescing of cracks, 13 cracks grow individually, and a/c does not change much. However, when 13 cracks are coalesced at the same time, a/c falls to 0.03. After crack coalescence, a shallow and long single crack grows rapidly to the thickness of flange in the depth direction, increasing the a/c to 0.18. The reason for this characteristics of crack growth is shown in Figure 33, which shows the crack growth rate. Figure 33(a) shows the crack growth rate in the depth direction. It can be seen that the growth rate increases steadily as the crack grows, and the growth rate increases by 52% after crack coalescence. As shown in Figure 33(b), which

shows crack growth rate in the length direction, the growth rate increases steadily as the crack grows, and the growth rate is also decreased by 96% after crack coalescence. This characteristic is found by the change of crack shape during crack growth as shown in Figure 34. Crack grows in the depth direction at a high speed without growth in the length direction while growing up to the thickness of the flange. It can be seen that fatigue life is significantly affected by accelerated crack growth rate due to crack coalescence as well as a lot of cracks.

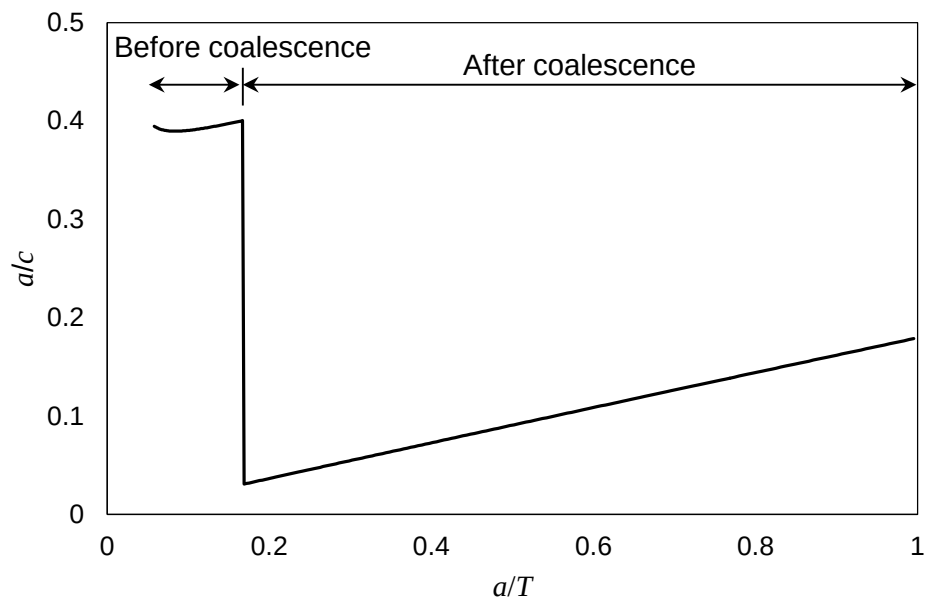

Figure 32. Crack shape development as a crack growth

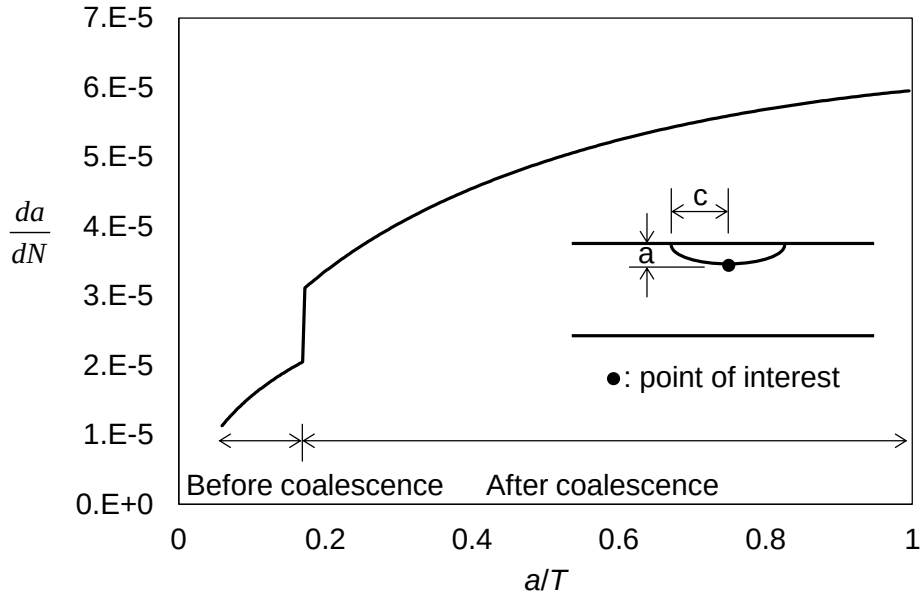

(a)

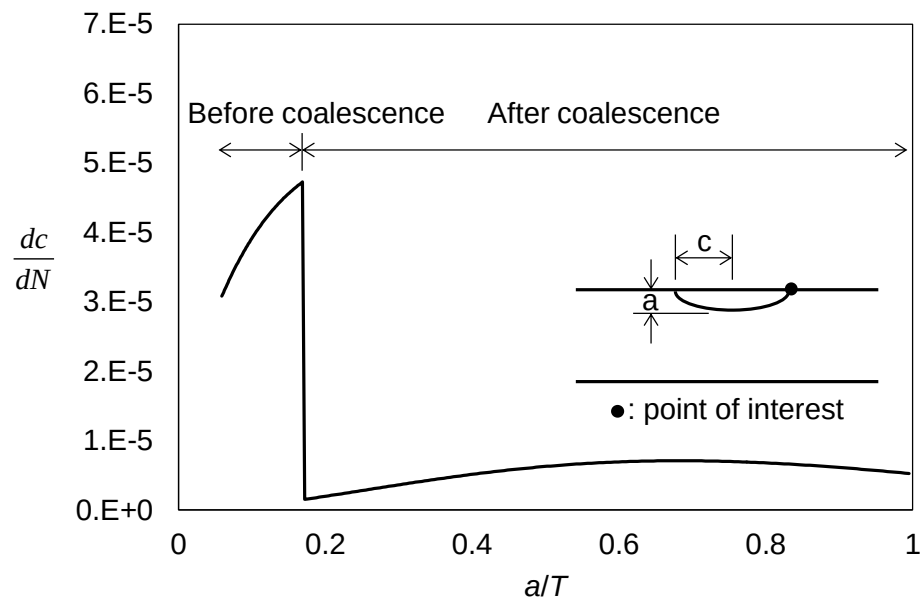

(b)

Figure 33. Change of crack growth rate as a crack growth: (a) at deepest crack depth; and (b) at crack tip surface

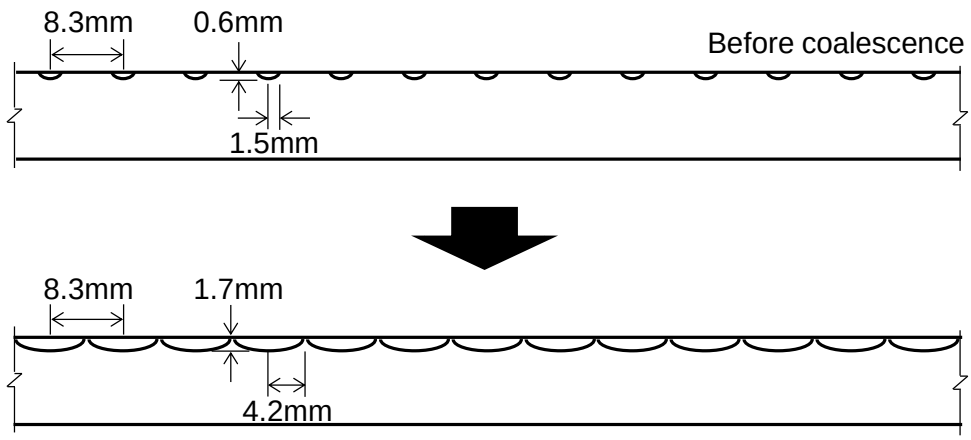

(a)

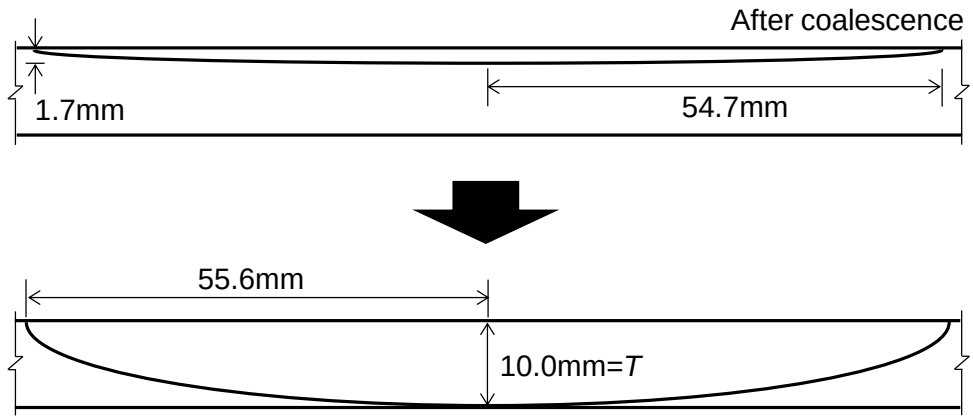

(b)

Figure 34. Propagation procedure of multiple crack: (a) before coalescence; and (b) after coalescence

3.2.3 Sample generation using Monte-Carlo simulation

The Monte-Carlo simulation (MCS) technique was used to generate a sample of the combination of the initial crack size, distance between cracks, and material parameter, which are random variables. The arrangement of the

multiple cracks was based on the probability model of crack distance and placed on the boundary between top flange and weldment with length of 114 mm. Since the distance between cracks is a random variable, the number of arranged cracks is distributed as shown in Figure 35. The average number of arranged cracks is 13.4 and arranged cracks ranges from 4 to 22.

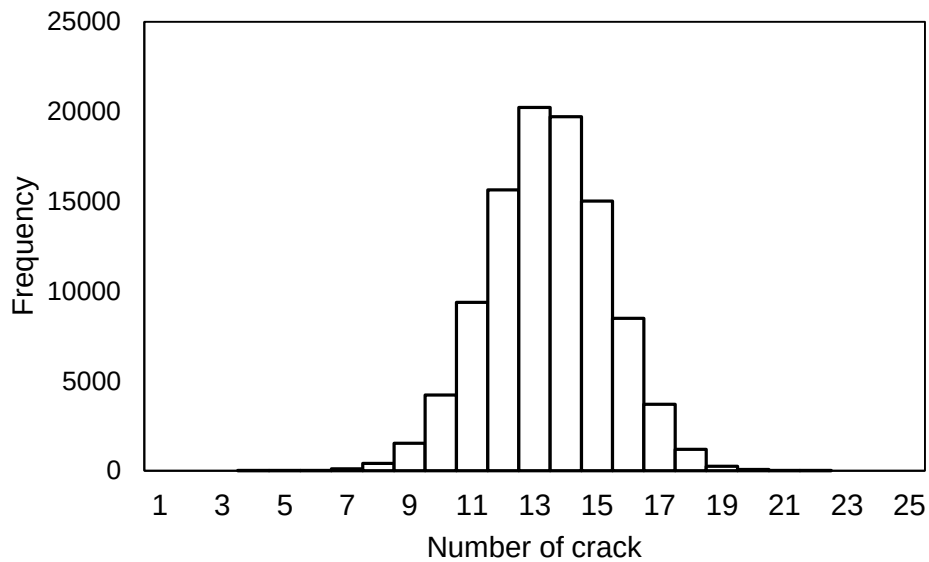

Figure 35. Histogram of the number of arranged cracks in cover plate detail

From 1 to 100,000 samples were generated for multiple crack simulation considering sufficiently various combinations. The fatigue life was obtained by crack growth analysis of each sample and the results are analyzed to identify the convergence of MCS. The mean and standard deviation of the fatigue life according to the number of samples are shown in Figure 36. The difference with result of 100,000 samples decreased to less than 1% from considering 30,000 samples, therefore, 100,000 samples were utilized to

assessment for sufficient convergence.

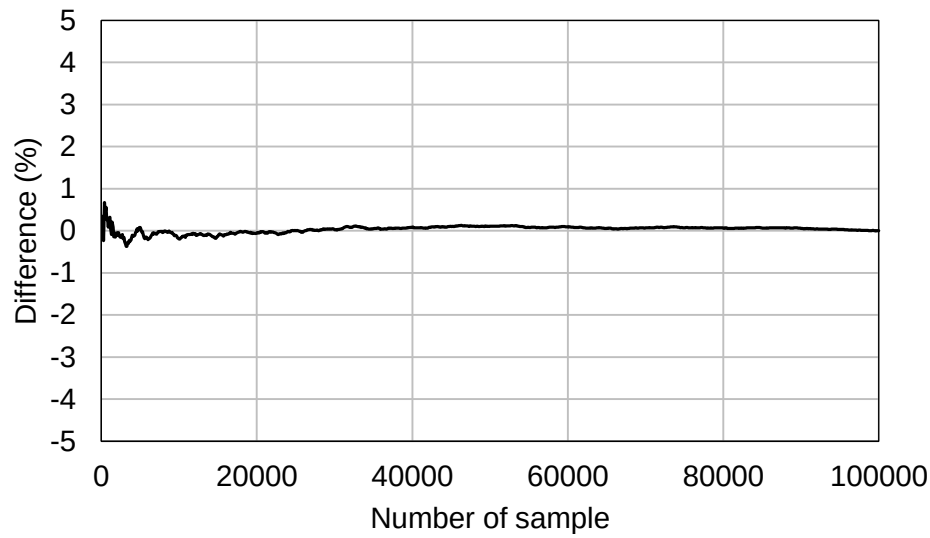

(a)

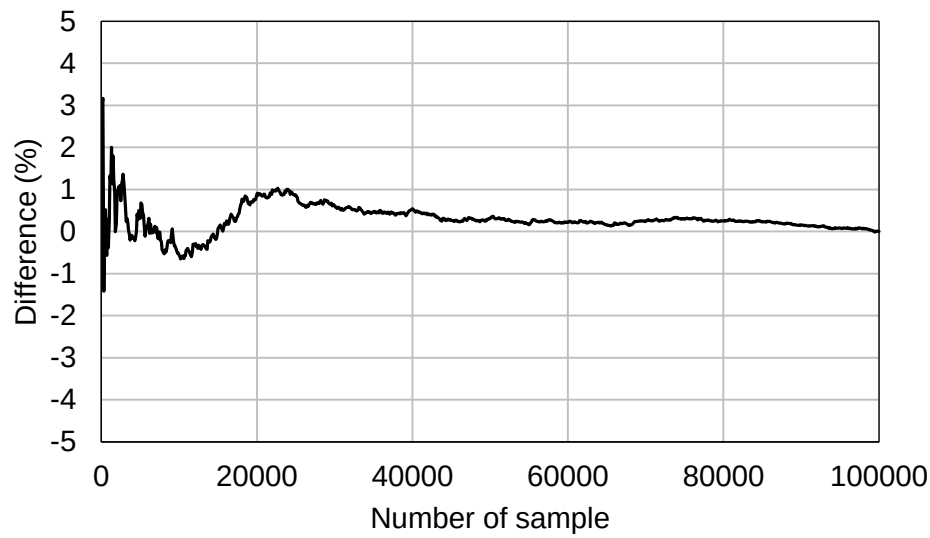

(b)

Figure 36. Convergence of result of simulation (a) mean of fatigue life; and (b) standard deviation of fatigue life

3.2.4 Appraisal of results

Distributions of fatigue life of three assessment cases obtained by MCS are plotted on the SN curve of AASHTO LRFD as shown in Figure 37. E^{mean} represents the mean life obtained based on the fatigue test, and E^{LB} and E^{UB} represent the fatigue life corresponding to the 95% confidence limit. E^{LB} is proposed as the design fatigue strength of Category E in AASHTO LRFD. In order to compare at a glance, the results of multiple cracks are plotted based on a stress range of 138 MPa (20 ksi) and results of single crack are plotted based on a stress range of 103 MPa (15 ksi). Results of distribution for multiple cracks and single cracks are shown as 95% confidence limit including LB of 2.5 percentile of fatigue life and UB of 97.5 percentile, and Mean.

LB of Case II and III are located similarly with the E^{Mean} of the distribution of experimental fatigue life, therefore, results of Case II and III overestimate the fatigue life. On the other hand, the distribution of Case I is similar to the distribution of experimental fatigue life than that of Case II and III. Lognormal distribution with a mean of 2.28 mm and a standard deviation of 0.53 mm can be recommended as equivalent single crack, which is result of Case IV. Although various SIFs were considered in Section 3.1.2, when SIF equations of Barsom and Rolfe (1999) and Zettlemoyer and Fisher (1977) are utilized to assessment, results of distribution were most similar to experimental fatigue life than result obtained using other SIF equation.

Therefore, for the fatigue assessment of cover plate detail and similar detail, it is recommended to consider SIF equation of Barsom and Rolfe (1999), Zettlemoyer and Fisher (1977) and multiple crack simulation at the same time.

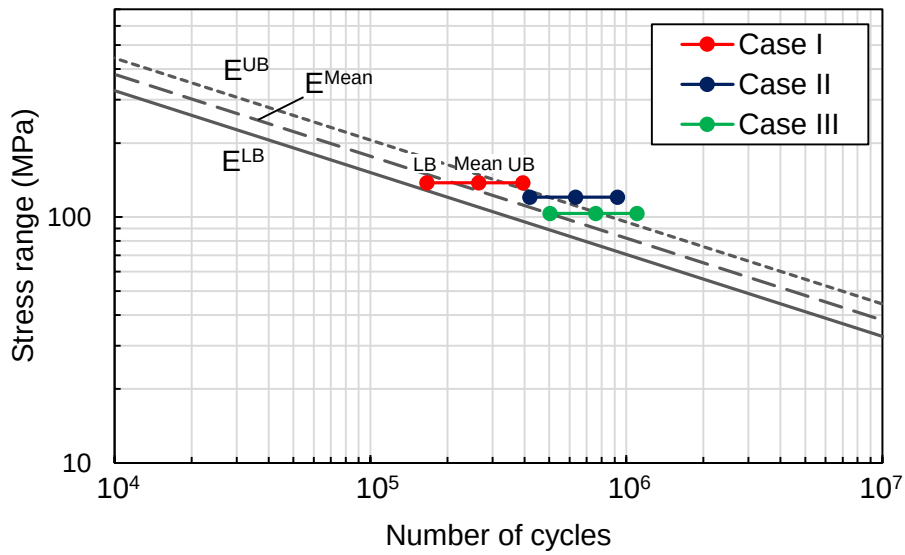

Figure 37. Distributions of fatigue life considering single and multiple cracks

Based on the same stress range of 138 MPa (20 ksi), histograms of fatigue life considering multiple cracks and single cracks were compared as shown in Figure 38. Similar to the results of fatigue test in NCHRP Report 102, the histogram of the fatigue life on the log scale obtained through MCS is also in the form of a normal distribution. The detailed comparison of fatigue life is shown in Table 17. As a result, it can be seen that the fit with the experimental fatigue life is high when the multiple crack conditions and developed probability models for initial crack are considered. On the other hand, the result of simulation assuming the conventional single crack condition can be

overestimated.

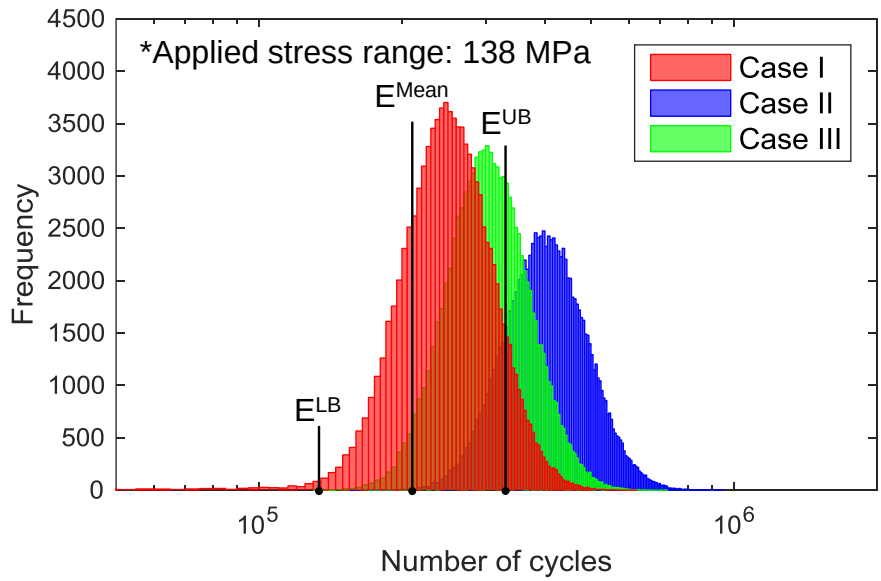

Figure 38. Histogram of fatigue life in log scale

Table 17. Distribution characteristics of fatigue life

	Fatigue life (cycles)*		
Type	Lower bound	Mean	Upper bound
AASHTO LRFD: Category E	134,000	211,000	332,000
Case I	166,000	265,000	394,000
Case II	281,000	425,000	619,000
Case III	213,000	321,000	465,000

* Applied stress range: 138 MPa

The sensitivity of the random variables to the distribution characteristics of fatigue life was identified by the importance vector as shown in Table 18. Size of initial crack is found to be the most sensitive variable to the mean of fatigue life since COV of size of initial crack is considerably larger than other random variables. Although the COV of the material parameter is the smallest,

it is identified that the sensitivity is quite high. Distance between crack initiation points is found to have the lowest sensitivity. It is identified that the number of arranged cracks differs by only one or two, which is not significant, even if 20 percent of the standard deviation were changed.

Table 18. Importance vector in cover plate detail

Case	Importance vector δ	Importance vector η
Size of initial crack, a_0	-106,000	8,340
Distance between crack initiation points, d	7,960	5,770
Material parameter, ln$C$	-53,100	49,900

CHAPTER 4

VERIFICATION FOR APPLICABILITY OF DEVELOPED PROBABILITY MODEL OF INITIAL CRACK TO TRANSVERSE STIFFENER DETAIL

Information of fatigue tests on transverse stiffener detail is referred to NCHRP Report 147 (Fisher et al., 1974). The results of fatigue test were used to suggest the design fatigue strength corresponding to Category C of AASHTO LRFD through statistical analysis (AASHTO, 2012). As shown in Figure 39, a crack propagation simulation was performed for cracks occurring at the boundary between the transverse stiffener fillet weld and the bottom flange of the test specimen. Assessment method in Section 3.1 is also applied to transverse stiffener in Chapter 4.

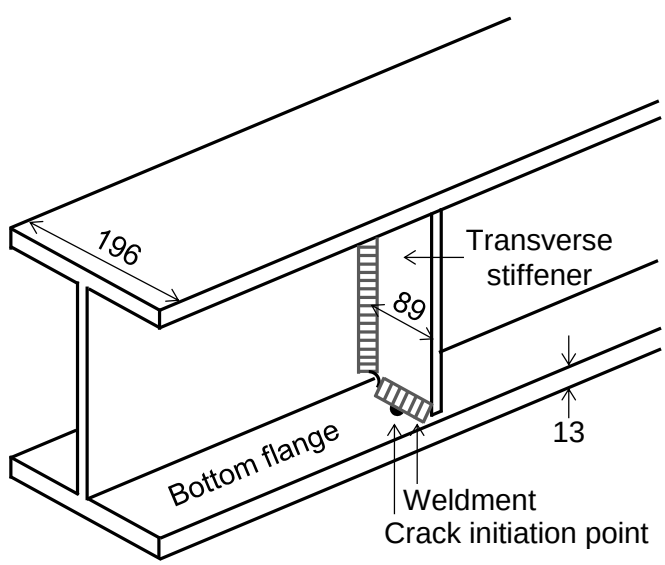

Figure 39. Transverse stiffener detail (Fisher et al., 1974) (unit: mm)

4.1 SIF equation for transverse stiffener detail

SIF Equation proposed by Barsom and Rolfe (1999) is adopted to calculate F_s, F_w, and F_e. SIF equation developed by Zettlemoyer and Fisher (1977) is adopted to calculate F_g. F_g could be calculated by:

$$F_{g,a} = \frac{SCF}{1 + \frac{1}{0.3602}\left(\frac{a}{T}\right)^{0.2487}} \tag{46}$$

$$SCF = 1.621 \log\left(\frac{Z}{T}\right) + 3.963 \tag{47}$$

In that equation, SCF is the stress concentration factor, T is the flange thickness, and Z is the weld height. Since equation of Zettlemoyer gives only the stress gradient correction factor in the depth direction, F_g equation which is proposed for transverse stiffener by Bowness and Lee (2002) is referred for analysis in length direction as described in Section 3.2.1. The reason for not referring to the equation of Bowness and Lee (2002), which suggests both length and depth direction of F_g for transverse stiffener, is that Bowness and Lee (2002) are based on the equation of Newman and Raju (1981), instead of Barsom and Rolfe (1999). Because F_s, F_w and F_e are determined by equation of Barsom and Rolfe (1999) for unity of evaluation conditions, F_g of Zettlemoyer and Fisher (1977), which presents only F_g in the depth direction, is applied.

4.2 Characteristics of multiple crack propagation and coalescence

Characteristics of multiple crack conditions is identified by performing multiple crack growth analysis using the mean value of each parameter. The mean values given in Table 13 are applied to multiple crack growth analysis.

Crack shape development is identified in terms of a/c as shown in Figure 40. Until crack coalescence, 9 cracks simulated based on mean value of crack distance grow individually, and a/c stays about the same. However, when 9 cracks are coalesced at the same time, a/c falls from 0.39 to 0.04. After crack coalescence, a shallow and long single crack grows rapidly to the thickness of flange in the depth direction, increasing the a/c to 0.32. The reason for this characteristics of crack growth is shown in Figure 41, which shows the crack growth rate. Figure 41(a) shows the crack growth rate in the depth direction. It can be seen that the growth rate increases steadily as the crack grows, and the growth rate increases by 49% after crack coalescence. As shown in Figure 41(b), which shows crack growth rate in the length direction, the growth rate increases steadily as the crack grows, and the growth rate is decreased by 94% after crack coalescence. In the region where the depth of cracks exceeds half of the thickness of flange, both the crack growth rate of depth and length direction are different from the result of cover plate detail. This is due to the influence of F_w. Cover plate detail shows that the web is resistant to bending, whereas the transverse stiffener shows a accelerated growth rate due to the

effect of bending.

Change of crack shape during crack growth is shown in Figure 42. Crack grows in the depth direction at a high speed without growth in the length direction while growing up to the thickness of the flange.

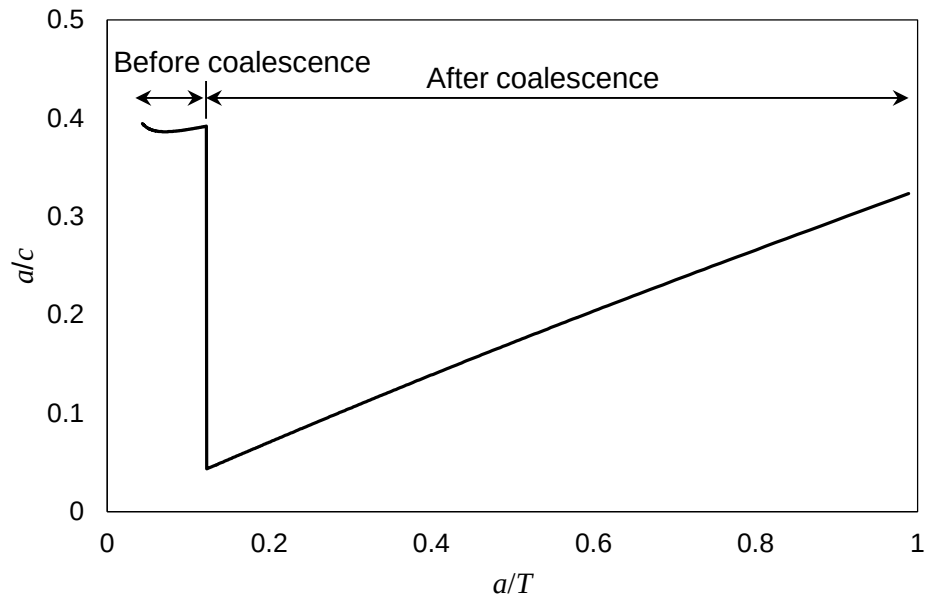

Figure 40. Crack shape development as a crack growth

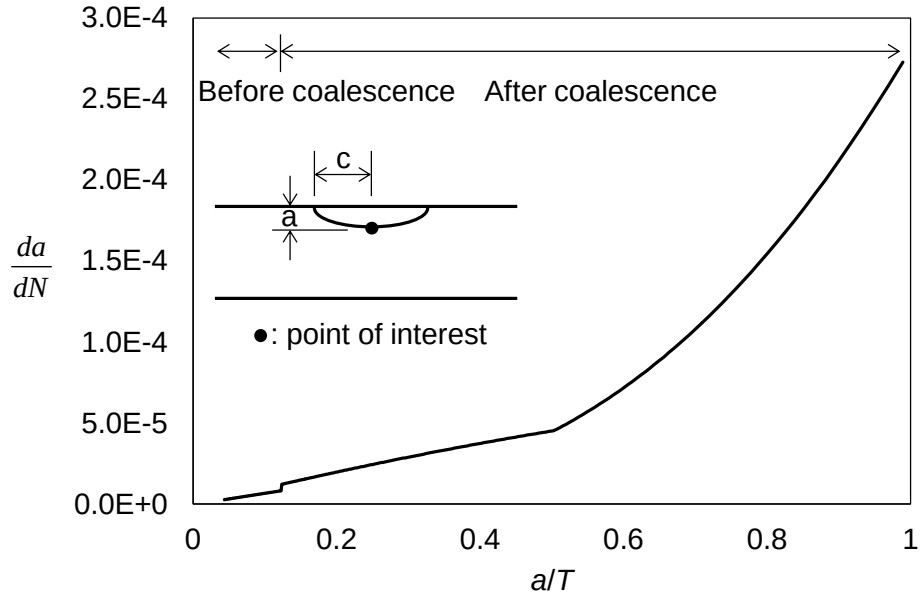

(a)

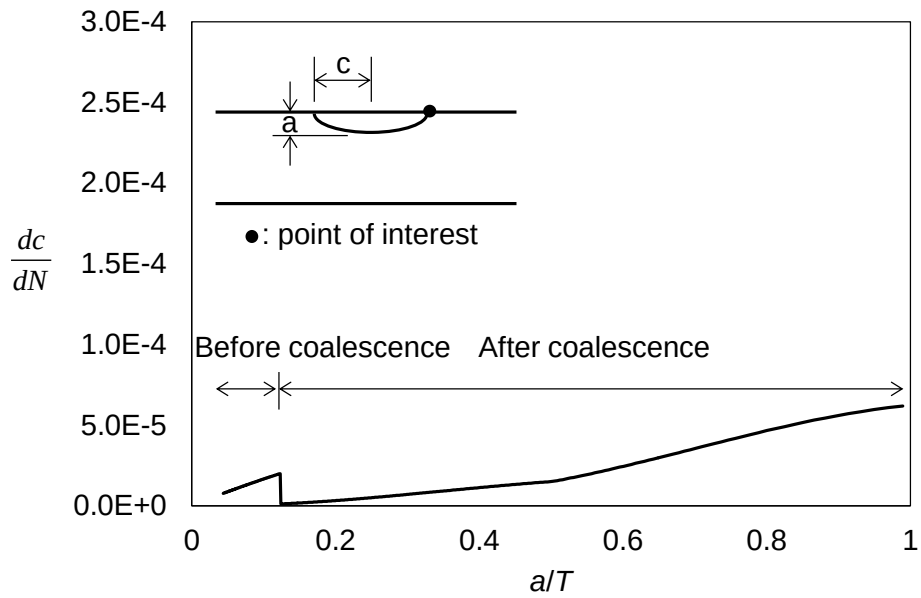

(b)

Figure 41. Change of crack growth rate as a crack growth: (a) at deepest crack depth (b) at crack tip surface

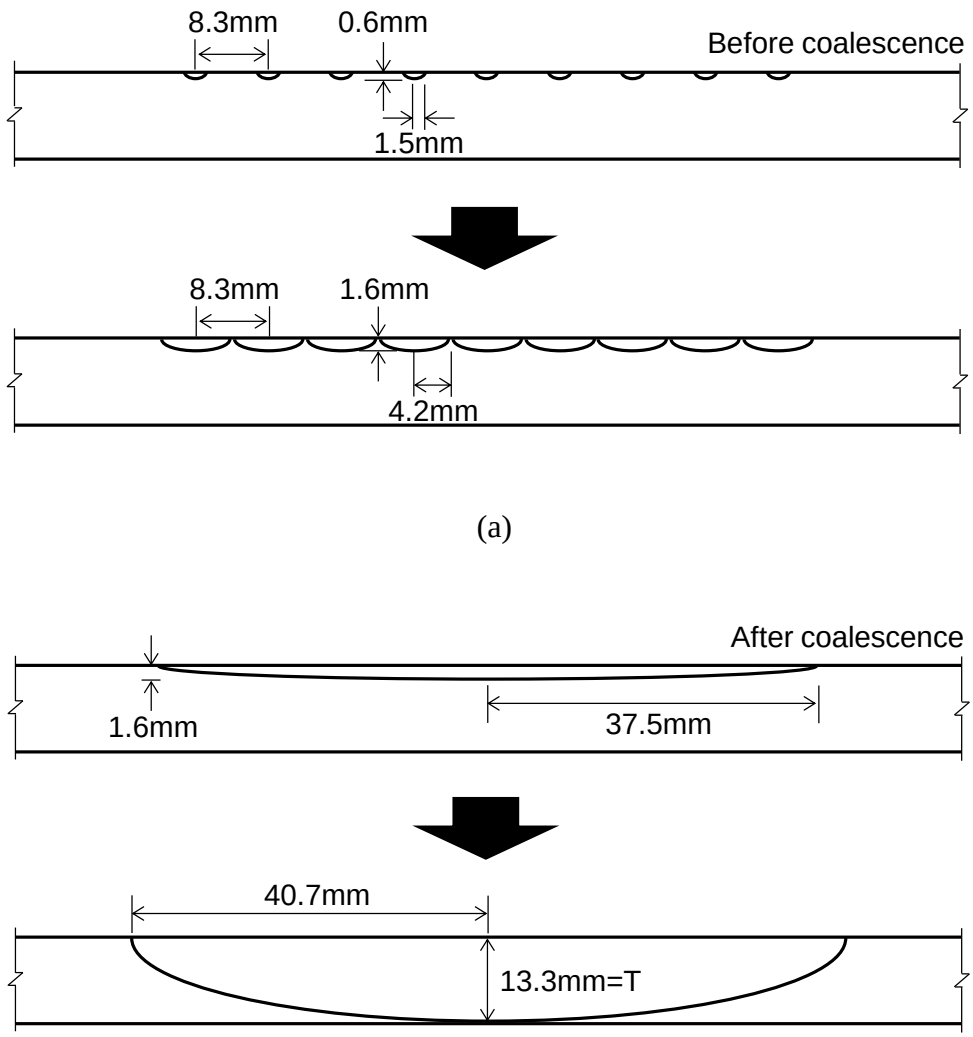

Figure 42. Propagation procedure of multiple crack: (a) before coalescence; and (b) after coalescence

4.3 Sample generation using Monte-Carlo simulation

MCS technique was used to generate a sample of the combination of the initial crack size, distance between cracks, and material parameter, which are random variables. The arrangement of the multiple cracks was based on the

probability model of crack distance and placed on the boundary between bottom flange and weldment with length of 83 mm. Since the distance between cracks is a random variable, the number of arranged cracks is distributed as shown in Figure 43. The average number of arranged cracks is 9.8 and arranged cracks ranges from 1 to 16.

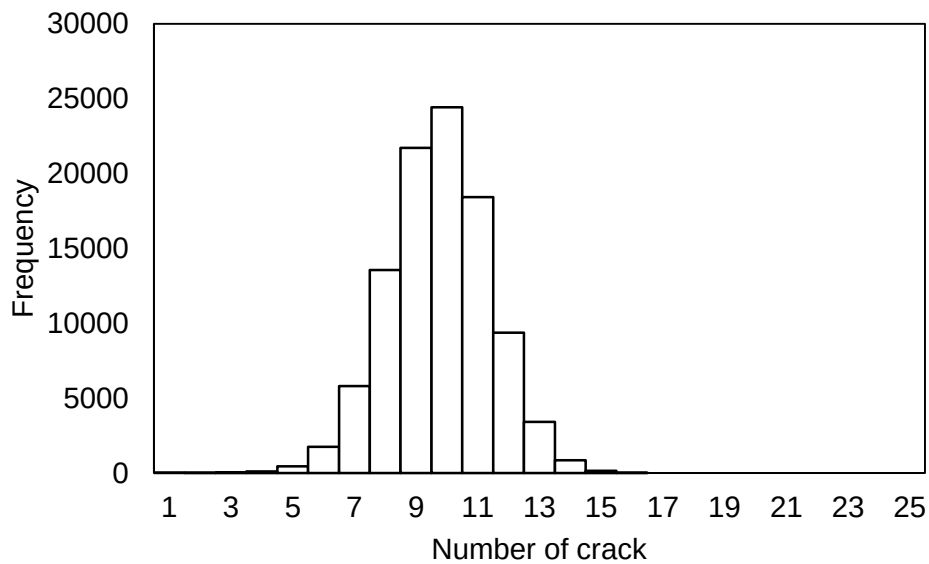

Figure 43. Histogram of the number of arranged cracks in transverse stiffener detail

Total 100,000 samples were utilized to assessment for sufficient convergence as described in Section 3.2.3. The fatigue life was obtained by crack growth analysis of each sample and the results are analyzed to identify the convergence of MCS. The mean and standard deviation of the fatigue life according to the number of samples are shown in Figure 44. It is found that difference with result of 100,000 samples decreased to less than 1% from considering 20,000 samples.

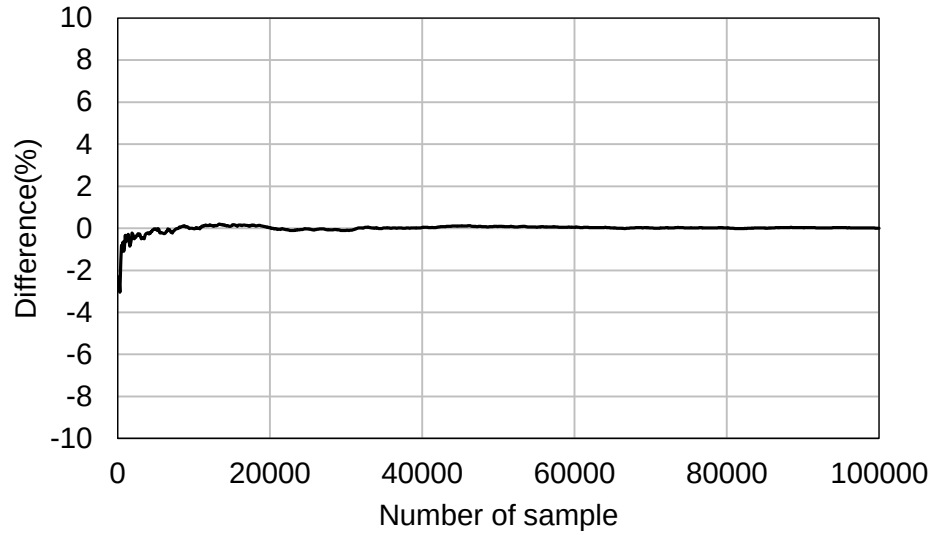

(a)

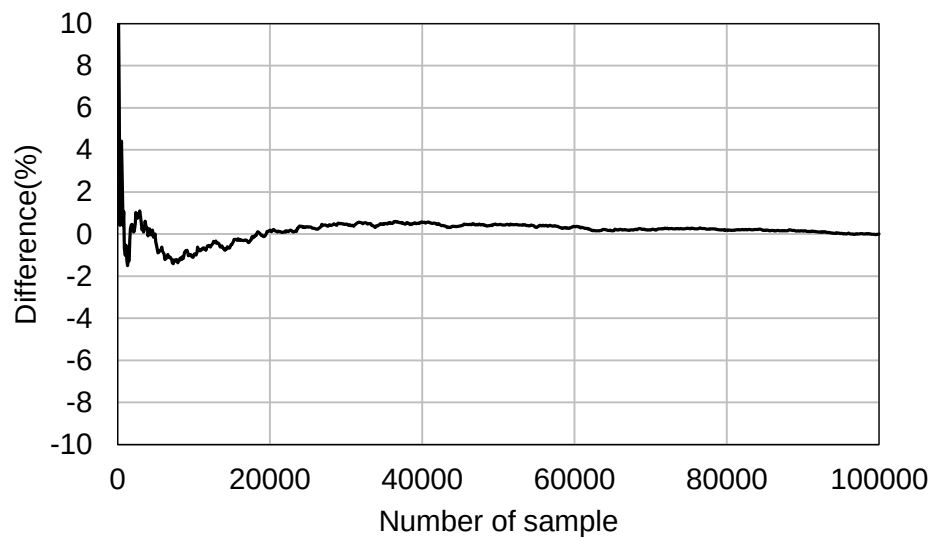

(b)

Figure 44. Convergence of result of simulation (a) mean of fatigue life; and (b) standard deviation of fatigue life

4.4 Appraisal of results

Distributions of fatigue life considering three assessment cases obtained by MCS are plotted on the SN curve of AASHTO LRFD as shown in Figure 45. Distribution of experimental fatigue life is represented by C^{mean}, C^{LB} and C^{UB}. In order to compare at a glance, the results of multiple cracks are plotted based on a stress range of 138 MPa (20 ksi) and results of single crack are plotted based on a stress range of 103 MPa (15 ksi). Results of distribution for multiple cracks and single cracks are also shown as Mean, LB and UB.

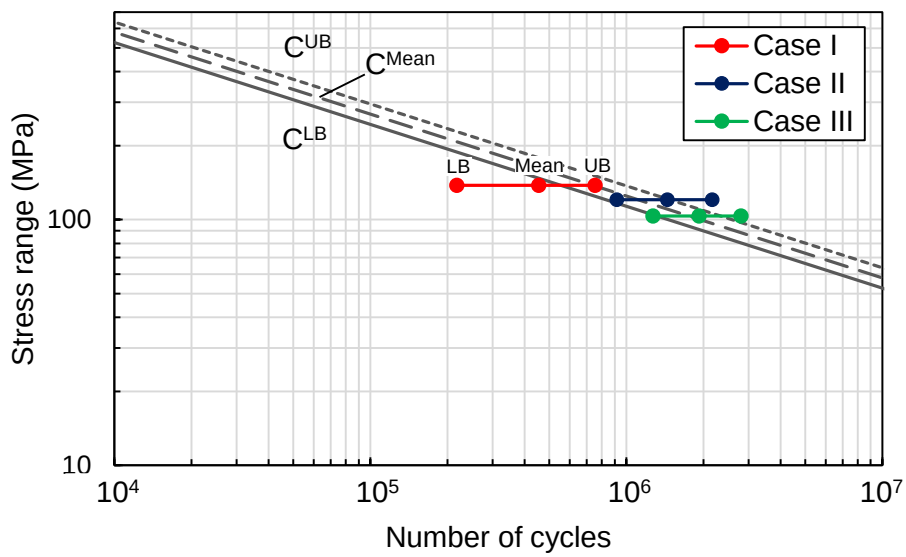

Figure 45. Distributions of fatigue life considering single and multiple cracks

Distribution of Case II and III are located similarly with that of experimental fatigue life, however, two cases overestimate the fatigue life. On the other hand, the distribution of Case I is underestimate the fatigue life.

It is reasonable to underestimate the results since simulation only considers stage of surface crack, although through-thickness crack beyond surface crack are considered in fatigue tests. Lognormal distribution with a mean of 1.37 mm and a standard deviation of 0.69 mm can be recommended as equivalent single crack, which is result of Case IV. In result of simulation cases, the width of the distribution is considerably wider than the experimental results, because the standard deviation of experimental results of Category C is very small compared to the results of other categories (Keating and Fisher, 1986). It can be seen that the standard deviation of the detail category constant in log scale with 0.063 is significantly smaller than Category E with 0.101.

Based on the same stress range of 138 MPa (20 ksi), histograms of fatigue life considering multiple cracks and single cracks were compared as shown in Figure 46. Similar to the results of fatigue test in NCHRP Report 147, the histogram of the fatigue life on the log scale obtained through MCS is also in the form of a normal distribution. Detailed comparison of fatigue life is described in Table 19.

Although various SIFs were considered in Section 3.1.2, when SIF equations of Barsom and Rolfe (1999) and Zettlemoyer and Fisher (1977) are utilized to assessment, results of distribution were most similar to experimental fatigue life than result obtained using other SIF equation. Therefore, for the fatigue assessment of transverse stiffener, it is recommended to consider SIF equation of Barsom and Rolfe (1999), Zettlemoyer and Fisher (1977) and multiple crack simulation at the same time.

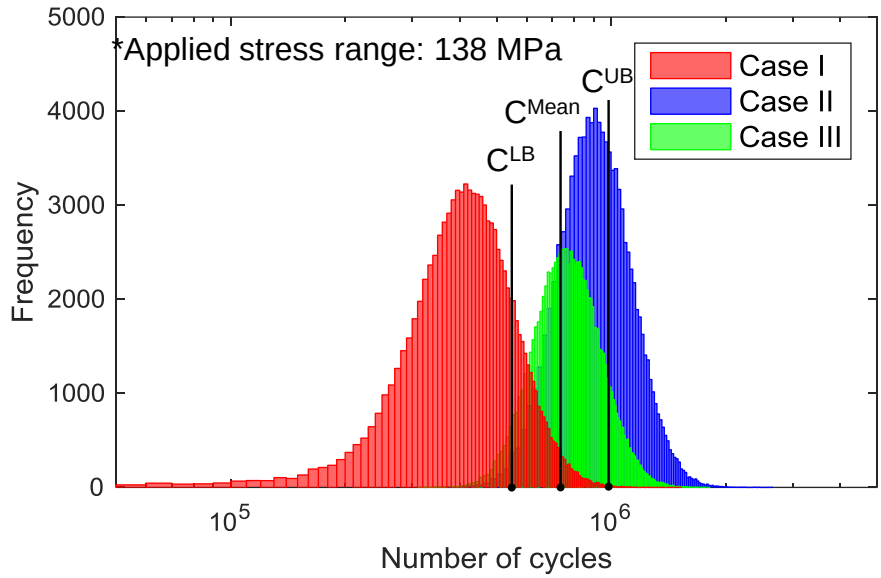

Figure 46. Histogram of fatigue life in log scale

Table 19. Distribution characteristics of fatigue life

	Fatigue life (cycles)*		
Type	Lower bound	Mean	Upper bound
AASHTO LRFD: Category C	556,000	739,000	981,000
Case I	217,000	454,000	753,000
Case II	614,000	967,000	1,449,000
Case III	535,000	812,000	1,183,000

* Applied stress range: 138 MPa

The sensitivity of the random variables to the distribution characteristics of fatigue life was identified by the importance vector as shown in Table 20. Size of initial crack is found to be the most sensitive variable to the mean of fatigue life since COV of size of initial crack is considerably larger than other random variables. Although the COV of the material parameter is the smallest, it is identified that the sensitivity is quite high. Distance between crack initiation points is found to have the lowest sensitivity. It is identified that the

number of arranged cracks differs by only one or two, which is not significant, even if 20 percent of the standard deviation were changed.

Table 20. Importance vector in transverse stiffener detail

Case	Importance vector δ	Importance vector η
Size of initial crack, a_0	-296,000	47,100
Distance between crack initiation points, d	1,530	8,190
Material parameter, ln$C$	-92,800	66,200

CHAPTER 5

VERIFICATION FOR APPLICABILITY OF DEVELOPED PROBABILITY MODEL OF INITIAL CRACK TO WEB ATTACHMENT DETAIL

Information of fatigue tests on transverse stiffener detail is referred to NCHRP Report 227 (Fisher et al., 1980). The results of fatigue test were used to suggest the design fatigue strength corresponding to Category E and E′ of AASHTO LRFD through statistical analysis (AASHTO, 2012). As shown in Figure 47, Category E specimen with thickness of attachment (T_{att}) less than 25 mm and Category E′ specimen with T_{att} thicker than 25 mm were used. Crack propagation simulation was performed for cracks occurring at the boundary between the longitudinal attachment fillet weld and web of the test specimen. Assessment method in Section 3.1 is also applied to transverse stiffener in Chapter 5.

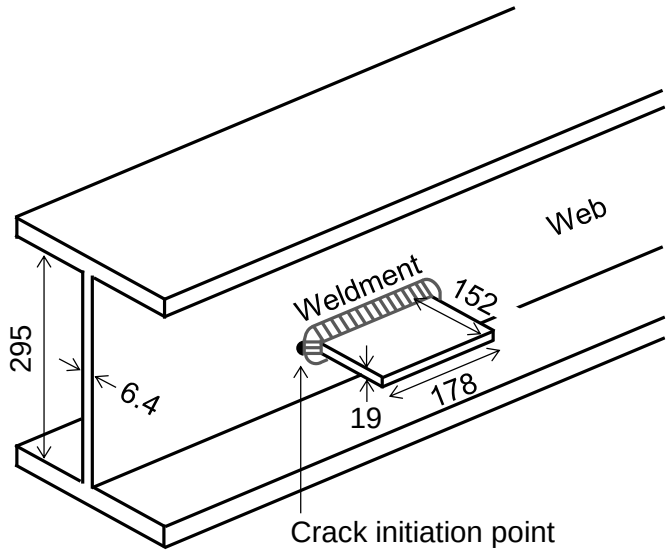

(a)

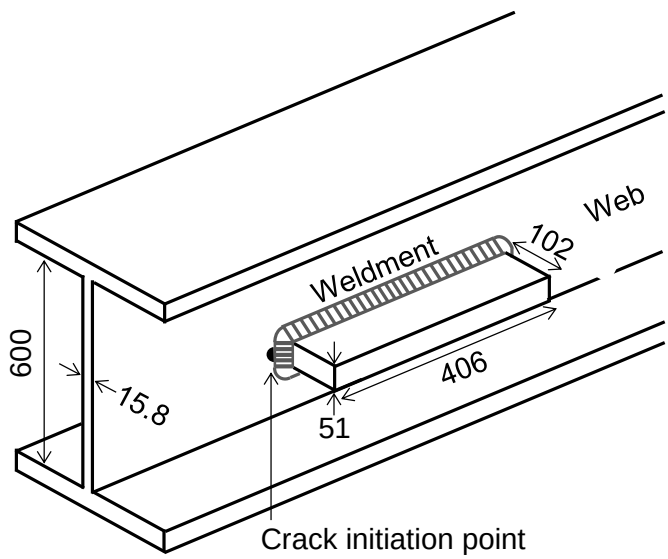

(b)

Figure 47. Web attachment detail: (a) Category E specimen with T_{att} less than 25 mm; and (b) Category E′ specimen with T_{att} thicker than 25 mm

5.1 SIF equation for web attachment detail

SIF Equation proposed by Barsom and Rolfe (1999) is adopted to calculate F_s, F_w, and F_e. SIF equation developed by Norris and Fisher (1981) is adopted to calculate F_g. Stress gradient factor, F_g could be calculated by:

$$F_{g,a} = \frac{SCF}{1 + \frac{1}{0.088} a^{0.576}} \tag{48}$$

In that equation, SCF is the stress concentration factor and has been found to have a value from 5.5 to 7.0. However, this equation is developed to apply to web attachment detail which has 20.3mm of thickness of web. Equation should be modified to apply other web attachment detail. In order to consider different thickness of web, variable a is substituted by a/T as shown in Eq. (49). This equation has same stress gradient factor with original equation developed by Norris and Fisher (1981) at the web attachment detail which has 20.3mm of thickness of web.

$$F_{g,a} = \frac{SCF}{1 + 4.942\left(\frac{a}{T}\right)^{0.576}} \tag{49}$$

In NCHRP Report 227, 7.0 and 8.0 of SCF were applied to the Category E' specimens for evaluation based on fracture mechanics, and then it was found that result of evaluation fit well with the experimental results (Fisher et al., 1980). Based on result in NCHRP Report 227, the lower limit value of the SCF with 5.5 was applied to the Category E specimen, and the upper limit

value of the SCF with 7.0 was applied to the Category E′ specimen. Since equation of Norris and Fisher (1981) gives only the stress gradient correction factor in the depth direction, F_g equation in length direction is estimated based on equation of Bowness and Lee (2002), as described in Section 3.2.1 and 4.1.

5.2 Characteristics of multiple crack propagation and coalescence

Characteristics of multiple crack conditions is identified by performing multiple crack growth analysis using the mean value of each parameter. The mean values given in Table 13 are applied to multiple crack growth analysis.

Crack shape development is identified in terms of *a*/*c* as shown in Figure 48. Until crack coalescence, 3 cracks simulated based on mean value of crack distance grow individually, and *a*/*c* stays about the same. However, when 3 cracks are coalesced at the same time, *a*/*c* falls from 0.42 to 0.14. After crack coalescence, a shallow and long single crack grows rapidly to the thickness of flange in the depth direction, increasing the *a*/*c* to 0.42. The reason for this characteristics of crack growth is shown in Figure 49, which shows the crack growth rate. Figure 49(a) shows the crack growth rate in the depth direction. It can be seen that the growth rate increases steadily as the crack grows, and the growth rate increases by 48% after crack coalescence. As shown in Figure 49(b), which shows crack growth rate in the length direction, the growth rate increases steadily as the crack grows, and the growth rate is decreased by 72%

after crack coalescence. In the region where the depth of cracks exceeds half of the thickness of flange, growth rate is accelerated due to the effect of bending in specimen.

Change of crack shape during crack growth is shown in Figure 50. Crack grows in the depth direction at a high speed without growth in the length direction while growing up to the thickness of the flange.

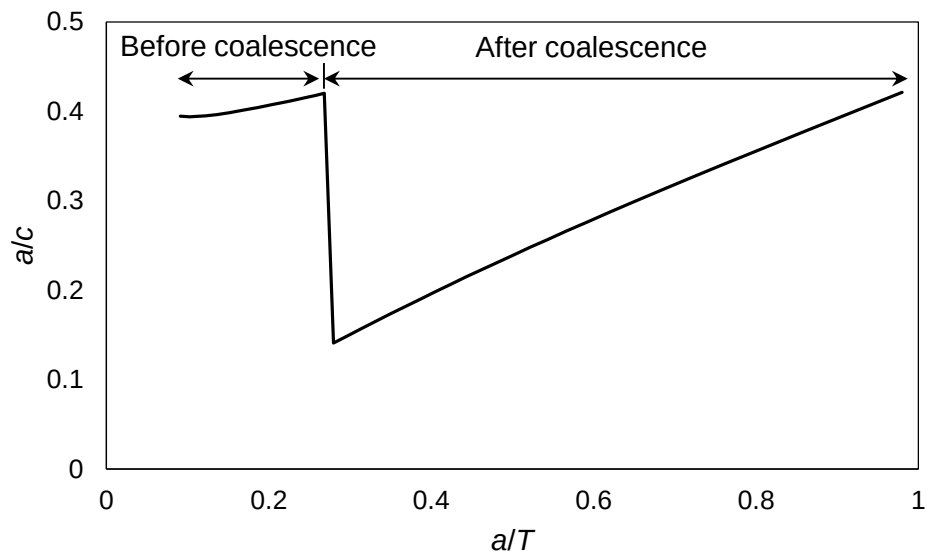

Figure 48. Crack shape development as a crack growth

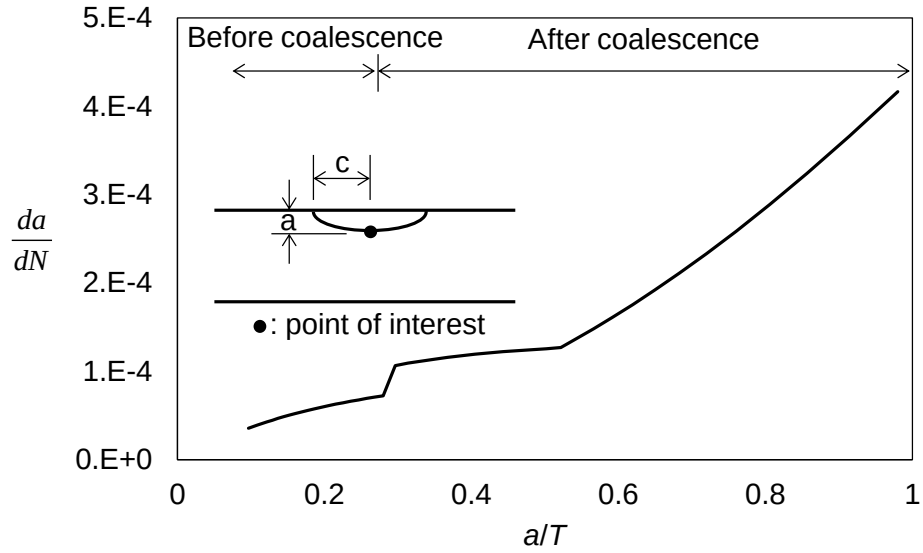

(a)

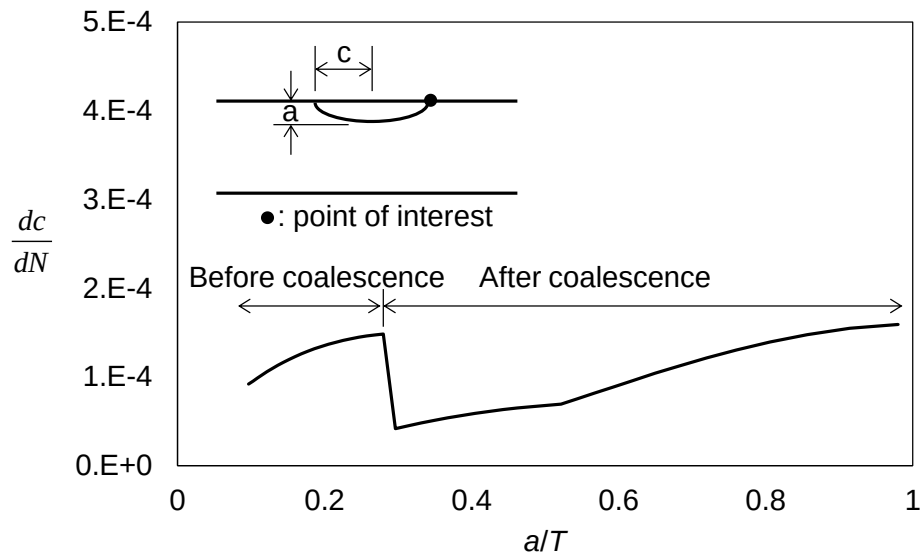

(b)

Figure 49. Change of crack growth rate as a crack growth: (a) at deepest crack depth (b) at crack tip surface

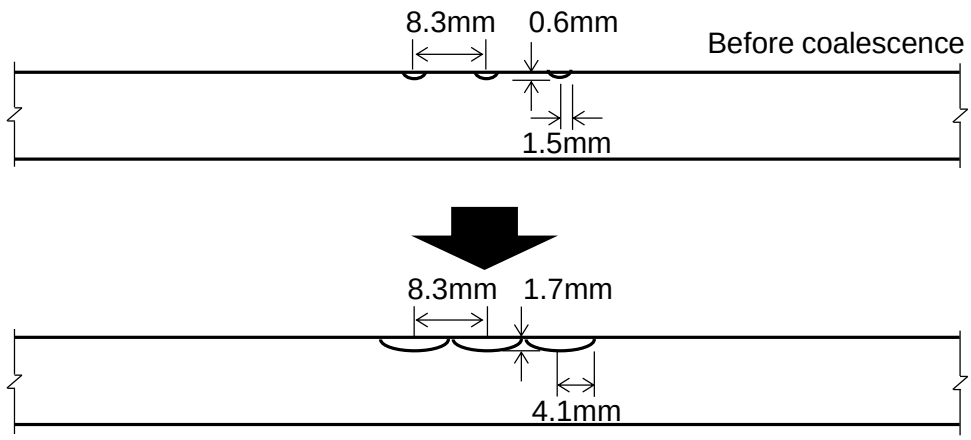

(a)

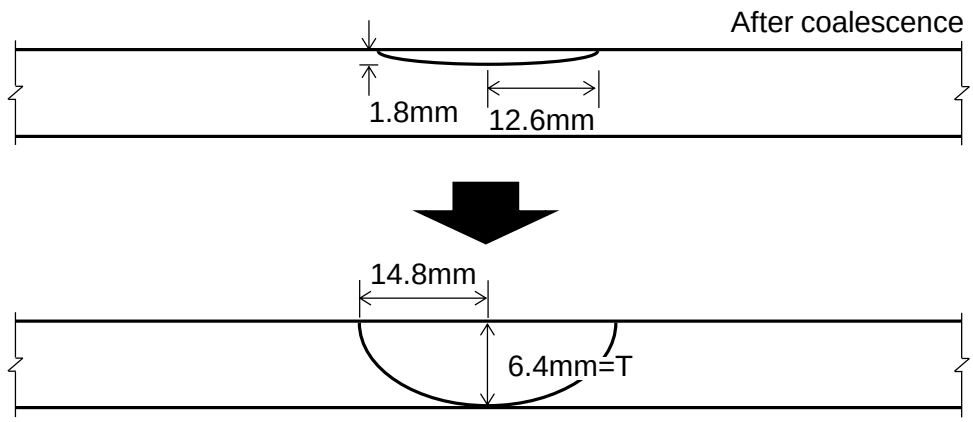

(b)

Figure 50. Propagation procedure of multiple crack: (a) before coalescence; and (b) after coalescence

5.3 Sample generation using Monte-Carlo simulation

MCS technique was used to generate a sample of the combination of the initial crack size, distance between cracks, and material parameter, which are random variables. The arrangement of the multiple cracks was based on the

probability model of crack distance and placed on the boundary between web and the longitudinal attachment fillet weld with length of 19 mm and 51 mm. Since the distance between cracks is a random variable, the number of arranged cracks is distributed as shown in Figure 51. The average number of arranged cracks in Category E specimen is 2.4 and arranged cracks ranges from 1 to 6. The average number of arranged cracks in Category E′ specimen is 6.1 and arranged cracks ranges from 1 to 12. Since the cracks are arranged symmetrically, the number of cracks arranged is odd number.

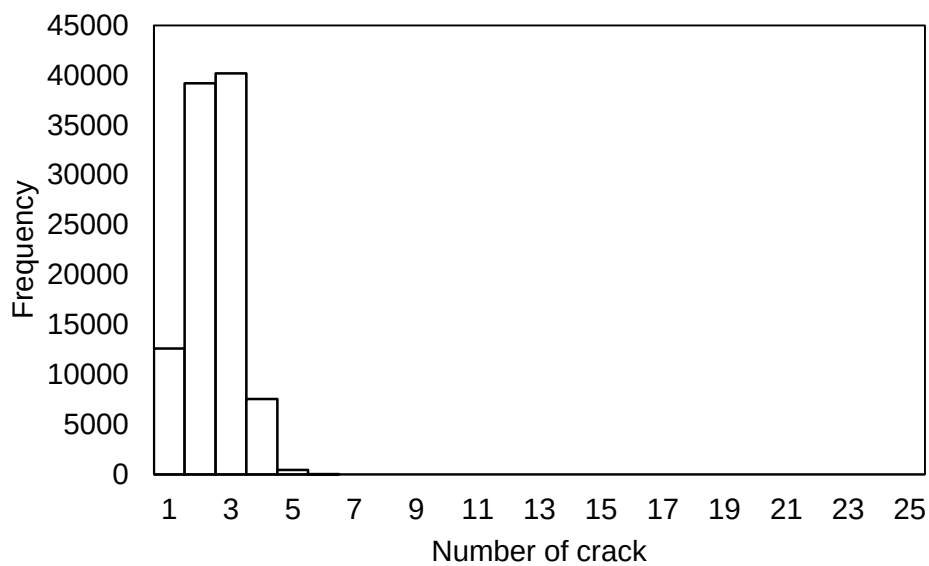

(a)

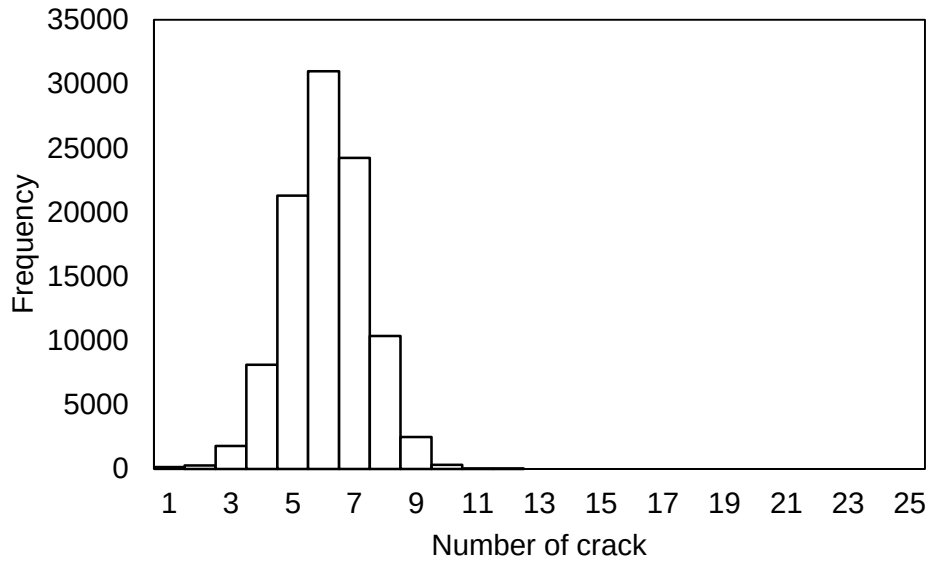

(b)

Figure 51. Histogram of the number of arranged cracks in web attachment detail: (a) T_{att}=19mm, Category E; and (b) T_{att}=51mm, Category E′

Total 100,000 samples were utilized to assessment for sufficient convergence as described in Section 3.2.3. The mean and standard deviation of the fatigue life according to the number of samples are calculated. It is found that difference with result of 100,000 samples decreased to less than 1% from considering 30,000 samples.

5.4 Appraisal of results

Distributions of fatigue life of three assessment cases obtained by MCS are plotted on the SN curve of AASHTO LRFD as shown in Figure 52. In case of Category E specimen, distribution of experimental fatigue life is

represented by E^{mean}, E^{LB} and E^{UB}. In case of Category E′ specimen, distribution of experimental fatigue life is represented by E^{LB} and E'^{LB} since there is no statistical properties of experimental result on Category E′. In order to compare at a glance, the results of multiple cracks are plotted based on a stress range of 138 MPa (20 ksi) and results of single crack are plotted based on a stress range of 103 MPa (15 ksi). Results of distribution for multiple cracks and single cracks are also shown as Mean, LB and UB.

In case of Category E specimen, the length of weldment is 19 mm, which is close to the condition of a single crack. Therefore, it can be seen that the results of the single crack model and that of the multiple crack model are similar, as shown in Figure 52(a). Distribution of Case II and III are located similarly with that of experimental fatigue life, however, two cases overestimate the fatigue life. On the other hand, the distribution of Case I is underestimate the fatigue life. It is reasonable to underestimate the results since simulation only considers stage of surface crack, although through-thickness crack beyond surface crack are considered in fatigue tests. Lognormal distribution with a mean of 1.00 mm and a standard deviation of 0.66 mm can be recommended as equivalent single crack, which is result of Case IV. The detailed comparison of fatigue life is shown in Table 21. It can be seen that the result of the Case I is more reasonable than Case II and III because the length of weldment is 19 mm and about 3 cracks are expected to occur.

Design SN curve of Category E′ is suggested based on the results of thick

cover plate detail and web attachment detail (Fisher et al., 1979). Unlike other Category, mean and standard deviation of experimental result were not suggested through statistical analysis. Therefore, the results of the single crack model and multiple crack model are compared with AASHTO E^{LB} and E'^{LB} as shown in Figure 52(b).

Results of the Case I and II are different because the length of weldment is 51 mm and the multiple crack condition is sufficiently satisfied for the Category E′ specimen. Distribution of Case I is underestimate the fatigue life like web attachment case of Category E. It is reasonable to underestimate the results since simulation only considers stage of surface crack, although through-thickness crack beyond surface crack are considered in fatigue tests. Lognormal distribution with a mean of 1.92 mm and a standard deviation of 0.69 mm can be recommended as equivalent single crack, which is result of Case IV. The detailed comparison of fatigue life is shown in Table 22.

Table 21. Distribution characteristics of fatigue life

	Fatigue life (cycles)*		
Type	Lower bound	Mean	Upper bound
AASHTO LRFD: Category E	134,000	211,000	332,000
Case I	89,000	191,000	307,000
Case II	172,000	261,000	379,000
Case III	150,000	230,000	339,000

* Applied stress range: 138 MPa

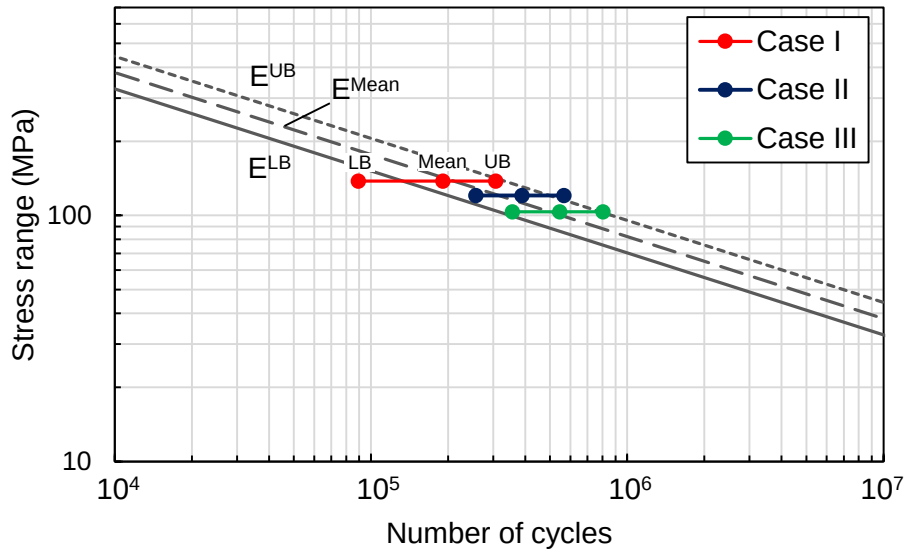

(a)

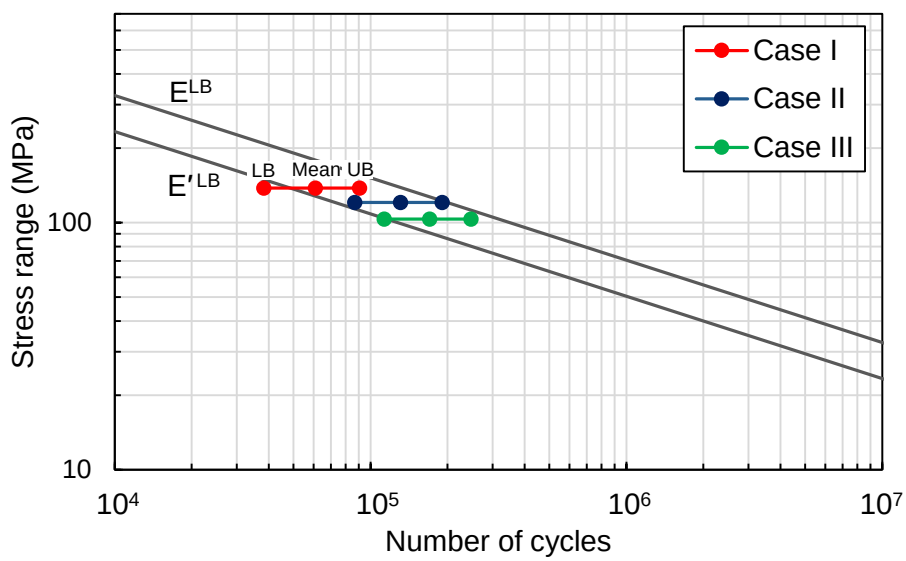

(b)

Figure 52. Distributions of fatigue life considering single and multiple cracks: (a) Category E specimen; and (b) Category E′ specimen

Table 22. Distribution characteristics of fatigue life

	Fatigue life (cycles)*		
Type	Lower bound	Mean	Upper bound
AASHTO LRFD: Category E′	49,000	-	-
Case I	38,000	61,000	90,000
Case II	58,000	88,000	127,000
Case III	48,000	72,000	104,000

* Applied stress range: 138 MPa

Based on the same stress range of 138 MPa (20 ksi), histograms of fatigue life considering multiple cracks and single cracks were compared as shown in Figure 53. Similar to the results of fatigue test in NCHRP Report 227, the histogram of the fatigue life on the log scale obtained through MCS is also in the form of a normal distribution.

Although various SIFs were considered in Section 3.1.2, when SIF equations of Barsom and Rolfe (1999) and Norris and Fisher (1981) are utilized to assessment, results of distribution were most similar to experimental fatigue life than result obtained using other SIF equation. Therefore, for the fatigue assessment of web attachment detail, it is recommended to consider SIF equation of Barsom and Rolfe (1999), Norris and Fisher (1981) and multiple crack simulation at the same time.

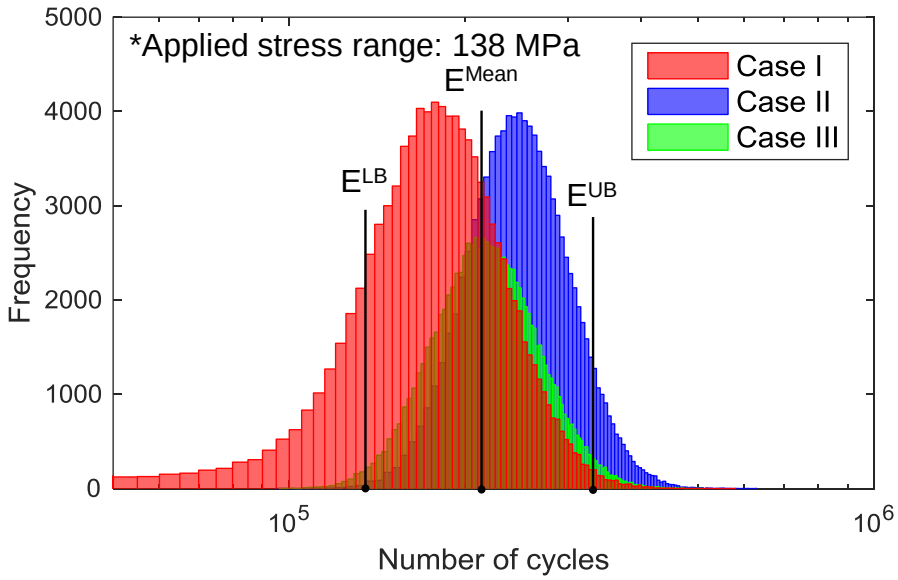

(a)

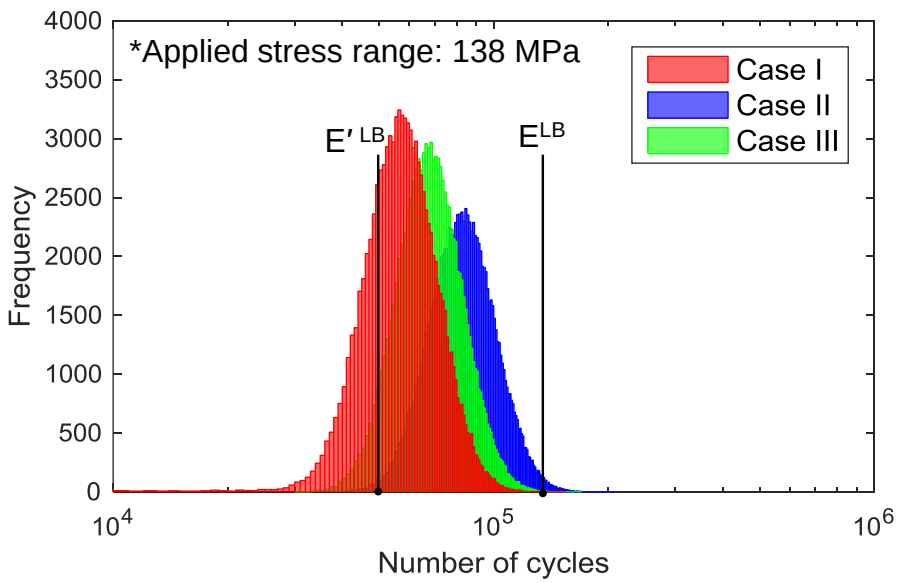

(b)

Figure 53. Histogram of fatigue life in log scale: (a) Category E specimen; and (b) Category E′ specimen

The sensitivity of the random variables to the distribution characteristics of fatigue life was identified by the importance vector as shown in Table 23. Size of initial crack is found to be the most sensitive variable to the mean of fatigue life since COV of size of initial crack is considerably larger than other random variables. Although the COV of the material parameter is the smallest, it is identified that the sensitivity is quite high. Distance between crack initiation points is found to have the lowest sensitivity. It is identified that the number of arranged cracks differs by only one or two, which is not significant, even if 20 percent of the standard deviation were changed.

Table 23. Importance vector in web attachment detail (Category E)

Case	Importance vector δ	Importance vector η
Size of initial crack, a_0	-97,600	14,500
Distance between crack initiation points, d	13,200	1,250
Material parameter, ln$C$	-38,600	26,600

Table 24. Importance vector in web attachment detail (Category E′)

Case	Importance vector δ	Importance vector η
Size of initial crack, a_0	-22,100	1,950
Distance between crack initiation points, d	1,980	1,040
Material parameter, ln$C$	-12,700	10,600

CHAPTER 6

CONCLUSIONS AND RECOMMENDATIONS FOR FURTHER STUDY

In order to evaluate fatigue reliability reflecting actual fatigue mechanism, both analysis methods for multiple crack growth and coalescence and a probability model of initial crack size and distance are suggested in this research. Probabilistic assessment to predict the fatigue performance of general welded connections is possible with suggested model instead of existing deterministic assessment based on measured multiple crack.

Analysis methods for multiple crack growth and coalescence were determined by referring to existing analysis methods. LEFM is adopted to simulate the propagation of single crack. Since the crack growth model proposed by Paris and Erdogan (1963) is based on large crack data, simulation of crack growth can be difficult in fatigue details with small cracks. Crack growth model suitable for the size of investigated crack should be adopted. However, it is difficult to establish the crack growth model as in the large crack since crack growth rate of small crack is affected by the grain size, grain orientation, and crack shape. To overcome this problem, EIFS concept, which utilize equivalent virtual crack size, is adopted. When EIFS is considered as initial crack size instead of actual initial crack size, crack growth simulation can be done with large crack growth model which is used to determine EIFS even if the initial crack size lies in the small crack region. Back-extrapolation

method, which find the initial crack size having the same life with experimental fatigue life, is adopted to estimate EIFS.

When multiple crack coalescence is simulated, the crack shape gradually differs from idealized semi-elliptical crack during crack coalescence. Therefore, FEA is adopted to simulate the crack coalescence since it is difficult to simulate the change of SIF occurring in the crack coalescence with existing solutions. For this reason, a re-characterization rule is adopted to replace the complex simulation of crack coalescence. Among the many proposed rules, re-characterization rule proposed by Kamaya (2008a) is adopted. In this rule, coalesced crack can be simulated by introducing a single crack having the same area with sum of two adjacent cracks.

For probabilistic simulation of multiple crack condition, probability model of initial crack size and distance that constitute the initial conditions of multiple cracks was developed by analyzing the fatigue fracture surface obtained from the actual fatigue tests performed in NCHRP Project 10-70 (Roy et al., 2011). Crack initiation point is estimated based on beach mark and ratchet mark on the fracture surface. From 6 to 23 of crack distance data were identified from each specimen and total 209 distance data were utilized to develop probability model of distance between initial cracks. As a result of goodness-of-fit test, the Lognormal distribution with a mean of 8.3 mm and a standard deviation of 4.4 mm is the most suitable distribution.

Since the initial crack size is not a variable that can be obtained directly from the fracture surface, it should be estimated based on the experimental

results. Initial crack size model suitable for the target structure was determined using the EIFS concept. In order to obtain EIFS, material parameters *C*, *m* and SIF equations appropriate for the target fatigue detail are necessary. Material parameters *C* and *m* are considered to be distribution model based on the experimental data of Barsom (1971). Since the material parameter *C* has a distribution, samples of *C* are generated based on experimental data of Barsom (1971) and then EIFS distribution corresponding to the samples of *C* is obtained. All EIFS distribution data obtained from each crack initiation point of the specimen is assembled and the probability model of the EIFS is suggested using these data. Most suitable distribution is Lognormal distribution with a mean of 0.58mm and a standard deviation of 0.91mm.

Multiple crack condition is not determined depending on the type of structure, but is common conditions in welded connection. In addition, general structural steel is utilized in test specimen and there is no significant difference with other type of structures in terms of welding materials and methods. Therefore, the distribution characteristics of the initial cracks extracted in Chapter 2 can be sufficiently applied to welded connection of other kinds of structures such as bridge. Welded details in bridge were selected for example to verify the validity of the developed assessment model. The validity of the developed assessment model was identified by comparing distribution of the fatigue life presented in the NCHRP Reports and that of the fatigue life obtained by the developed assessment model. In addition,

distribution of fatigue life obtained by applying single crack model is also considered to compare with multiple crack model. As a result, it can be seen that the fit with the experimental fatigue life is high when the multiple crack conditions are considered. In case of transverse stiffener, model for multiple crack gives conservative results. However, it is reasonable to underestimate the results since simulation only considers stage of surface crack, although through-thickness crack beyond surface crack are considered in fatigue tests. Result of simulation assuming the conventional single crack condition gives overestimated fatigue life. Through the assessment of the three welded details, the basis for application of welded details of various steel structures are identified.

From the practical point of view, fatigue assessment considering multiple cracks for maintenance of actual bridges is more complicated than conventional fatigue assessment based on single crack. As a further study, there is a need for a simplified assessment method that yields the same results of assessment considering multiple crack condition.

REFERENCES

AASHTO. (2012). *AASHTO LRFD Bridge design specifications*. 6th ed. Washington, D.C., USA: American Association of State Highway and Transportation Officials.

Ali, A., Brown, M. W., and Rodopoulos, C. A. (2008). Modelling of crack coalescence in 2024-T351 Al alloy friction stir welded joints. *International Journal of Fatigue*, 30(10-11), 2030-2043.

API. (2007). *API 579-1/ASME FFS-1- Fitness-for-Service*: American Petroleum Institute (API), American Society of Mechanical Engineers (ASME).

ASME. (1995). *Boiler and Pressure Vessel Code Section XI: Rules for in-service inspection of nuclear power plant components*. American Society of Mechanical Engineers (ASME).

Barsom, J. M. (1971). Fatigue-Crack Propagation in Steels of Various Yield Strengths. *Journal of Engineering for Industry*, 93(4), 1190-1196.

Barsom, J. M. and Rolfe, S. T. (1999). *Fracture and Fatigue Control in Structures: Applications of Fracture Mechanics* (3rd ed.). West Conshohocken: PA.

Becher, P. and Hansen, B. (1974). Statistical evaluation of defects in welds. *Danish Institute of Welding*.

Beier, H. T., Schork, B., Bernhard, J., Tchoffo Ngoula, D., Melz, T., Oechsner, M., and Vormwald, M. (2015). Simulation of fatigue crack growth in welded joints. *Materialwissenschaft und Werkstofftechnik*, 46(2), 110-122.

Bergman, M. (1995). STRESS INTENSITY FACTORS FOR

CIRCUMFERENTIAL SURFACE CRACKS IN PIPES. *Fatigue & Fracture of Engineering Materials & Structures*, 18(10), 1155-1172.

Bokalrud, T. and Karlsen, A. (1982). Probabilistic fracture mechanics evaluation of fatigue failure from weld defects in butt welded joints. *Proceedings of the Conference on fitness for purpose validation of welded constructions*.

Bowness, D. and Lee, M. M. K. (2002). *Fracture mechanics assessment of fatigue cracks in offshore tubular structures*. Health and Safety Executive.

BSI. (2014). *BS 7608: Guide to fatigue design and assessment of steel products*. London: BSI.

BSI. (2015). *BS 7910: Guide to methods for assessing the acceptability of flaws in metallic structures*. London: BSI.

Chen, N.-Z., Wang, G., and Guedes Soares, C. (2011). Palmgren–Miner's rule and fracture mechanics-based inspection planning. *Engineering Fracture Mechanics*, 78(18), 3166-3182.

Chew, Y. and Pang, J. H. L. (2016). Fatigue life prediction model for laser clad AISI 4340 specimens with multiple surface cracks. *International Journal of Fatigue*, 87, 235-244.

DNV. (1984). *Fatigue strength analysis for mobile offshore units Classification Note No. 30-2*.

El Haddad, M. H., Smith, K. N., and Topper, T. H. (1979). Fatigue crack propagation of short cracks. *Journal of Engineering Materials and Technology*, Transactions of the ASME, 101(1), 42-46.

El Haddad, M. H., Topper, T. H., and Smith, I. F. C. (1980). Fatigue Life

Prediction of Welded Components Based on Fracture Mechanics. *Journal of Testing and Evaluation*, 8(6), 301-307.

El Haddad, M. H., Topper, T. H., and Smith, K. N. (1979). Prediction of non-propagating cracks. *Engineering Fracture Mechanics*, 11(3), 573-584.

Engesvik, K. M. and Moan, T. (1983). Probabilistic Analysis of the Uncertainty in the Fatigue Capacity of Welded-Joints. *Engineering Fracture Mechanics*, 18(4), 743-762.

Fawaz, S. A. (2000). Equivalent initial flaw size testing and analysis.

Fawaz, S. A. (2003). Equivalent initial flaw size testing and analysis of transport aircraft skin splices. *Fatigue & Fracture of Engineering Materials & Structures*, 26(3), 279-290.

Fisher, J. W. (1984). *Fatigue and fracture in steel bridges. Case studies*.

Fisher, J. W., Albrecht, P. A., Yen, B. T., Klingerman, D. J., and McNamee, B. M. (1974). Fatigue strength of steel beams with welded stiffeners and attachments. *NCHRP Report 147*. Transportation Research Board, Washington, DC.

Fisher, J. W., Barthelemy, B. M., Mertz, D. R., and Edinger, J. A. (1980). Fatigue behavior of full-scale welded bridge attachments. *NCHRP Report 227*. Transportation Research Board, Washington, DC.

Fisher, J. W., Frank, K. H., Hirt, M. A., and McNamee, B. M. (1970). Effect of weldments on the fatigue strength of steel beams. *NCHRP Report 102*. Transportation Research Board, Washington, DC.

Fisher, J. W., Hausammann, H., Sullivan, M. D., and Pense, A. W. (1979). Detection and repair of fatigue damage in welded highway bridges.

NCHRP Report 206. Transportation Research Board, Washington, DC.

Forth, S. C., Everett, R. A., and Newman, J. A. (2002). A novel approach to rotorcraft damage tolerance. *6th Joint FAA/DoD/NASA aging aircraft conference*.

Frise, P. R. and Bell, R. (1992). Modeling Fatigue Crack-Growth and Coalescence in Notches. *International Journal of Pressure Vessels and Piping*, 51(1), 107-126.

Frost, N. E. (1959). A Relation between the Critical Alternating Propagation Stress and Crack Length for Mild Steel. *Proceedings of the Institution of Mechanical Engineers*, 173(1), 811-836.

Grandt, A., Thakker, A., and Tritsch, D. (1986). An Experimental and Numerical Investigation of the Growth and Coalescence of Multiple Fatigue Cracks at Notches. *Fracture Mechanics: Seventeenth Volume, ASTM STP 905*.

Harrington, D. S. (1995). *Fatigue crack coalescence and shape development: an experimental investigation*. Master's thesis, Carleton University, Department of Mechanical and Aerospace Engineering.

Hirt, M. A. and Fisher, J. W. (1973). Fatigue crack growth in welded beams. *Engineering Fracture Mechanics*, 5(2), 415-429.

Hobbacher, A. (1993). Stress Intensity Factors of Welded-Joints. *Engineering Fracture Mechanics*, 46(2), 173-182.

Hoh, H. J., Pang, J. H. L., and Tsang, K. S. (2016). Stress intensity factors for fatigue analysis of weld toe cracks in a girth-welded pipe. *International Journal of Fatigue*, 87, 279-287.

Hudak Jr, S., McClung, R., Bartlett, M., Fitzgerald, J., and Russell, D.

(1990). A comparison of single-cycle versus multiple-cycle proof testing strategies. *Contractor report no. 4318*. National Aeronautics and Space Administration, Washington, DC.

Iida, K. and Kawahara, M. (1980). Propagation and coalescence of fatigue cracks initiated from collinear or parallel adjacent surface flaws. *Proceedings of 4th International Conference on Pressure Vessel Technology*, 257-263.

Irwin, G. R. (1962). Crack-extension force for a part-through crack in a plate. *Journal of Applied Mechanics*, 29(4), 651-654.

JCSS. (2011). *JCSS Probabilistic model code Part 3: Resistance models*: Joint Committee on Structural Safety (JCSS).

Johnson, W. S. (2010). The history, logic and uses of the Equivalent Initial Flaw Size approach to total fatigue life prediction. *Procedia Engineering*, 2(1), 47-58.

Kamaya, M. (2008a). Growth evaluation of multiple interacting surface cracks. Part I: Experiments and simulation of coalesced crack. *Engineering Fracture Mechanics*, 75(6), 1336-1349.

Kamaya, M. (2008b). Influence of the Interaction on Stress Intensity Factor of Semielliptical Surface Cracks. *Journal of Pressure Vessel Technology*, 130(1), 011406-011406-011407.

Keating, P. B. and Fisher, J. W. (1986). Evaluation of Fatigue Tests and Design Criteria on Welded Details. *NCHRP Report 286*. Transportation Research Board, Washington, DC.

King, R. (1998). A review of fatigue crack growth rates in air and seawater', *HSE Report OTH 511*. Health and Safety Executive Books, London.

Leander, J. and Al-Emrani, M. (2016). Reliability-based fatigue assessment of steel bridges using LEFM - A sensitivity analysis. *International Journal of Fatigue*, 93, 82-91.

Leek, T. H. and Howard, I. C. (1996). An examination of methods of assessing interacting surface cracks by comparison with experimental data. *International Journal of Pressure Vessels and Piping*, 68(2), 181-201.

Lie, S. T., Zhao, H. S., and Vipin, S. P. (2017). New weld toe magnification factors for semi-elliptical cracks in plate-to-plate butt-welded joints. *Fatigue & Fracture of Engineering Materials & Structures*, 40(2), 207-220.

Lin, X. B. and Smith, R. A. (1997). Fatigue growth analysis of interacting and coalescing surface defects. *International Journal of Fracture*, 85(3), 283-299.

Liu, Y. M. and Mahadevan, S. (2009). Probabilistic fatigue life prediction using an equivalent initial flaw size distribution. *International Journal of Fatigue*, 31(3), 476-487.

Lukic, M. and Cremona, C. (2001). Probabilistic assessment of welded joints versus fatigue and fracture. *Journal of Structural Engineering-Asce*, 127(2), 211-218.

Maljaars, J., Steenbergen, H. M. G. M., and Vrouwenvelder, A. C. W. M. (2012). Probabilistic model for fatigue crack growth and fracture of welded joints in civil engineering structures. *International Journal of Fatigue*, 38, 108-117.

Marshall, W. (1982). *An assessment of the integrity of PWR pressure vessels*. Second report by a study group under the chairmanship of Dr.

W Marshall.

Miller, K. J. (1987). The Behavior of Short Fatigue Cracks and Their Initiation .2. A General Summary. *Fatigue & Fracture of Engineering Materials & Structures*, 10(2), 93-113.

Murakami, Y. and Nemat-Nasser, S. (1983). Growth and stability of interacting surface flaws of arbitrary shape. *Engineering Fracture Mechanics*, 17(3), 193-210.

Newman, J. C. (1979). A Review and Assessment of the Stress-Intensity Factors for Surface Cracks. *STP 687*. ASTM

Newman, J. C., Phillips, E. P., and Swain, M. H. (1999). Fatigue-life prediction methodology using small-crack theory. *International Journal of Fatigue*, 21(2), 109-119.

Newman, J. C. and Raju, I. S. (1981). An Empirical Stress-Intensity Factor Equation for the Surface Crack. *Engineering Fracture Mechanics*, 15(1-2), 185-192.

Norris, S. N. and Fisher, J. W. (1981). The fatigue behaviour of welded web attachments. *Journal of Constructional Steel Research*, 1(2), 27-38.

Pang, J. H. L., Hoh, H. J., Tsang, K. S., Low, J., Kong, S. C., and Yuan, W. G. (2017). Fatigue crack propagation analysis for multiple weld toe cracks in cut-out fatigue test specimens from a girth welded pipe. *International Journal of Fatigue*, 94, 158-165.

Pang, J. H. L., Tsang, K. S., and Hoh, H. J. (2016). 3D stress intensity factors for weld toe semi-elliptical surface cracks using XFEM. *Marine Structures*, 48, 1-14.

Paris, P. C. and Erdogan, F. (1963). A Critical Analysis of Crack

Propagation Laws. *Journal of Basic Engineering*, 85(4), 528-533.

Paris, P. C. and Sih, G. C. (1965). Stress Analysis of Cracks. *STP 381*. ASTM.

Pipinato, A., Pellegrino, C., and Modena, C. (2011). Fatigue assessment of highway steel bridges in presence of seismic loading. *Engineering Structures*, 33(1), 202-209.

Raju, I. S. and Newman, J. C. (1986). *STRESS-INTENSITY FACTORS FOR CIRCUMFERENTIAL SURFACE CRACKS IN PIPES AND RODS UNDER TENSION AND BENDING LOADS*. ASTM Special Technical Publication.

Recho, N. (1984). Potential use of fracture mechanics in the fatigue design of fillet welded joints. *Proceedings of the 5th European Conference on Fracture*.

Ritchie, R. O. and Lankford, J. (1986). Small Fatigue Cracks - a Statement of the Problem and Potential Solutions. *Materials Science and Engineering*, 84(1-2), 11-16.

Roy, S., Park, Y. C., Sause, R., Fisher, J. W., and Kaufmann, E. J. (2011). Cost-effective connection details for highway sign, luminaire, and traffic signal structures. *NCHRP Web-Only Document 176*. Transportation Research Board, Washington, DC.

Rudd, J. L. and Gray, T. D. (1976). Equivalent initial quality method. *AFFDL-TM-76-83-FBE*.

Shahani, A. R. and Moayeri Kashani, H. (2013). Assessment of equivalent initial flaw size estimation methods in fatigue life prediction using compact tension specimen tests. *Engineering Fracture Mechanics*, 99,

48-61.

Snijder, H. H., Gijsbers, F. B. J., Dijkstra, O. D., and Avest, F. J. T. (1987). Probabilistic fracture mechanics approach of fatigue and brittle fracture in tubular joints. *Proc. Steel in Marine Structures*, Amsterdam: Elsevier, 927-939.

Soboyejo, W. O., Knott, J. F., Walsh, M. J., and Cropper, K. R. (1990). Fatigue crack propagation of coplanar semi-elliptical cracks in pure bending. *Engineering Fracture Mechanics*, 37(2), 323-340.

Tanaka, T., Sakai, T., and Okada, K. (1985). A statistical study on fatigue life distribution based on the coalescence of cracks from surface defects. *Bulletin of JSME*, 28(236), 209-216.

Twaddle, B. R. and Hancock, J. W. (1988). The development of cracks by defect coalescence. *Proceedings of Conference on Fatigue of Offshore Structures*, 185–198.

Venkateswaran, P., Raman, S. G. S., and Pathak, S. D. (2005). Short fatigue crack growth behaviour of a ferritic steel weld metal. *Science and Technology of Welding and Joining*, 10(1), 95-102.

Vialaton, G., Lhermet, G., Vessiere, G., Boivin, M., and Bahuaud, J. (1976). Field of stresses in an infinite plate containing two collinear cuts loaded at an arbitrary location. *Engineering Fracture Mechanics*, 8(3), 525-538.

Yamada, K. and Nagatsu, S. (1989). Evaluation of scatter in fatgue life of welded details using fracture mechanics. *Structural Engineering/Earthquake Engineering*, 6(1), 13-21.

Yazdani, N. and Albrecht, P. (1990). Probabilistic Fracture-Mechanics Application to Highway Bridges. *Engineering Fracture Mechanics*,

37(5), 969-985.

Zettlemoyer, N. and Fisher, J. W. (1977). Stress gradient correction factor for stress intensity at welded stiffeners and cover plates. *Welding Research Supplement*, 56(12), 393-398.

Zettlemoyer, N. and Fisher, J. W. (1978). Stress gradient and Crack shape effects on stress intensity at welded details. *Welding Journal Research Supplement*, 57(8), 246-250.

Zhang, Y. H., Maddox, S. J., and Razmjoo, G. R. (2002). Experimental Study and Prediction of Fatigue Crack Growth in Girth Welded Pipes. (36134), 525-533.

Zhou, H., Shi, G., Wang, Y., Chen, H., and De Roeck, G. (2016). Fatigue evaluation of a composite railway bridge based on fracture mechanics through global–local dynamic analysis. *Journal of Constructional Steel Research*, 122, 1-13.

APPENDIX A. FATIGUE TEST RESULTS

In this appendix, information of fatigue tests performed in NCHRP Project 10-70 are summarized in Table A1 and A2. Identified number of crack initiation points is shown in Table A3. Fatigue fracture surfaces and identified crack initiation points are shown in Figure A1 to Figure A16.

Table A1. Applied parameters in specimens

Specimen type	Detail	$S_{r,hs}$ due to membrane stress (MPa)*	$S_{r,hs}$ due to bending stress (MPa)*	DOB	L/T	θ (degree)
Type I-1	Arm	78.0	181.9	0.70	12.6	42
Type I-2	Arm	78.0	181.9	0.70	12.6	26
Type I-3	Arm	78.0	181.9	0.70	12.6	20
Type I-4	Arm	45.5	106.1	0.70	12.6	30
Type I-5	Arm	45.5	106.1	0.70	12.6	30
Type I-5	Pole	26.0	82.7	0.76	9.4	34
Type I-6	Arm	45.5	106.1	0.70	12.6	30
Type I-7	Arm	45.5	106.1	0.70	12.6	30
Type I-7	Pole	18.2	58.0	0.76	9.4	35
Type II-1	Pole	28.0	65.7	0.70	9.4	30
Type III-1	Arm	77.9	107.6	0.58	12.6	30
Type III-2	Arm	77.9	107.6	0.58	12.6	30
Type III-3	Arm	77.9	107.6	0.58	12.6	30
Type III-4	Arm	103.9	143.5	0.58	12.6	30
Type III-8	Arm	103.9	143.5	0.58	12.6	30
Type V-1	Pole	50.9	75.2	0.60	9.4	30

* Applied nominal stress is 82.7MPa in case of arm and 46.9MPa in case of pole

Table A2. Results of fatigue test at fracture state

Specimen	Detail	Length of crack (mm)	Number of cycles
Type I-1	Arm	191	180,200
Type I-2	Arm	71+48*	406,300
Type I-3	Arm	89+31*	1,773,000
Type I-4	Arm	109	2,741,000
Type I-5	Arm	97	5,986,000
Type I-5	Pole	152	3,634,000
Type I-6	Arm	112	2,136,000
Type I-7	Arm	109	2,868,000
Type I-7	Pole	170	8,319,000
Type II-1	Pole	94+33*	2,395,000
Type III-1	Arm	91+31*	1,422,000
Type III-2	Arm	112	5,085,000
Type III-3	Arm	104	2,202,000
Type III-4	Arm	74+41*	284,500
Type III-8	Arm	53	6,666,000
Type V-1	Pole	38+58*	270,600

* two large cracks exist in fracture surface

Table A3. Number of identified crack initiation points

Specimen	Detail	Number of crack initiation point
Type I-1	Arm	24
Type I-2	Arm	17
Type I-3	Arm	12
Type I-4	Arm	20
Type I-5	Arm	12
Type I-5	Pole	20
Type I-6	Arm	10
Type I-7	Arm	10
Type I-7	Pole	14
Type II-1	Pole	13
Type III-1	Arm	16
Type III-2	Arm	12
Type III-3	Arm	10
Type III-4	Arm	14
Type III-8	Arm	7
Type V-1	Pole	12

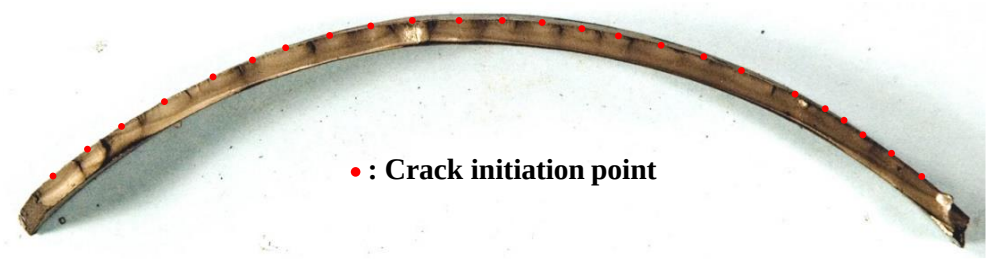

Figure A1. Fatigue fracture surface and identified crack initiation points in Type I-1 Arm

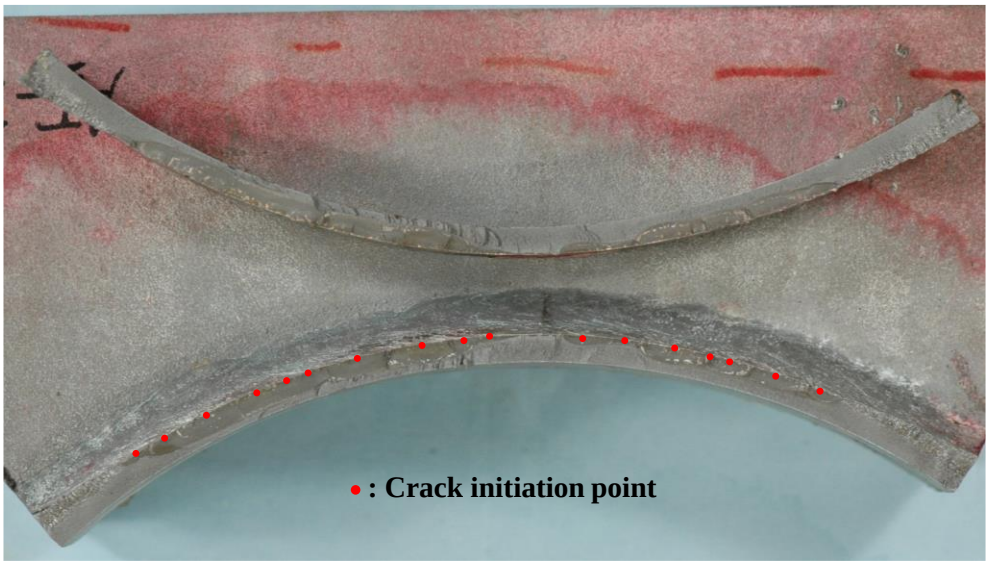

Figure A2. Fatigue fracture surface and identified crack initiation points in Type I-2 Arm

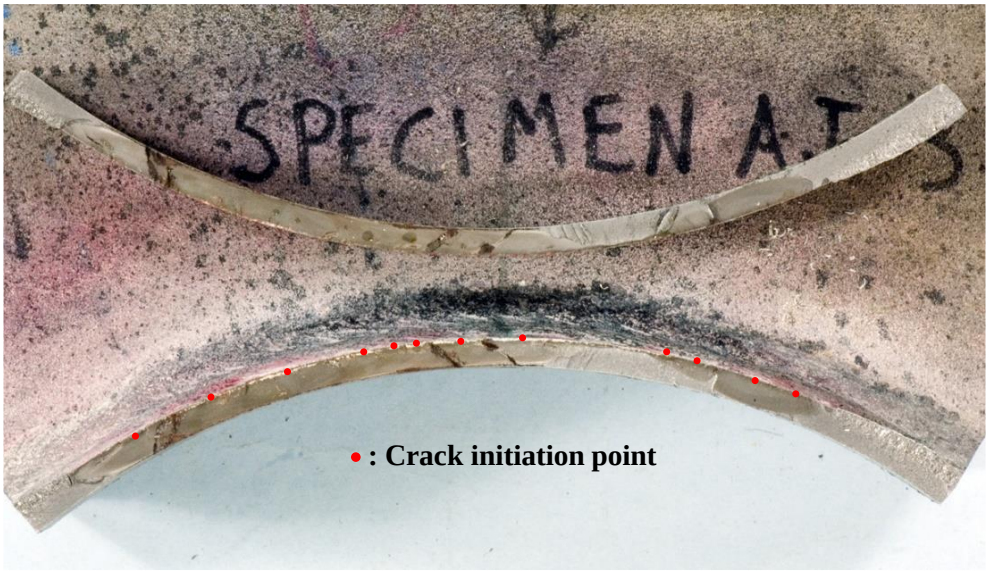

Figure A3. Fatigue fracture surface and identified crack initiation points in Type I-3 Arm

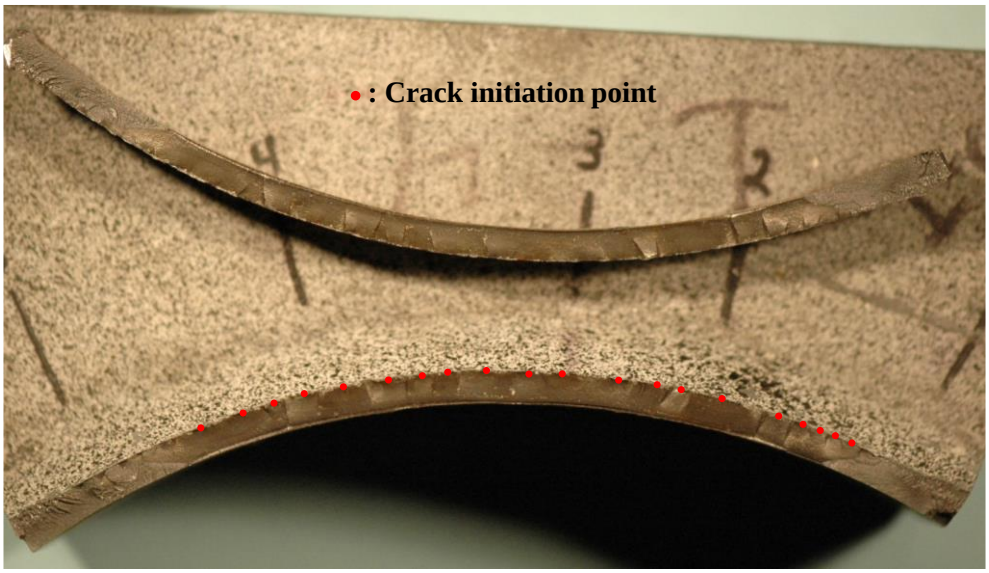

Figure A4. Fatigue fracture surface and identified crack initiation points in Type I-4 Arm

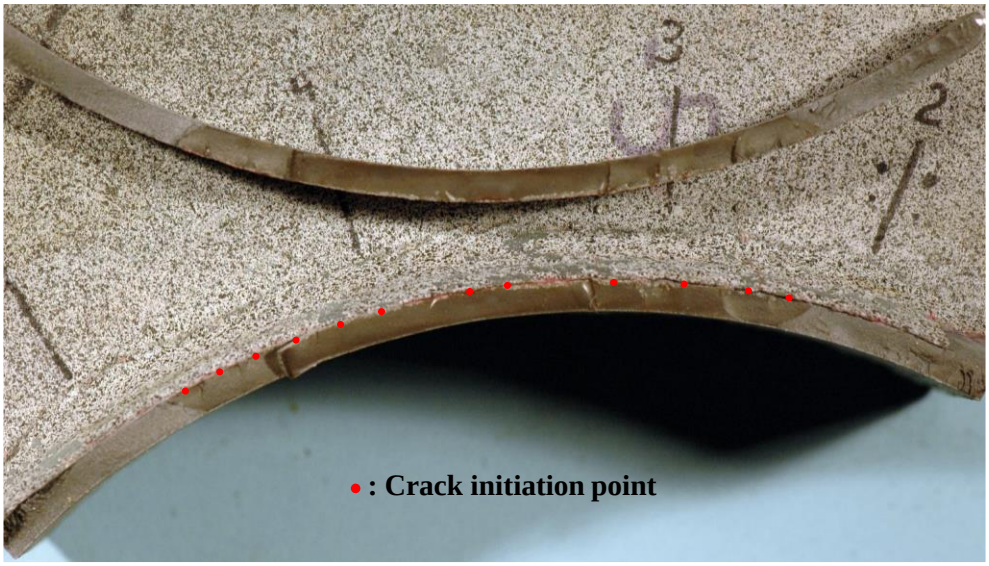

Figure A5. Fatigue fracture surface and identified crack initiation points in Type I-5 Arm

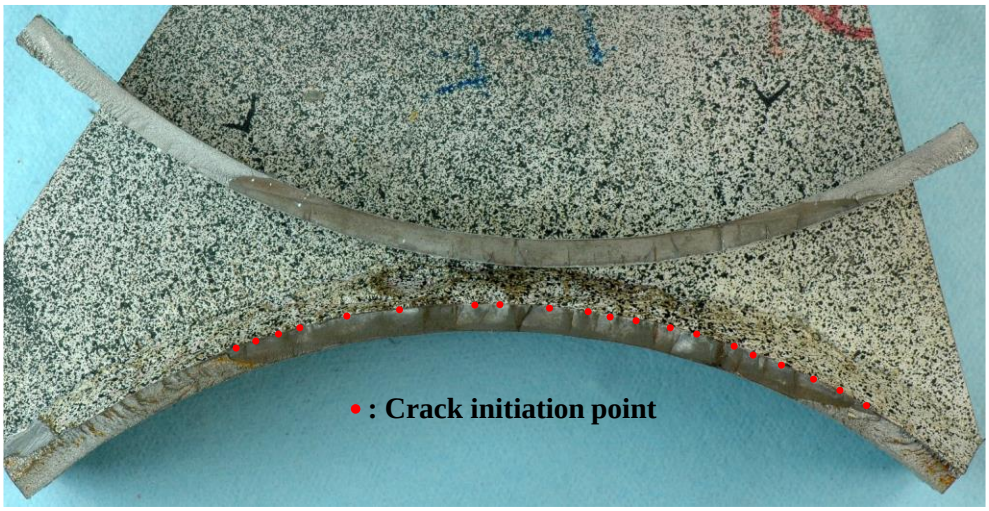

Figure A6. Fatigue fracture surface and identified crack initiation points in Type I-5 Pole

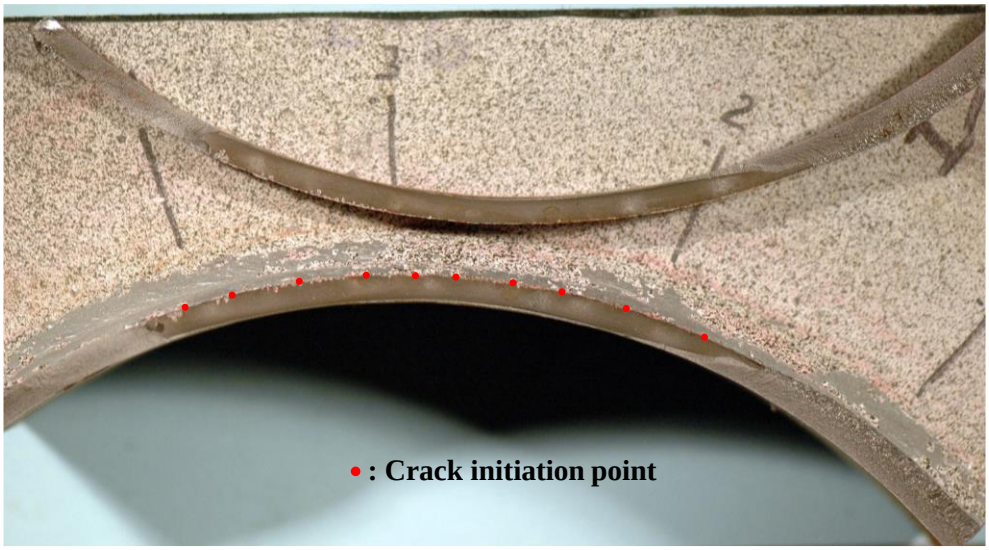

Figure A7. Fatigue fracture surface and identified crack initiation points in Type I-6 Arm

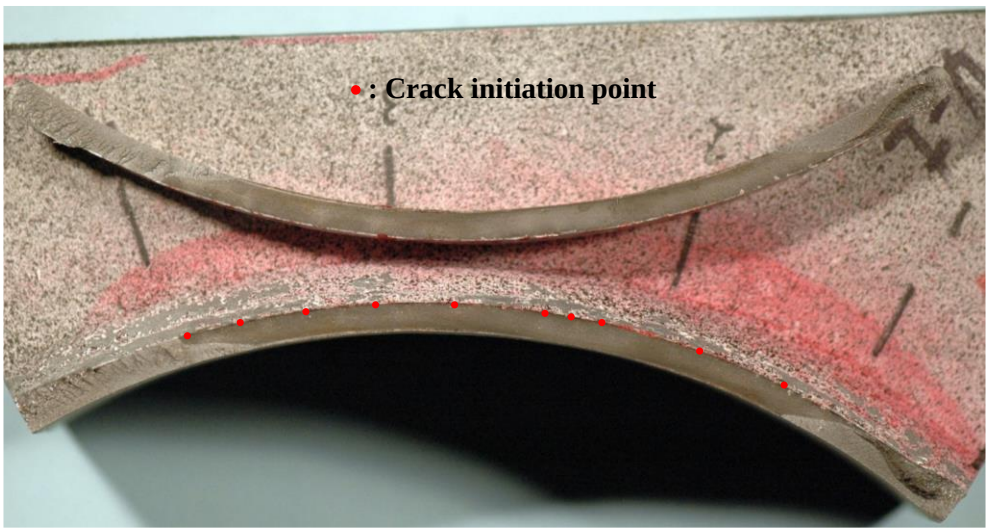

Figure A8. Fatigue fracture surface and identified crack initiation points in Type I-7 Arm

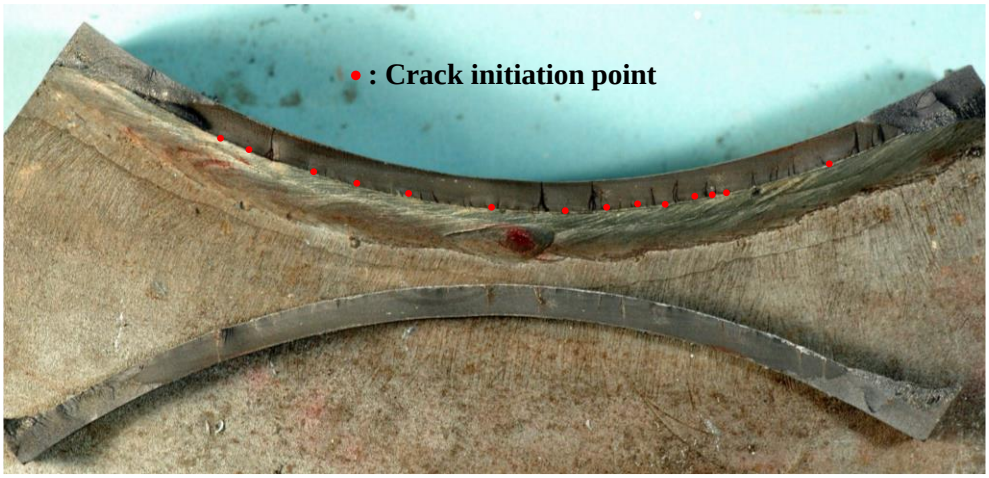

Figure A9. Fatigue fracture surface and identified crack initiation points in Type I-7 Pole

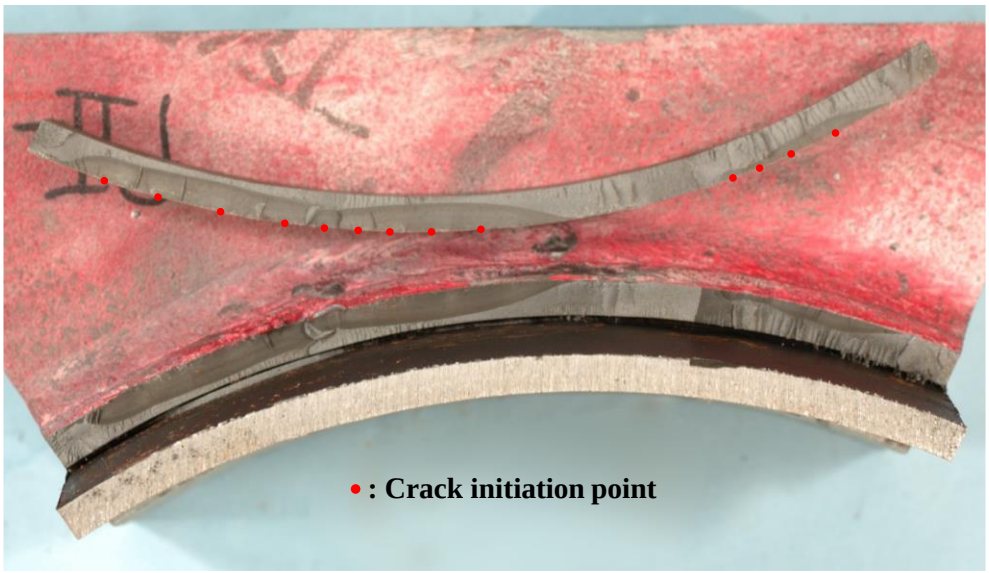

Figure A10. Fatigue fracture surface and identified crack initiation points in Type II-1 Pole

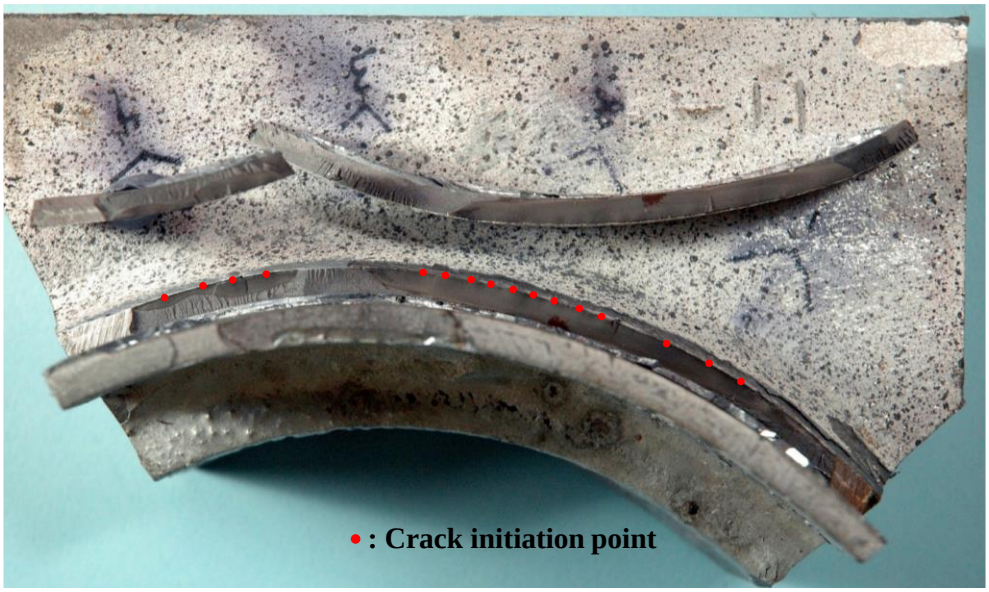

Figure A11. Fatigue fracture surface and identified crack initiation points in Type III-1 Arm

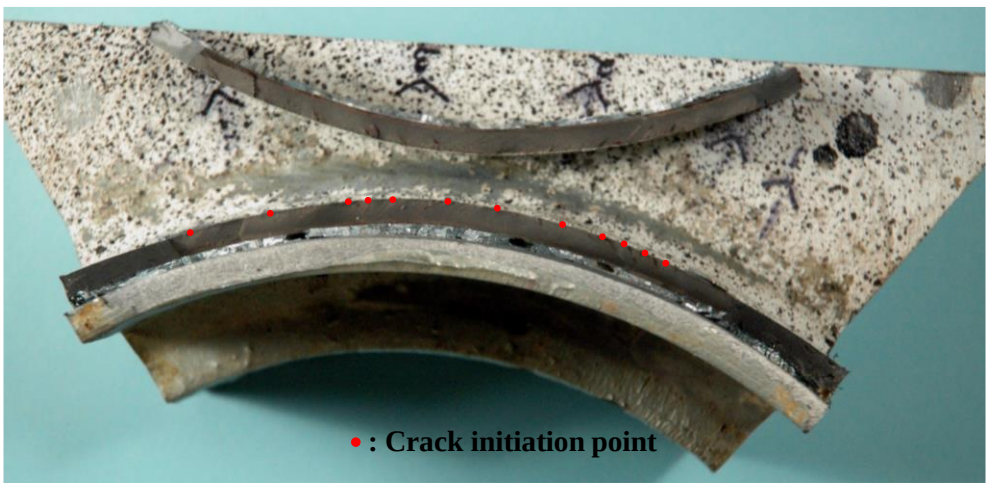

Figure A12. Fatigue fracture surface and identified crack initiation points in Type III-2 Arm

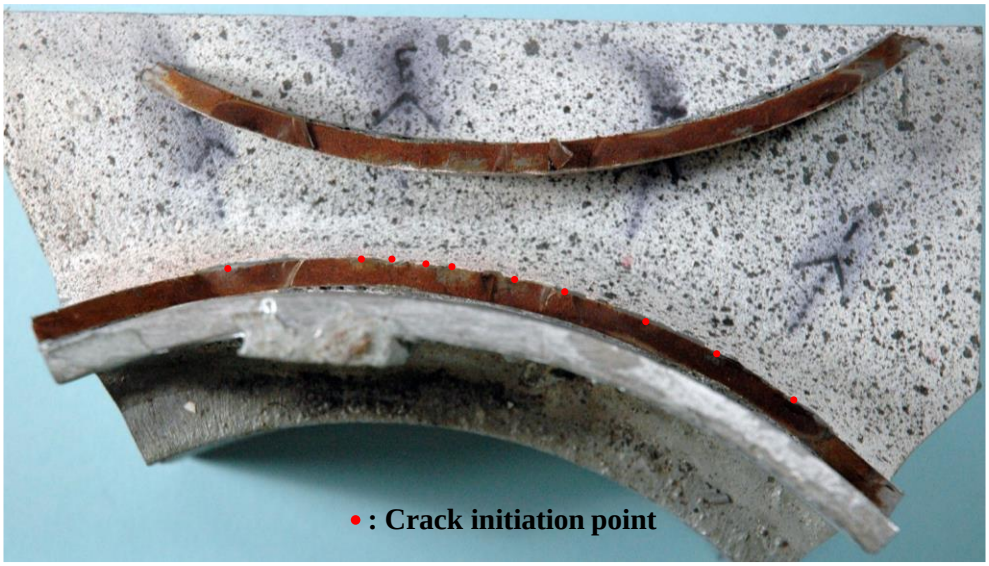

Figure A13. Fatigue fracture surface and identified crack initiation points in Type III-3 Arm

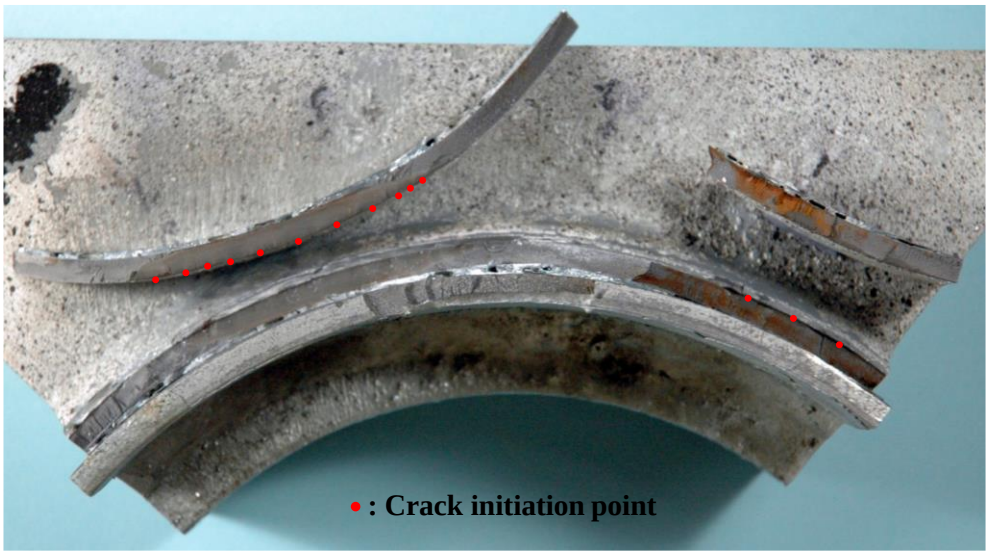

Figure A14. Fatigue fracture surface and identified crack initiation points in Type III-4 Arm

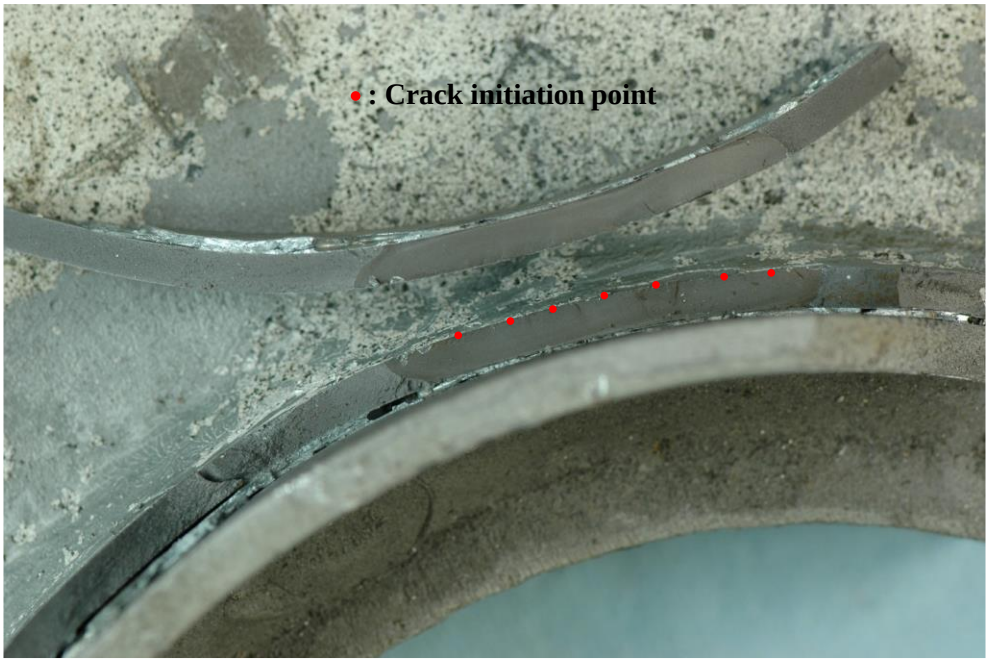

Figure A15. Fatigue fracture surface and identified crack initiation points in Type III-8 Arm

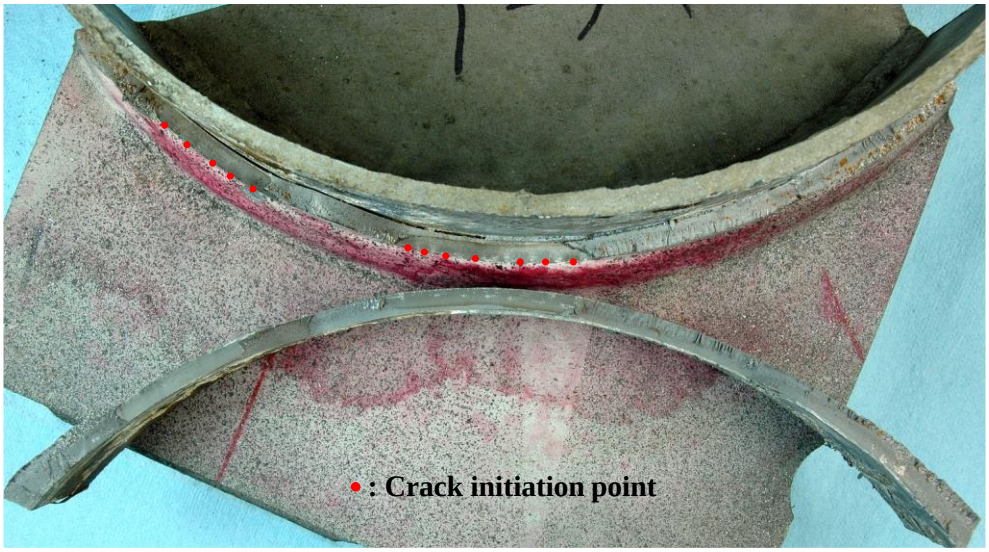

Figure A16. Fatigue fracture surface and identified crack initiation points in Type V-1 Pole

APPENDIX B. EIFS DISTRIBUTION

Information about EIFS obtained from 46 crack initiation points is included in Table B1. Table B1 shows the type of crack in each test specimen and the number of outlier. Outlier represents the invalid EIFS lower than depth of crack of lower validity limit in SIF equation. Histogram of EIFS is shown in Figure B1 to Figure B40. If outliers are more than 95% of total number of simulation, the histogram is not drawn, but valid EIFS is included for determining probability model.

Table B1. Information about EIFS obtained from 46 crack initiation points

Specimen type	Crack No.	Types of crack	Number of outlier	Ratio of outlier (%)
I-1 Arm	1	Thickness	3	0.1
I-2 Arm	1	Surface	365	12.2
	2	Surface	16	0.5
	3	Surface	8	0.3
	4	Surface	10	0.3
	5	Surface	9	0.3
	6	Surface	14	0.5
	7	Surface	14	0.5
	8	Surface	14	0.5
	9	Surface	48	1.6

Specimen type	Crack No.	Types of crack	Number of outlier	Ratio of outlier (%)
	10	Surface	1876	62.5
	11	Surface	176	5.9
	12	Surface	881	29.4
	13	Surface	16	0.5
	14	Surface	71	2.4
	15	Surface	20	0.7
	16	Surface	15	0.5
	17	Surface	83	2.8
I-3 Arm	1	Thickness	3000	100.0
	2	Thickness	2999	100.0
I-4 Arm	1	Thickness	2380	79.3
I-5 Arm	1	Thickness	3000	100.0
I-5 Pole	1	Thickness	171	5.7
I-6 Arm	1	Thickness	441	14.7
I-7 Arm	1	Thickness	1969	65.6
I-7 Pole	1	Thickness	7	0.2
II-1 Pole	1	Thickness	0	0.0
	2	Thickness	0	0.0

Specimen type	Crack No.	Types of crack	Number of outlier	Ratio of outlier (%)
	3	Surface	0	0.0
	4	Surface	0	0.0
	5	Surface	0	0.0
	6	Surface	0	0.0
III-1 Arm	1	Surface	2132	71.1
	2	Surface	2569	85.6
	3	Surface	1378	45.9
	4	Surface	1479	49.3
	5	Thickness	2434	81.1
III-2 Arm	1	Thickness	3000	100.0
III-3 Arm	1	Thickness	2988	99.6
III-4 Arm	1	Thickness	5	0.2
	2	Surface	0	0.0
	3	Surface	3	0.1
	4	Surface	5	0.2
III-8 Arm	1	Thickness	3000	100.0
V-1 Pole	1	Thickness	0	0.0
	2	Thickness	0	0.0

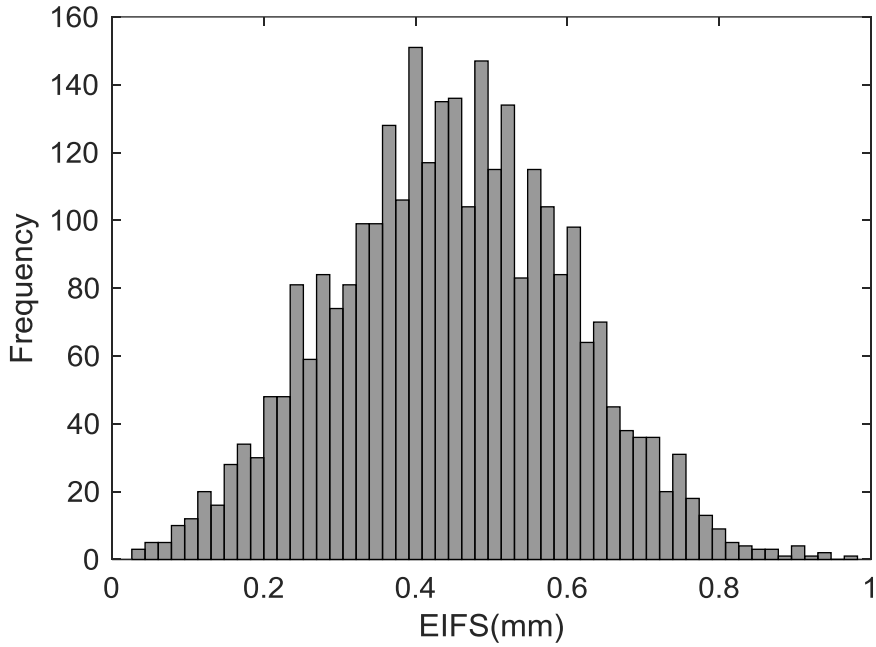

Figure B1. Histogram of EIFS in Type I-1 Arm

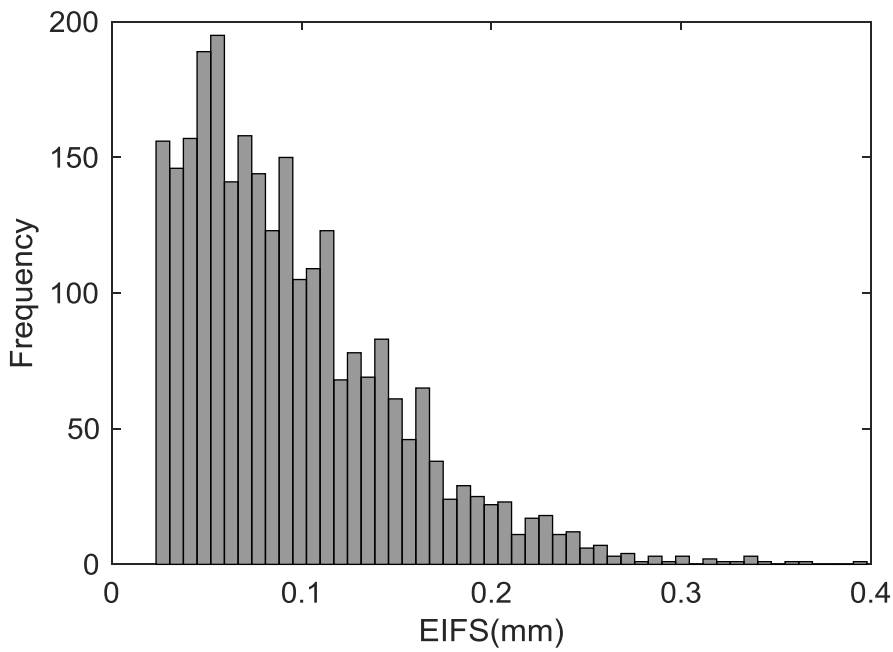

Figure B2. Histogram of EIFS in 1st crack of Type I-2 Arm

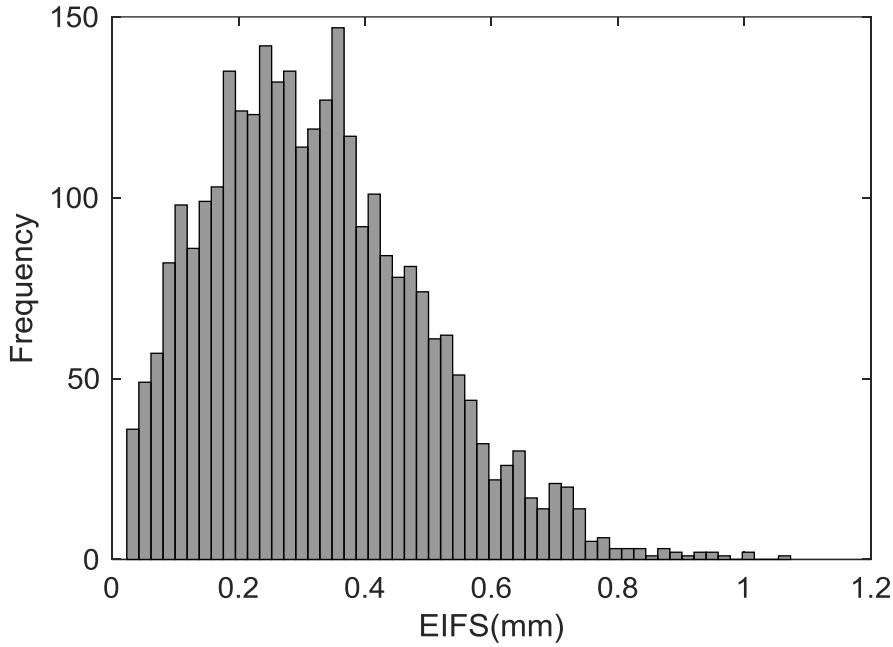

Figure B3. Histogram of EIFS in 2nd crack of Type I-2 Arm

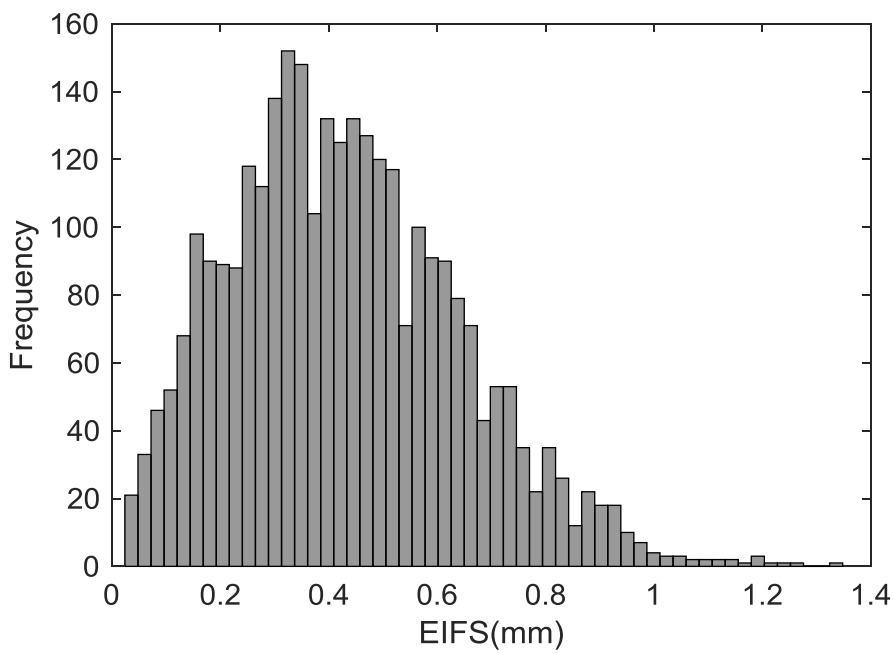

Figure B4. Histogram of EIFS in 3rd crack of Type I-2 Arm

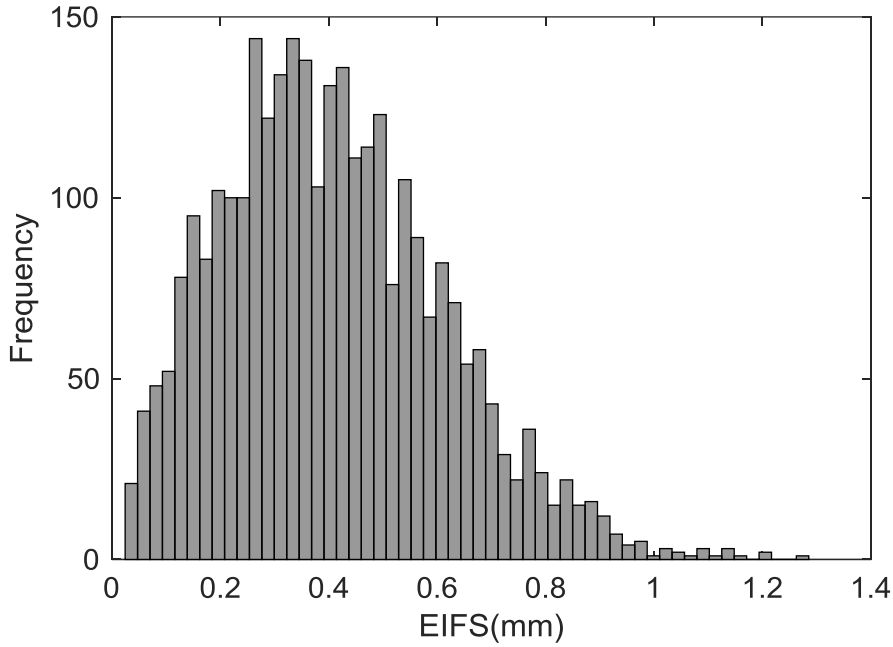

Figure B5. Histogram of EIFS in 4th crack of Type I-2 Arm

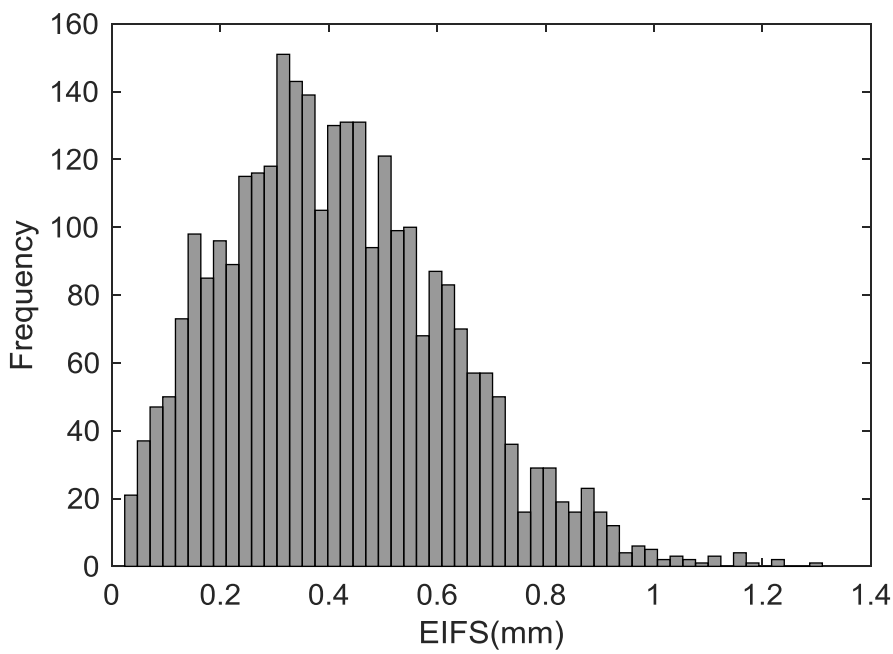

Figure B6. Histogram of EIFS in 5th crack of Type I-2 Arm

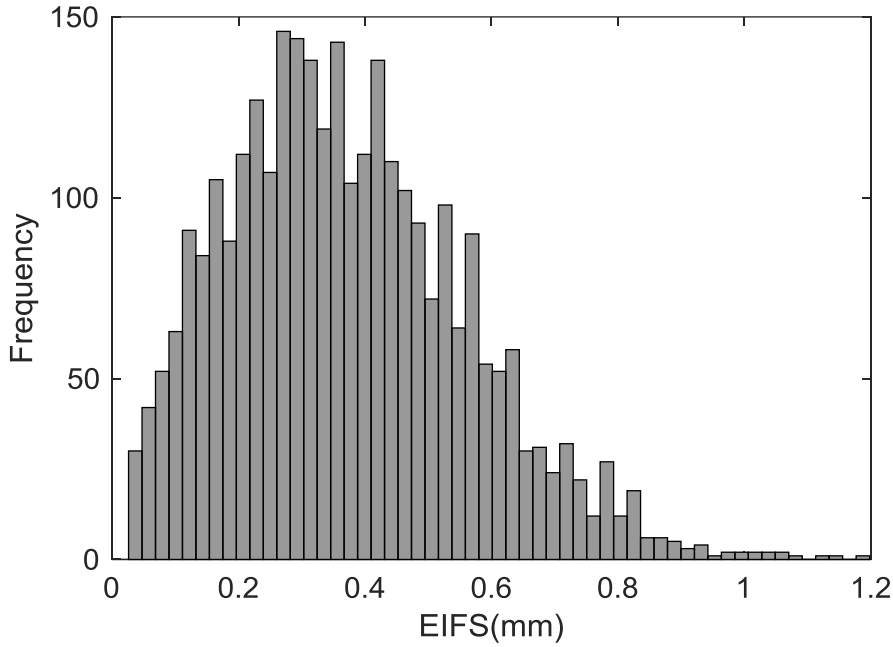

Figure B7. Histogram of EIFS in 6th crack of Type I-2 Arm

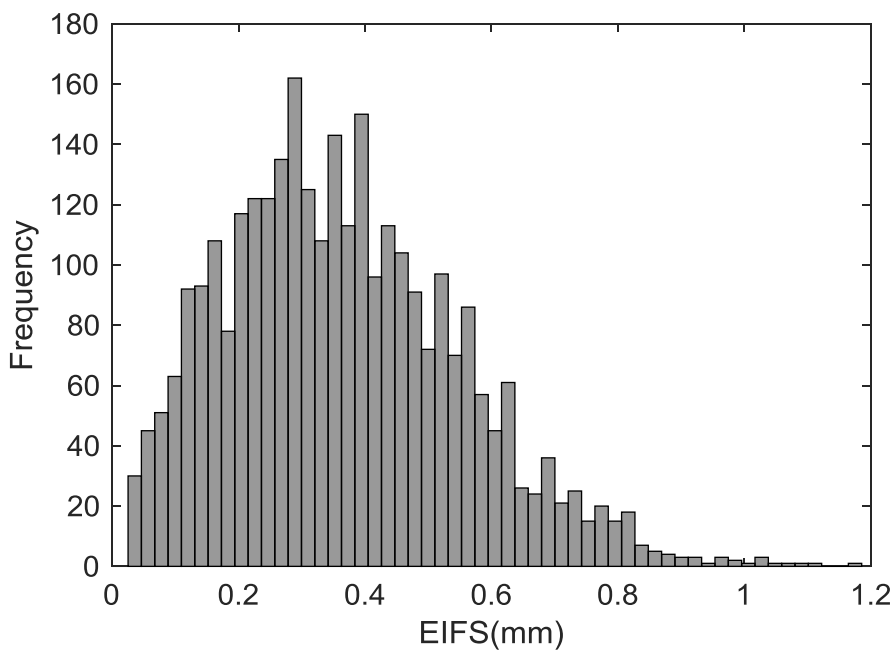

Figure B8. Histogram of EIFS in 7th crack of Type I-2 Arm

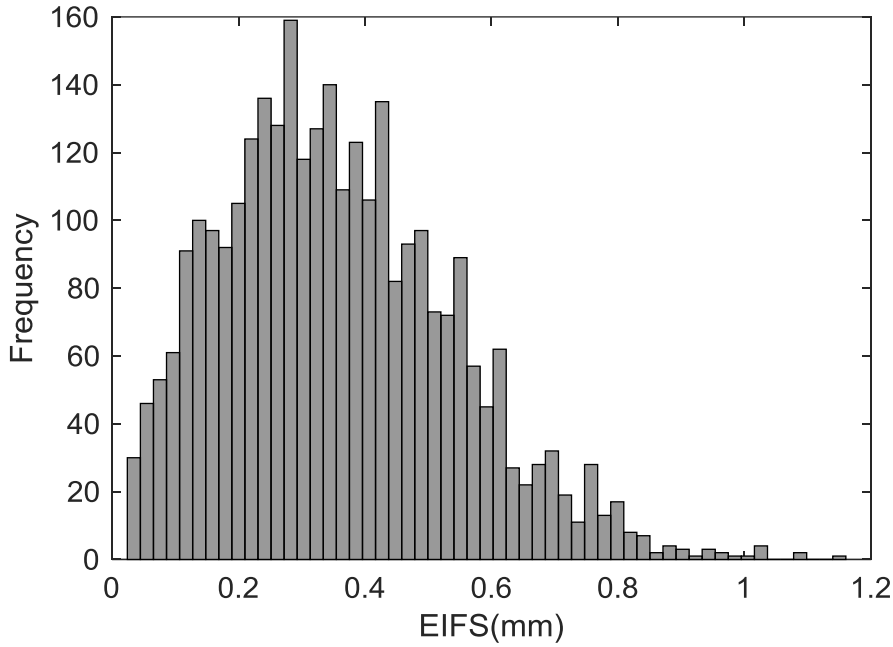

Figure B9. Histogram of EIFS in 8th crack of Type I-2 Arm

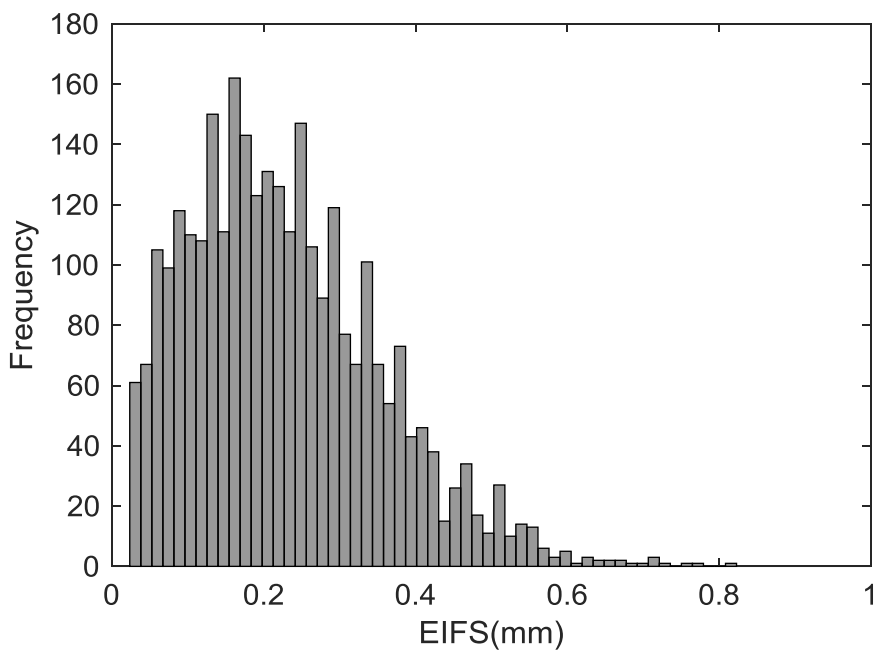

Figure B10. Histogram of EIFS in 9th crack of Type I-2 Arm

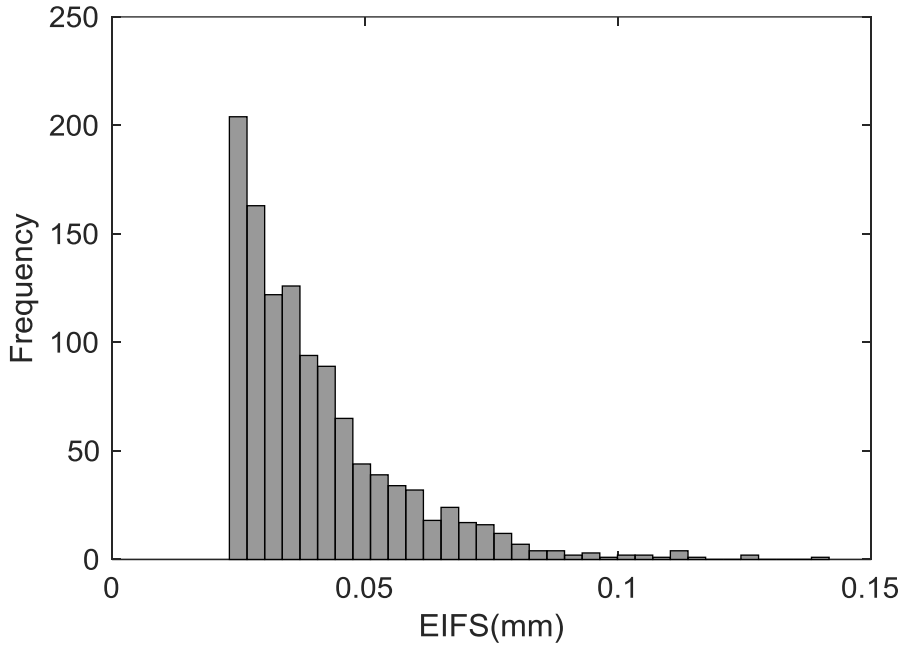

Figure B11. Histogram of EIFS in 10th crack of Type I-2 Arm

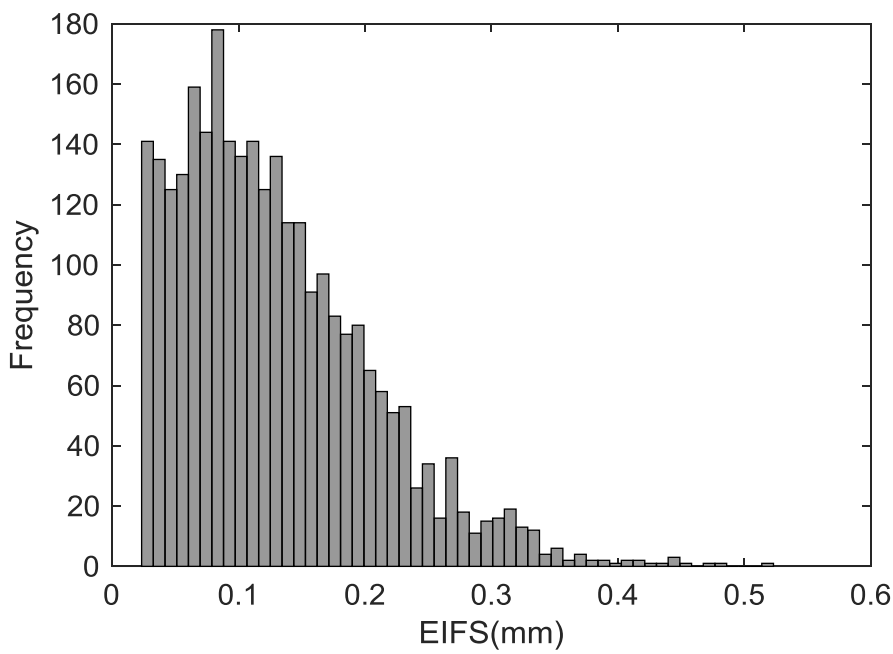

Figure B12. Histogram of EIFS in 11th crack of Type I-2 Arm

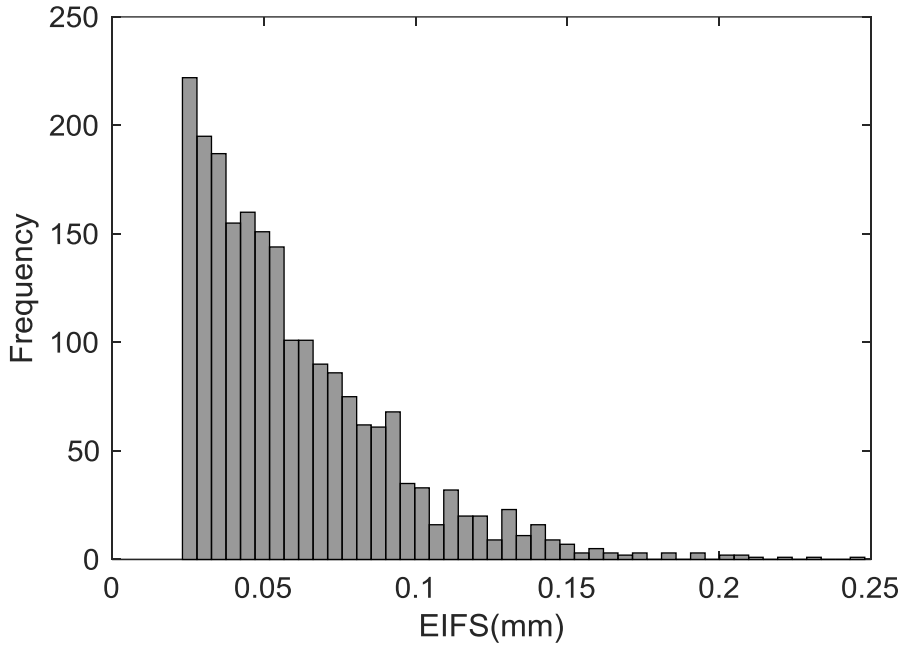

Figure B13. Histogram of EIFS in 12th crack of Type I-2 Arm

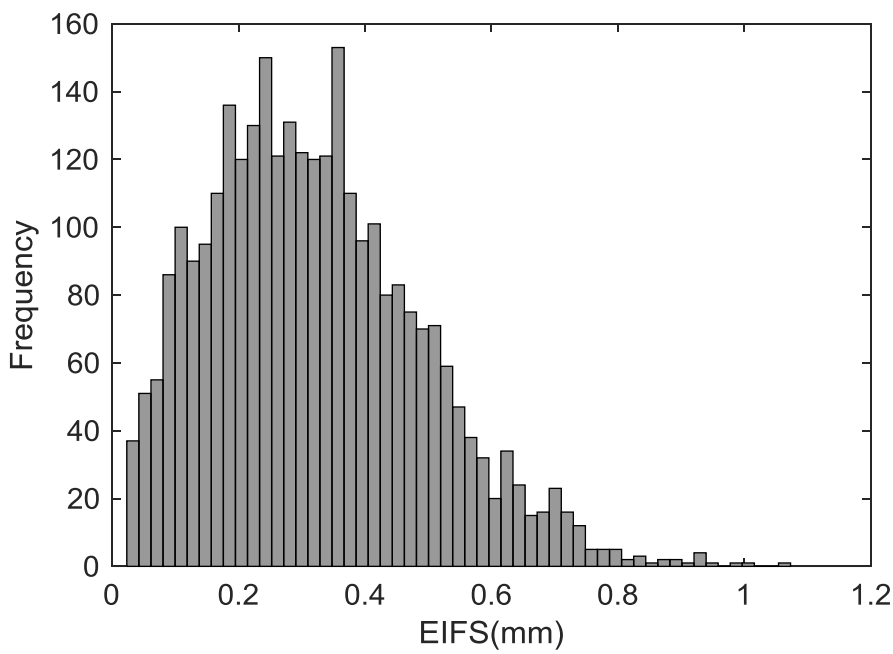

Figure B14. Histogram of EIFS in 13th crack of Type I-2 Arm

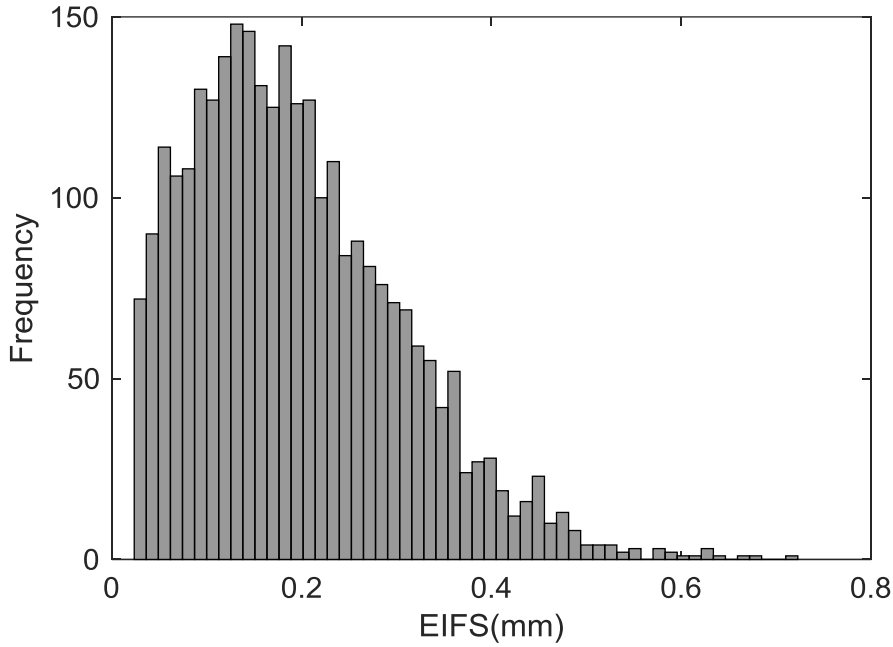

Figure B15. Histogram of EIFS in 14th crack of Type I-2 Arm

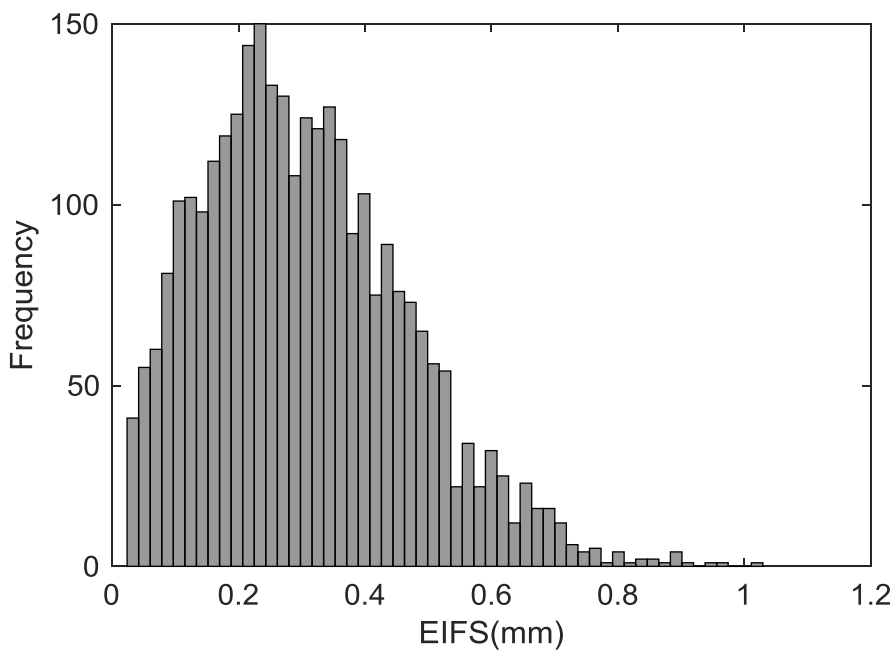

Figure B16. Histogram of EIFS in 15th crack of Type I-2 Arm

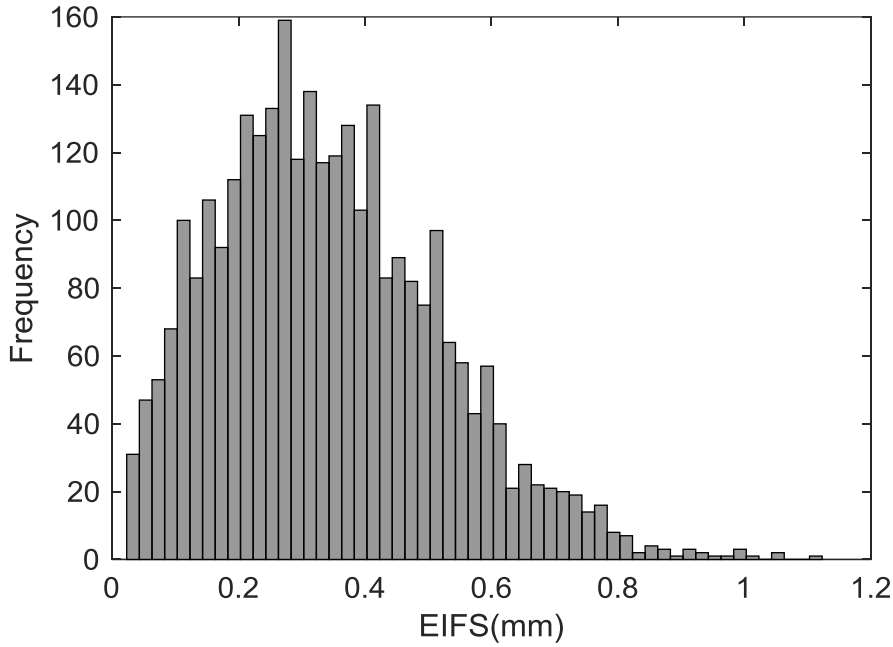

Figure B17. Histogram of EIFS in 16th crack of Type I-2 Arm

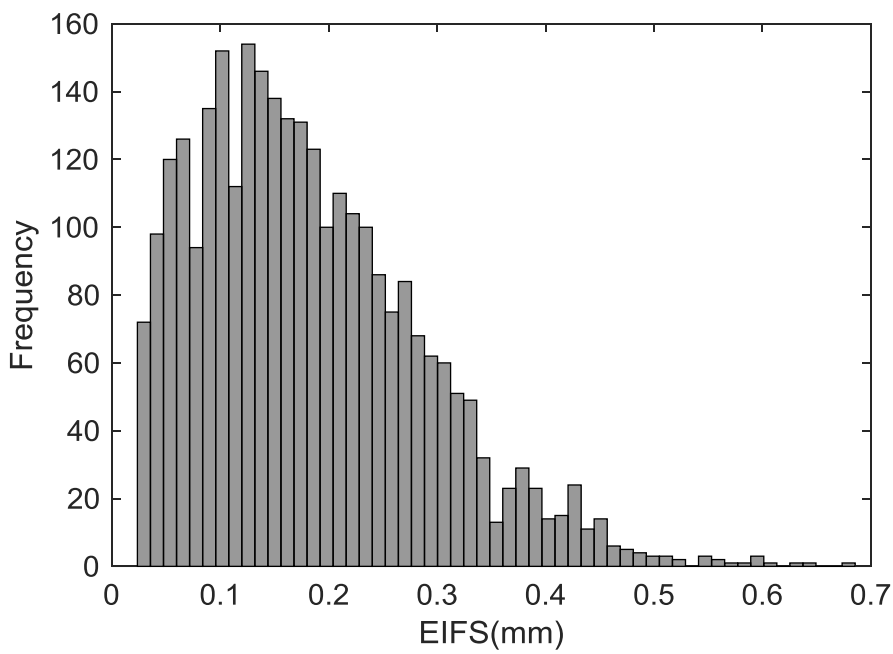

Figure B18. Histogram of EIFS in 17th crack of Type I-2 Arm

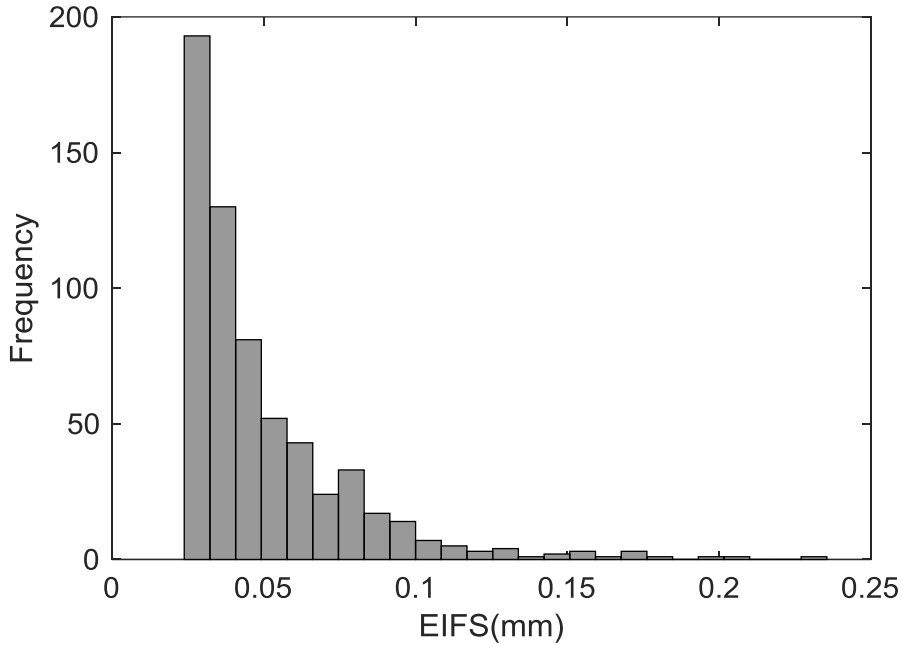

Figure B19. Histogram of EIFS in Type I-4 Arm

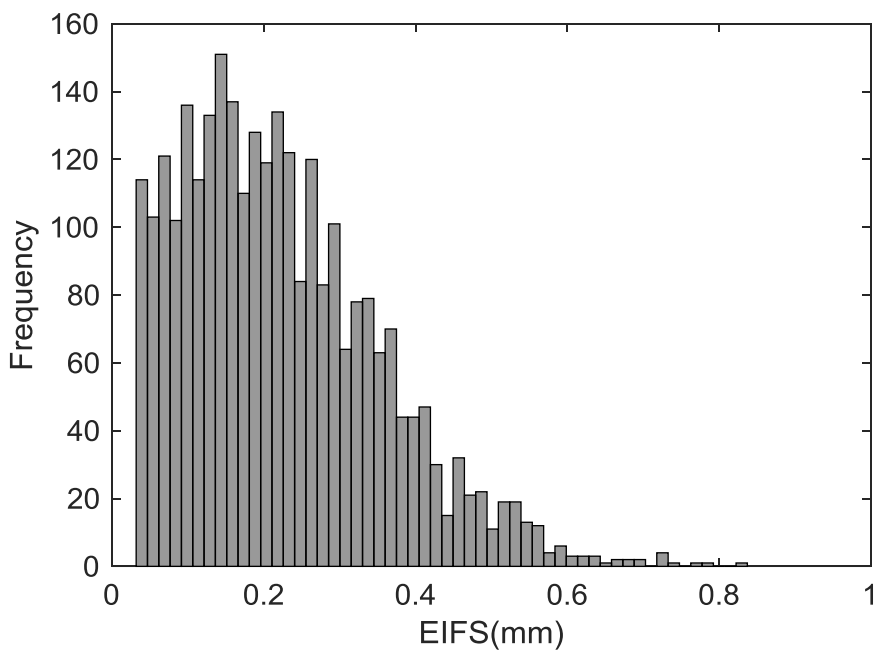

Figure B20. Histogram of EIFS in Type I-5 Pole

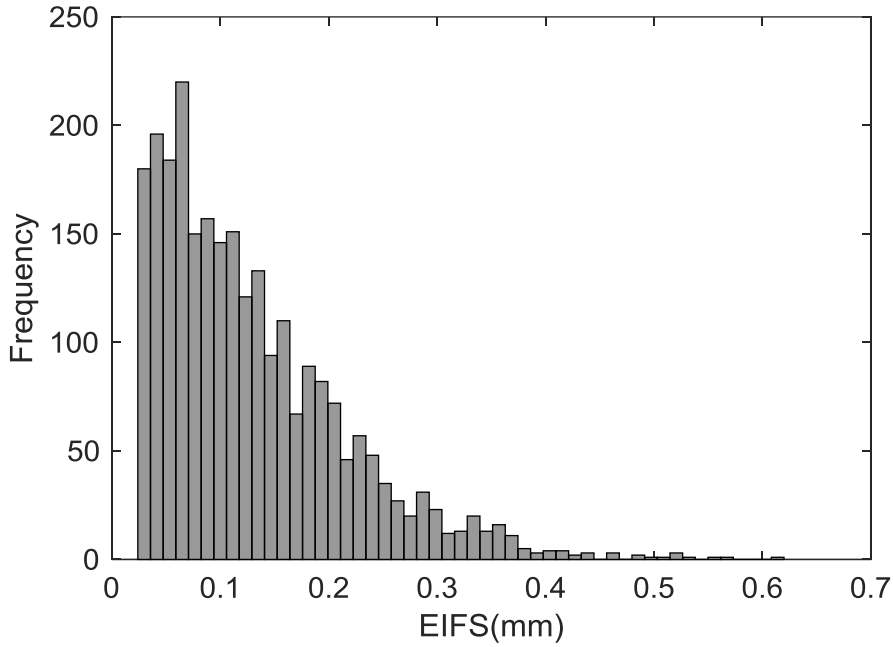

Figure B21. Histogram of EIFS in Type I-6 Arm

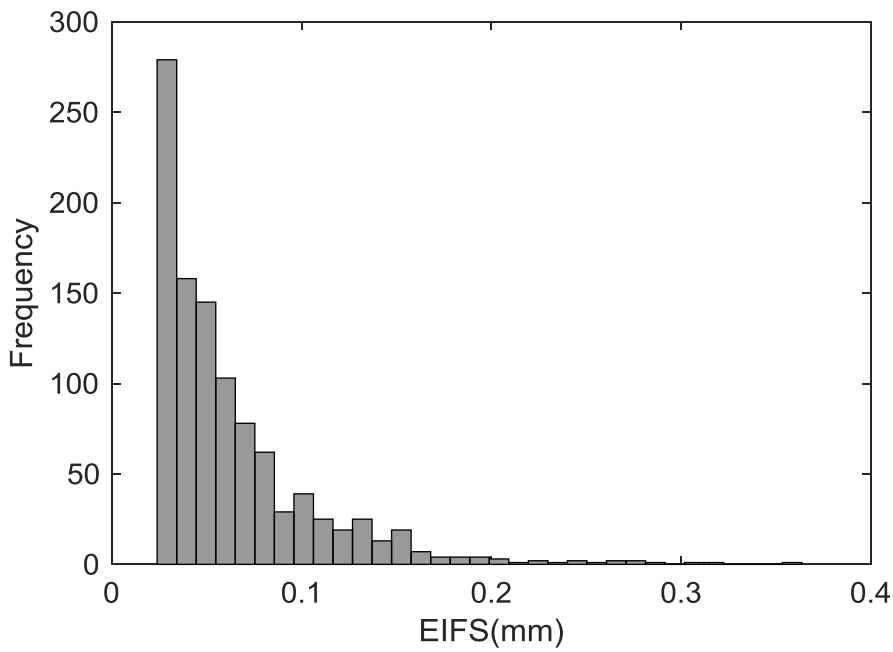

Figure B22. Histogram of EIFS in Type I-7 Arm

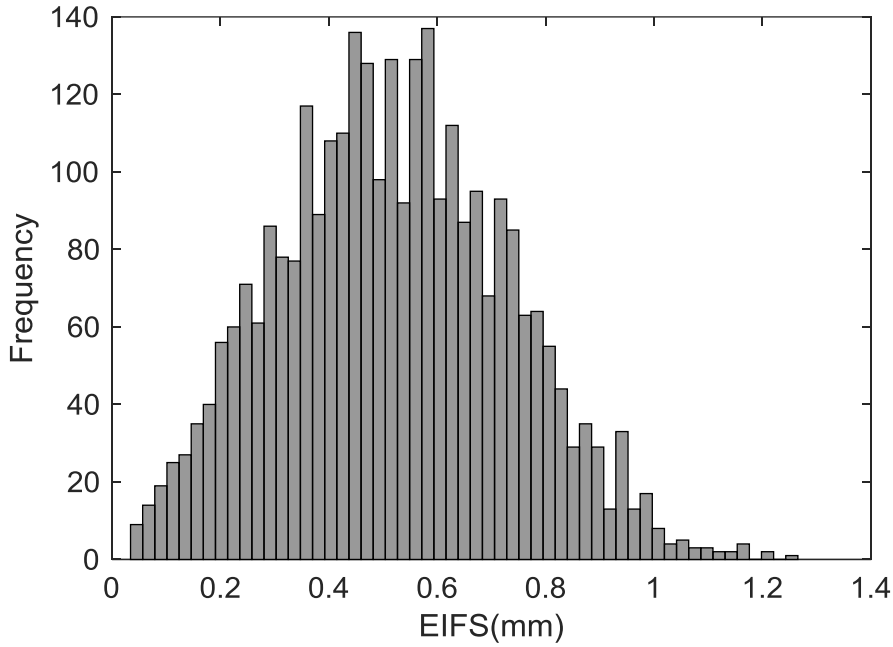

Figure B23. Histogram of EIFS in Type I-7 Pole

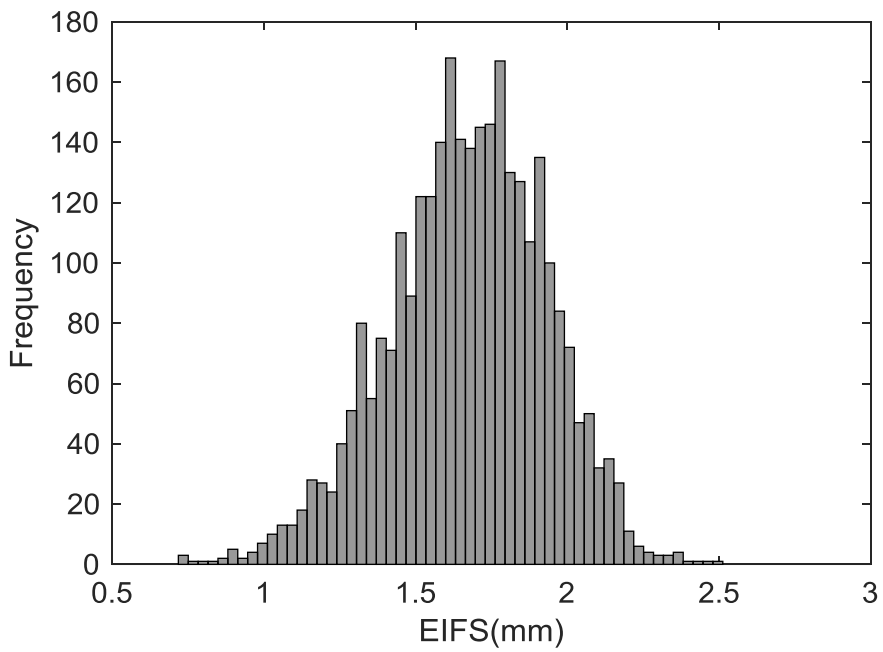

Figure B24. Histogram of EIFS in 1st crack of Type II-1 Pole

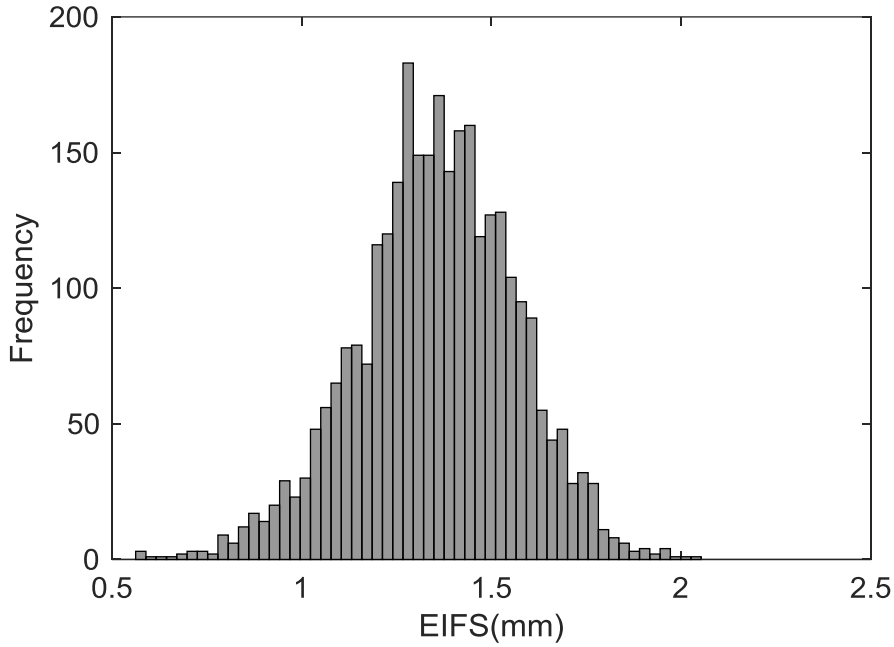

Figure B25. Histogram of EIFS in 2nd crack of Type II-1 Pole

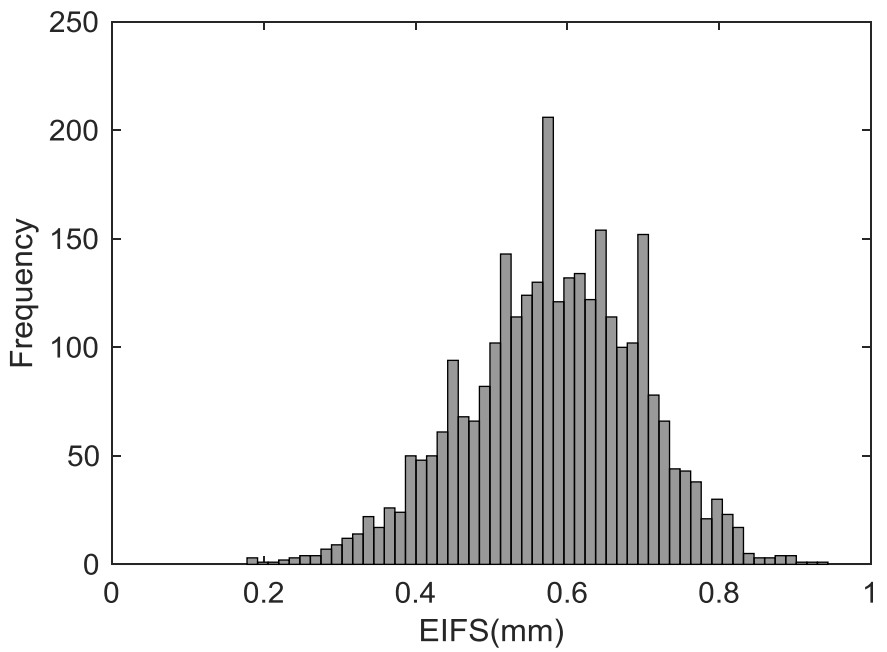

Figure B26. Histogram of EIFS in 3rd crack of Type II-1 Pole

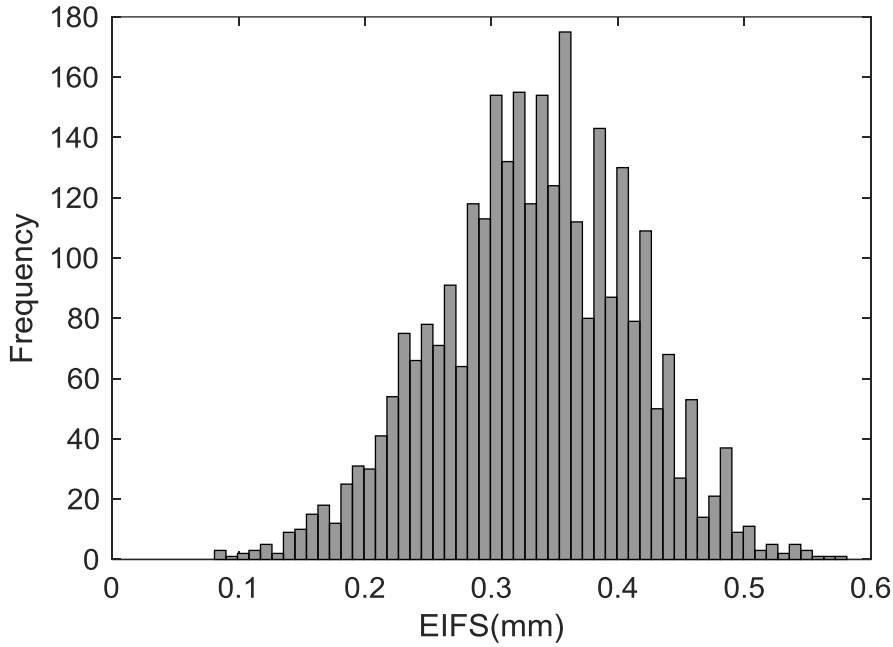

Figure B27. Histogram of EIFS in 4th crack of Type II-1 Pole

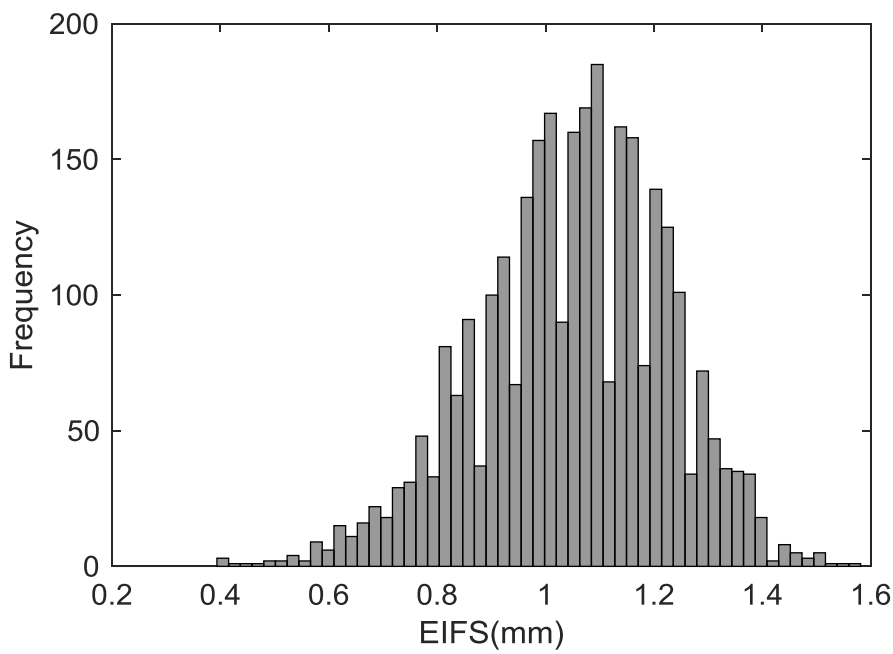

Figure B28. Histogram of EIFS in 5th crack of Type II-1 Pole

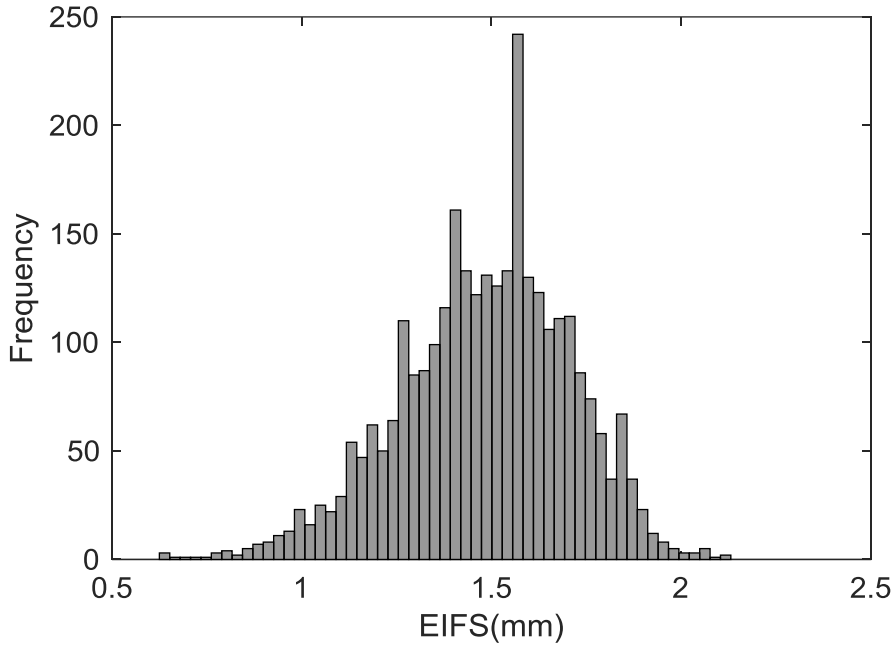

Figure B29. Histogram of EIFS in 6th crack of Type II-1 Pole

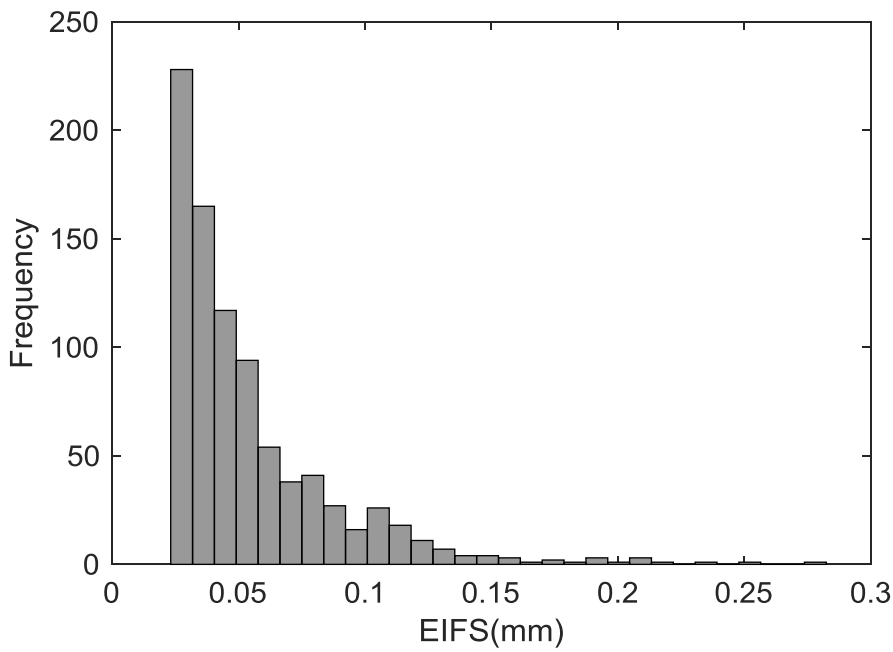

Figure B30. Histogram of EIFS in 1st crack of Type III-1 Arm

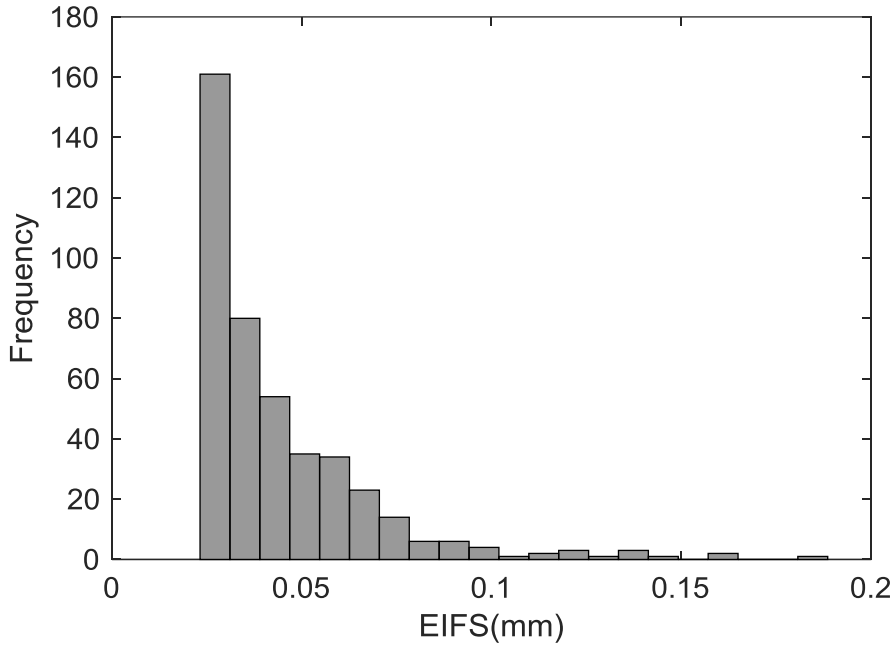

Figure B31. Histogram of EIFS in 2nd crack of Type III-1 Arm

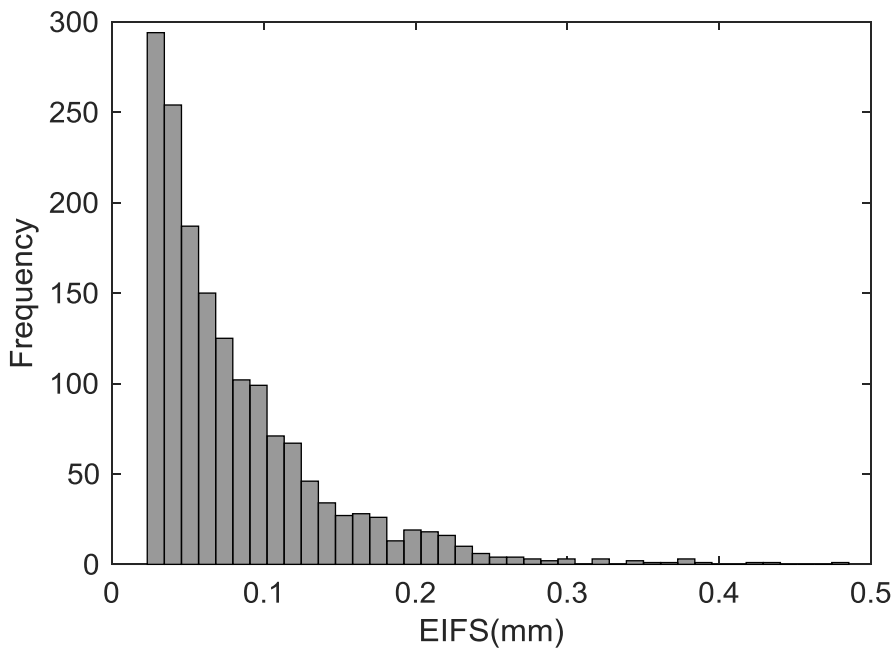

Figure B32. Histogram of EIFS in 3rd crack of Type III-1 Arm

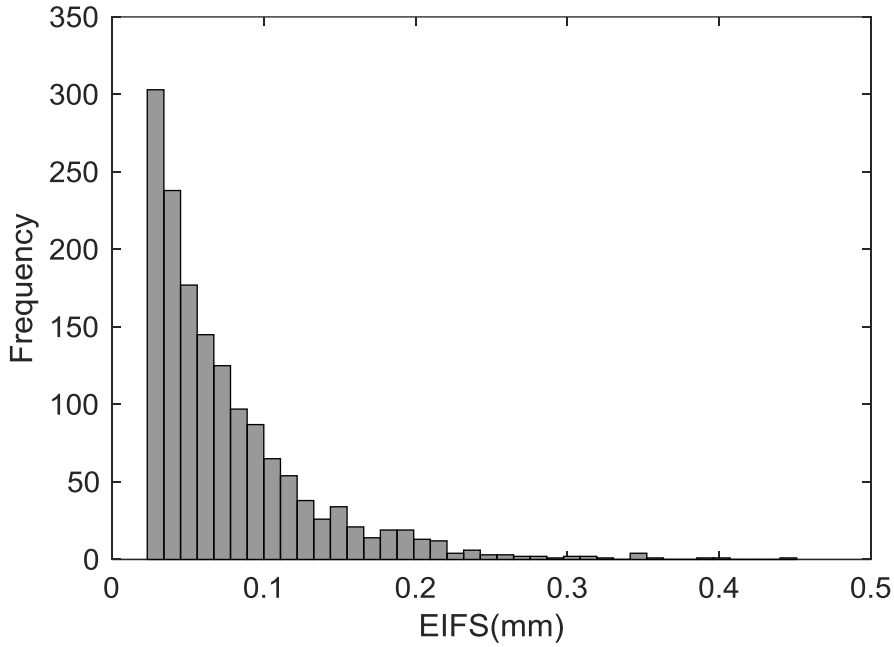

Figure B33. Histogram of EIFS in 4th crack of Type III-1 Arm

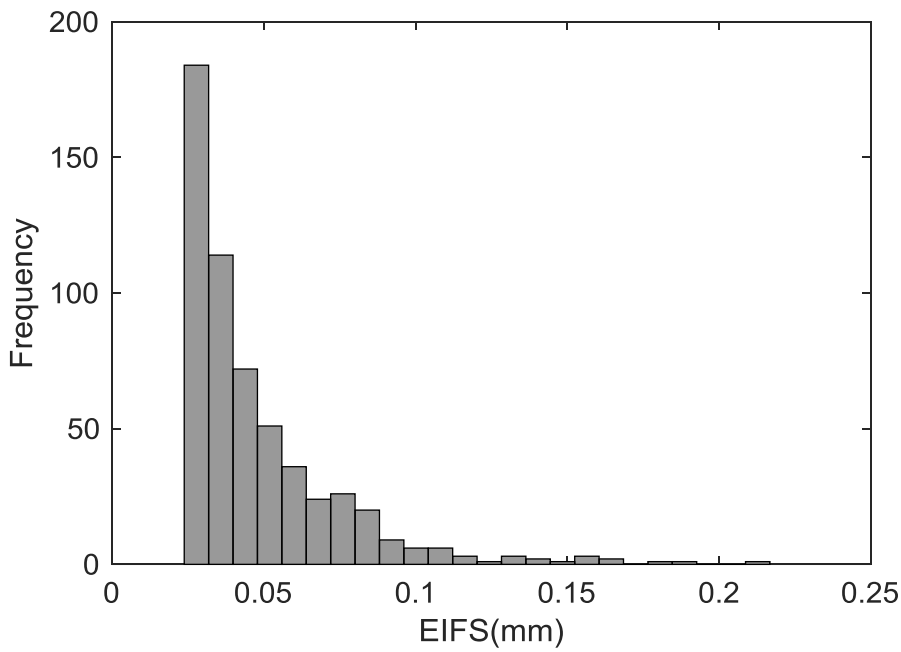

Figure B34. Histogram of EIFS in 5th crack of Type III-1 Arm

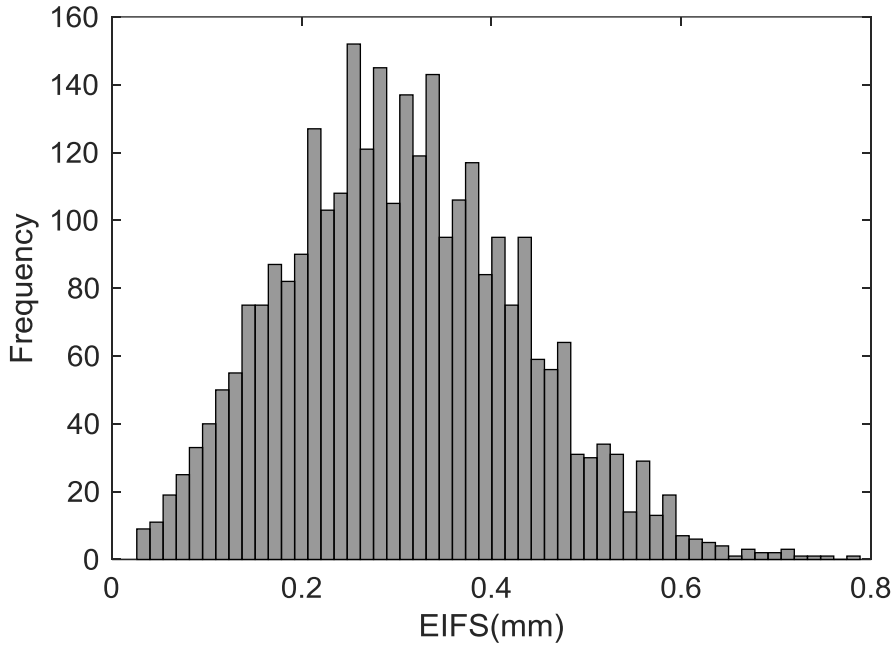

Figure B35. Histogram of EIFS in 1st crack of Type III-4 Arm

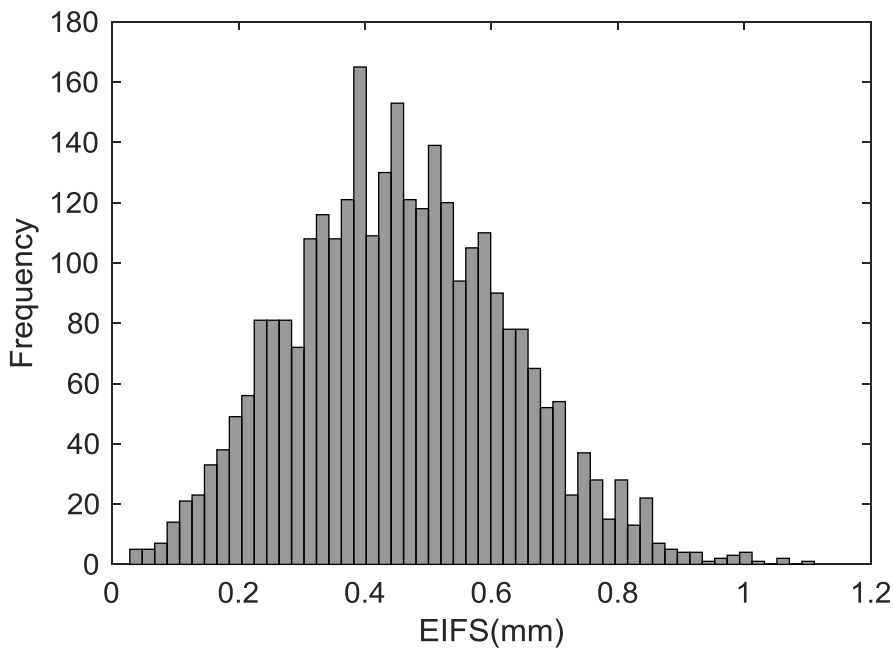

Figure B36. Histogram of EIFS in 2nd crack of Type III-4 Arm

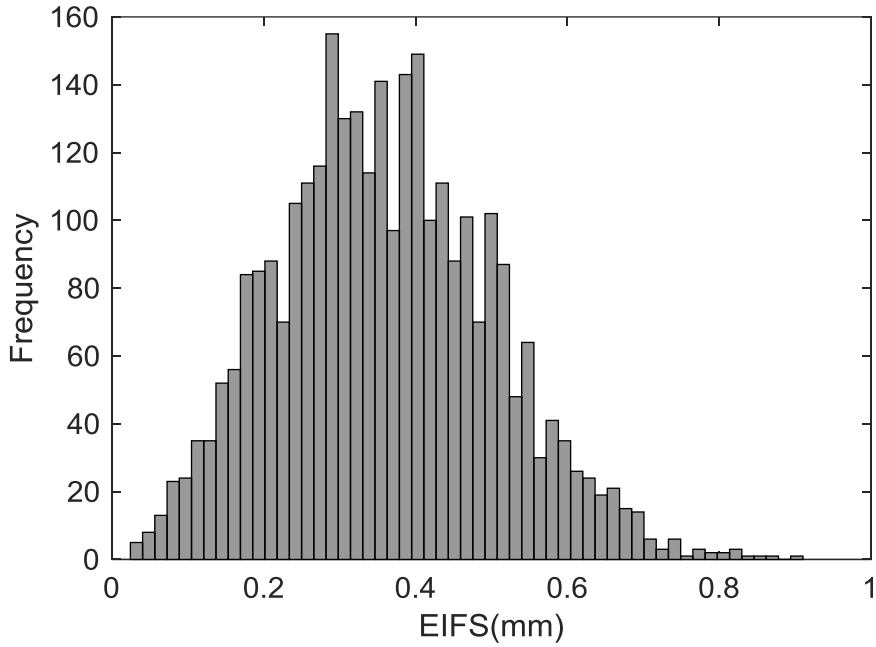

Figure B37. Histogram of EIFS in 3rd crack of Type III-4 Arm

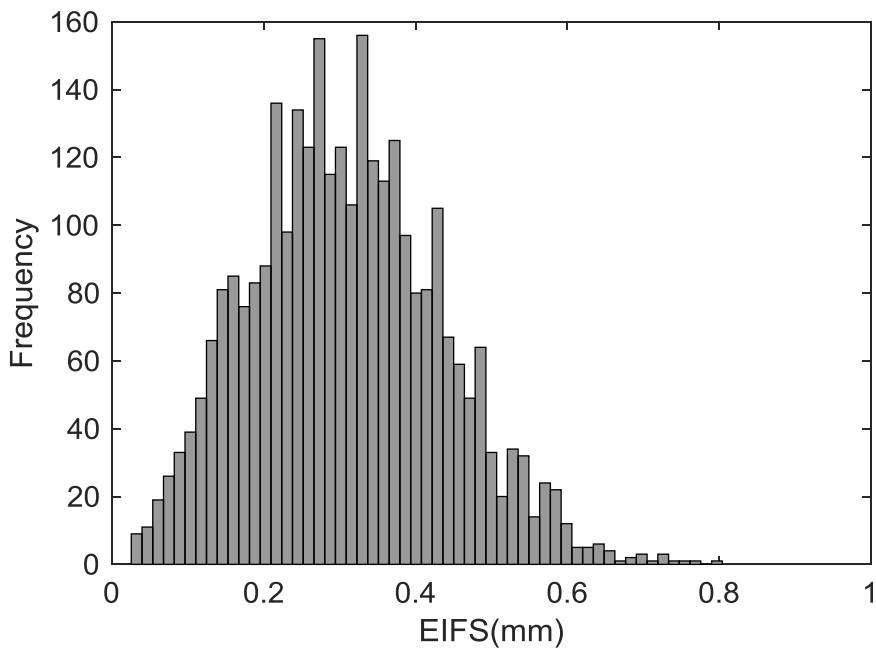

Figure B38. Histogram of EIFS in 4th crack of Type III-4 Arm

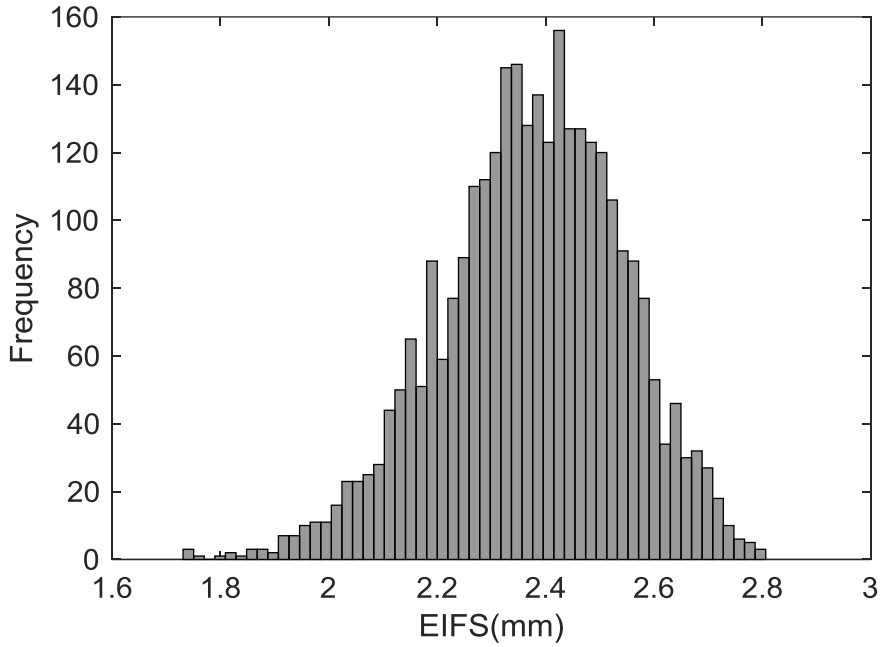

Figure B39. Histogram of EIFS in 1st crack of Type V-1 Pole

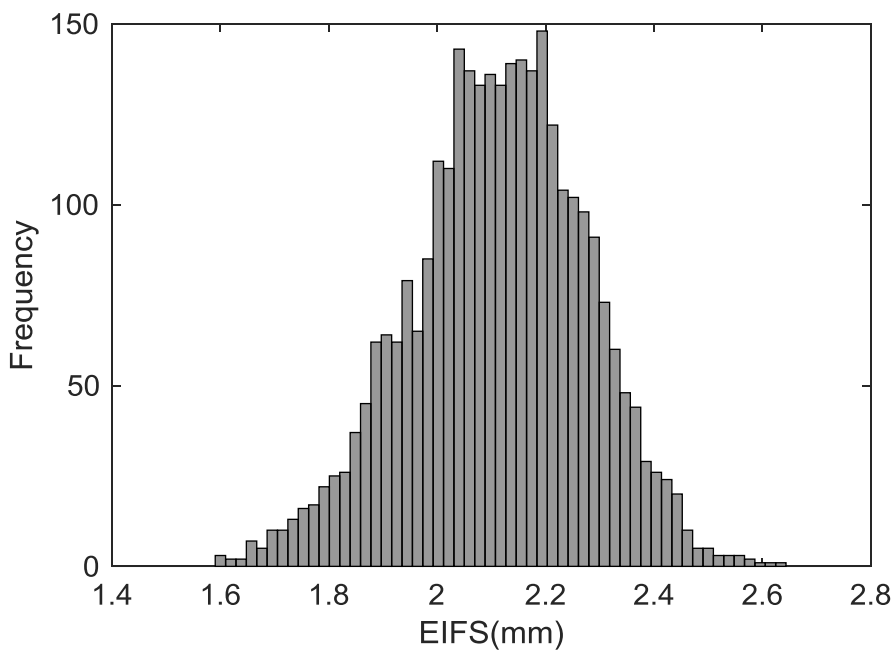

Figure B40. Histogram of EIFS in 2nd crack of Type V-1 Pole

초 록

박준용
건설환경공학부
서울대학교 대학원

실제 피로 메커니즘을 반영하는 피로 신뢰도 평가를 수행하기 위하여 다중균열의 성장과 병합을 고려한 균열성장해석법과 다중균열 조건의 모사를 위한 초기 균열 크기와 균열 간 간격의 확률모델을 제안하였다. 계측된 다중균열 정보에 기반한 기존의 결정론적 평가방법을 대체하여, 제안한 평가 모델을 통해 보다 일반적인 용접상세에 적용 가능한 확률론적 평가가 가능하다.

기존의 연구결과를 참고하여 다중균열의 성장과 병합을 고려한 균열성장해석법을 결정하였다. 단일균열의 성장을 모사하기 위하여 LEFM을 활용하였다. Paris와 Edrogan이 제안한 균열성장모델은 Large crack에 유효하기 때문에, 일반적으로 1mm보다 작은 균열을 나타내는 small crack의 성장해석은 유효하지 않다. Small crack의 성장은 불확실성이 큰 이유로 Paris' law와 같이 널리 알려진 균열성장모델이 개발되지 않았다. 이 문제를 해결하기 위하여, 가상의 등가균열크기를 나타내는 EIFS를 도입하였다. Back-extrapolation method를 통해 실험 피로수명과 동일한 피로수명을 도출하는 가상

의 균열크기를 추정하며 이를 EIFS라고 한다. 가상의 균열 크기를 나타내기 때문에 균열 크기가 small crack의 영역에 위치하더라도 Large crack에 유효한 Paris' law를 활용한 균열성장해석이 가능하다.

다중균열의 병합을 모사하는 경우, 병합 과정에서 균열 형상은 초기에 가정한 반타원 균열에서 점차 다른 형상으로 바뀌게 된다. 그러므로 기존의 SIF 식으로는 균열 병합 과정에서 발생하는 SIF의 변화를 모사할 수 없으며, FEA를 통해 균열 병합을 모사할 수 있다. 이런 이유로 복잡한 균열 병합 과정의 모사를 대체하기 위하여, re-characterization rule을 도입하였다. 다양한 re-characterization rule 중에서 Kamaya의 연구결과를 활용하여 인접한 두 균열의 면적의 합과 동일한 면적을 가지는 단일균열로 치환함으로써 복잡한 병합 과정을 대체하였다.

다중균열 조건의 확률론적 모사를 위하여 초기 균열의 크기 및 균열 간 간격의 확률모델을 개발하였다. 확률모델 개발을 위해 NCHRP Project 10-70에서 수행된 피로시험의 실제 피로 파단면들을 분석하였다. 파단면에서 발생한 beach mark와 ratchet mark를 통해 균열시작점을 구분하였으며, 하나의 시험체에서 6~23개의 균열시작점을 확인하였다. 균열시작점 간의 간격을 측정하여 총 209개의 균열 간격 데이터를 확보하였고, 이를 활용하여 확률모델을 개발하였다. 적합도 검정을 통해 평균 8.3mm와 표준편차 4.4mm를 가

지는 Lognormal 분포의 적합도가 가장 높음을 확인하였다.

초기 균열의 크기는 피로 파단면으로부터 직접적으로 확인하기 힘드므로, 균열시작점의 위치와 피로수명을 기반으로 역으로 추정하였다. EIFS를 초기 균열의 크기로 간주하였다. Paris' law의 재료상수 C는 분포특성을 가지므로 Barsom의 실험데이터를 활용하여 확률모델로 적용하였다. 재료상수 C가 확률모델로 적용되었으므로, 재료상수 C에 대응하여 추정되는 EIFS 또한 분포를 가진다. 모든 균열시작점에서 추정된 EIFS 분포 데이터를 취합하여 초기 균열 크기의 확률모델을 개발하였다. 적합도 검정 결과 평균 0.58mm와 표준편차 0.91mm를 가지는 Lognormal 분포가 가장 적합하다는 것을 확인하였다.

다중균열 조건은 구조물의 종류와 무관하게 용접부에서 나타나는 특징이다. 그리고 활용된 시험체는 강관이지만 일반 구조용강을 사용하였고, 적용된 용접 재료와 방법이 다른 구조물의 용접부와 다르지 않다. 그러므로 제안한 초기 균열의 분포특성은 충분히 다른 강구조물의 용접부에 적용될 수 있다. 강교의 용접상세들을 예제로 구성하여 제안한 평가모델의 타당성을 검증하였다. 타당성을 검증하기 위하여 NCHRP Report에 수록되어 있는 피로수명의 분포특성과 제안한 평가모델을 통해 얻은 피로수명의 분포특성을 비교하였다. 기존에 단일균열을 가정한 평가모델의 결과 또한 함께

비교하였다. 결과적으로 제안한 다중균열을 고려한 평가모델이 피로상세에 따라 보수적인 결과를 주기도 하였지만, 전체적으로 실험피로수명의 분포특성과 유사한 결과를 주고 있음을 확인하였다. 반면 단일균열을 가정한 평가모델의 결과는 전반적으로 피로수명을 과대평가하는 결과를 주고 있음을 확인하였다. 강교의 피로상세에 제안한 평가모델을 적용하여 타당성을 확인함으로써 다양한 강구조물의 용접부에 대한 피로신뢰도 해석에 적용할 수 있는 근거를 확보하였다.

주요어: 피로신뢰도; LEFM; 다중균열 병합; Equivalent initial flaw size (EIFS); Re-characterization rule

Student Number: 2011-20977